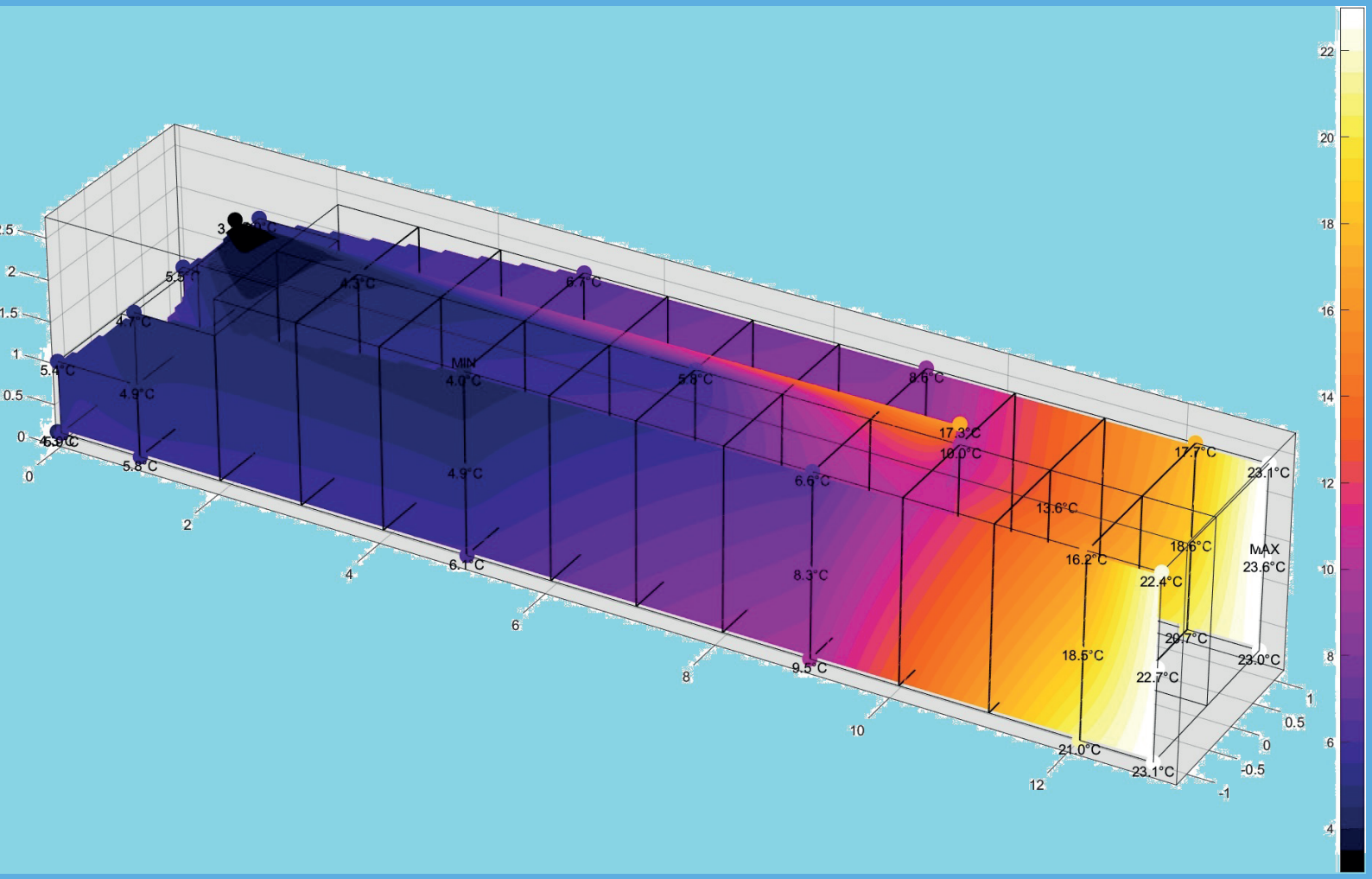

Temperature uniformity, air flow and air pressure in a 45ft reefer container

Climate chamber tests on 45ft intermodal refrigerated container PVDU380268[0]

L. J. S. Lukasse, M. G. Staal, J. Wildschut

CONFIDENTIAL

WAGENINGEN
UNIVERSITY & RESEARCH

Temperature uniformity, air flow and air pressure in a 45ft reefer container

Climate chamber tests on 45ft intermodal refrigerated container PVDU380268[0]

Authors: L. J. S. Lukasse, M. G. Staal, J. Wildschut

Institute: Wageningen Food & Biobased Research

This study was carried out by Wageningen Food & Biobased Research, subsidised by TKI Horticulture (the Dutch Ministry of Agriculture, Nature and Food Quality) under TKI number TU18098, funded by commissioners and commissioned by Anthos, H. Essers, Unit45 and Thermo King.

Wageningen Food & Biobased Research
Wageningen, September 2021

Confidential until 08-2023

Report 2211

WAGENINGEN
UNIVERSITY & RESEARCH

WFBR Project number: 6234166203
Version: Final
Reviewer: Hans de Wild
Approved by: Nicole Koenderink
Subsidised by: TKI Horticulture (the Dutch Ministry of Agriculture, Nature and Food Quality) under TKI number TU18098
Funded by: commissioners
Commissioned by: Anthos, H. Essers, Unit45 and Thermo King
This report is confidential until: August 2023

PO box 17, 6700 AA Wageningen, The Netherlands, T + 31 (0)317 48 00 84, E info.wfbr@wur.nl, www.wur.eu/wfbr.

Contents

Summary 5

1 Introduction 6

1.1 Aim 6

2 Theory (Key Performance Indicators) 7

3 Equipment specifications 9

3.1 Reefer container 9
3.1.1 Insulated body 9
3.1.2 Return air duct (bulkhead) 10
3.1.3 Supply air duct 11
3.1.4 Refrigeration unit type and settings 13
3.2 Dummy load during testing 13
3.3 Logger types and positions 14

4 Test program 18

4.1 K-value 18
4.2 Supply air flow rate 18
4.3 Mapping of temperature, air velocity and static pressure difference 18
4.3.1 Tested configurations 18
4.3.2 Sensor positions 19
4.3.3 Temperature mapping tests 21
4.4 Inner surface temperatures 22

5 Results 24

5.1 Measured K-value 24
5.1.1 Measuring results 24
5.2 Supply air flow rate 24
5.3 Air velocities and static pressure differences 25
5.4 Temperature mapping 29
5.5 Inner surface temperatures 32

6 Discussion 33

6.1 K-value 33
6.2 Supply air flow rate 33
6.3 Air velocities and static pressure differences 33
6.4 Temperature mapping 34
6.4.1 General temperature distribution patterns 34
6.4.2 Maximal cargo temperature difference ΔT_{cargo} 34
6.4.3 ΔT_{cargo} in heating mode vs. cooling mode 34
6.4.4 Effect of supply air duct 35
6.4.5 Effect of distance between cargo and walls (23 or 26 pallets) 36
6.4.6 Air flow distribution 36
6.4.7 Return air temperature control 36
6.4.8 Effect of method of drive 36
6.4.9 Effect of run mode 37
6.5 Inner surface temperatures 37

7 Conclusions 39

Literature **40**

Acknowledgements **41**

Annex 1 Temperature graphs **42**

Annex 2 steady state temperatures in 3D **51**

Annex 3 Static pressure differences **59**

Annex 4 Air velocities measured with anemometers **61**

Annex 5 Test log **64**

Summary

Project partners Essers, Thermo King and Unit45 are developing a new type of 45ft reefer container. They would like to compare the performance of a first version of the new type of 45ft reefer container to a reference 45ft container. To that end a series of climate chamber tests has been performed on a reference 45ft container.
In the tests the following parameters were measured and evaluated: K-value, air flow rate, distribution of air flow, static air pressure distribution, and temperature distribution in extreme ambient temperatures. The distribution of air flow, static air pressure distribution, and temperature distribution were measured for three configurations:

1. Configuration 1 (reference): standard container with standard stowage.
2. Configuration 2 (no air chute): reference + removed supply air duct.
3. Configuration 3 (23 pallets): reference + right row of pallets 90° rotated to increase space between walls and cargo from 2 to 12 cm.

In these tests a dense grid with more than 50 internal temperature loggers was used, which allows a 3D comparison of temperature distribution in the different conditions.
Important is the temperature uniformity requirement: for long-distance carriage of lily bulbs, the difference between the warmest and the coldest cargo temperature shall never be more than 3 °C.
In all tests especially the door-end temperatures deviate from setpoint, illustrating the need to carry more supply air towards the door-end. The most important conclusion is that temperature differences inside the container are too large, especially in cooling mode. In cooling mode at T_{set} = 4 °C and T_{amb} = 40 °C, method of drive = diesel, and run mode = continuous, even in the favorable reference configuration the difference between the warmest and the coldest cargo temperature is 7.7 °C.
Other important conclusions are:

1. This container's supply air duct is susceptible to improvement, despite its significant contribution to making the temperature distribution more uniform.
2. Increasing the distance between cargo and walls from 2 to 12 cm in this container adversely effects door-end temperatures, and hence temperature uniformity.

1 Introduction

Project partners Essers, Thermo King and Unit45 are developing a new type of 45ft reefer container. A purpose of the development is that the new 45ft reefer container should be suited for the long-distance carriage of lily bulbs. In that case it is required that the difference between the warmest and the coldest steady state cargo temperature is never more than 3 °C.
The project partners would like to compare the performance of a first version of the new type of 45ft reefer container to a reference 45ft container.
Key performance indicators of refrigerated transport equipment are K-value of the container and cargo temperature distribution under extreme ambient temperatures. In a series of climate chamber tests these KPIs are measured and evaluated for an existing 45ft container, which will then serve as a reference point in the future development.
The cargo temperature distribution inside reefers directly relates to air flow distribution. That's why also the unit's air flow rate, distribution of air flow, and static air pressure distribution inside the container are measured.
The air and temperature distribution are affected by multiple parameters, amongst which: difference between internal and external temperature, the presence of a supply air duct, air flow rate of the unit's evaporator fans, and cargo stowage pattern. Therefore, the following factors were varied in the tests: 1) Internal and external temperature settings T_{set} / T_{amb}, 2) unit's run mode, 3) unit's method of drive, 4) presence of supply air duct, 5) cargo stowage. Note that the unit's evaporator fan speed is not varied, because the test container's refrigeration unit does not allow such setting.

1.1 Aim

The tests have multiple purposes:
1. Assess K-value.
2. To measure steady state temperature distribution, pull down and pull up curves in extreme ambient temperatures.
3. To quantify the effect of T_{set} / T_{amb}, run mode, method of drive, supply air duct and a cargo stowage variation on temperature distribution.
4. To collect data suitable for CFD model calibration afterwards.

2 Theory (Key Performance Indicators)

In an experimental study on temperature distribution in reefer containers lots of data need to be evaluated. The three typical stages of interest are: steady state, power off, and pulldown. In an experiment a natural procedure is to first prepare for pulldown by establishing steady state at initial temperature (stage 0), then pulldown (stage 1) to steady state (stage 2), then introduce a power off period of a predefined duration (stage 3), and then recover the temperatures (stage 4) to steady state again (stage 2). Fig. 1 shows an arbitrary example (note: recovery stage missing from this illustration). The 'temperature recovery' stage has similarities with the initial pulldown stage after hot stuffing. The difference is that at the start of a recovery period there are typical temperature gradients in the cargo from warm side temperatures to a colder core, while at the start of an initial pulldown stage all cargo temperatures are approximately equal.

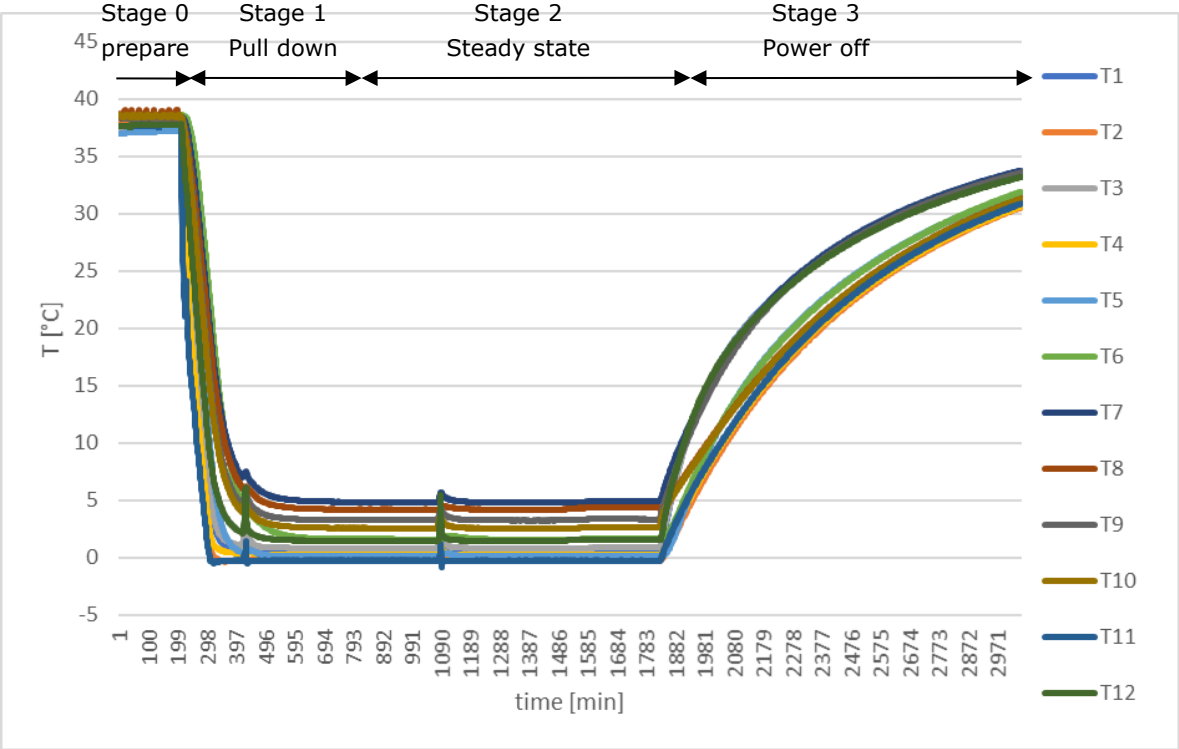

Figure 1 ***Example of temperatures recorded during four consecutive test stages. Series T1 till T12 show temperatures recorded by temperature sensors placed at different positions in cargo.***

To condense the information contained in the temperature readings to one, or a few, informative numbers, this report uses the key performance indicators listed in Table 1.
The maximal cargo temperature range is the measure for the cargo temperature uniformity:

$$\Delta T_{cargo} = T_{warmest} - T_{coldest} \quad [°C] \quad (1)$$

where

$T_{warmest}$ = warmest time-averaged cargo temperature sensor during steady state
$T_{coldest}$ = coldest time-averaged cargo temperature sensor during steady state

Note that in this report cargo temperature is defined as temperature measured by a temperature sensor taped to the dummy load of cartons. Under ideal air distribution conditions ΔT_{cargo} is the same as the absolute value of the temperature difference between the unit's return and supply air temperature, defined as ΔT_{unit}:

$$\Delta T_{unit} = |T_{ret} - T_{sup}| \quad [°C] \quad (2)$$

where

T_{ret} = refrigeration unit's time-averaged return air temperature during steady state

T_{sup} = refrigeration unit's time-averaged supply air temperature during steady state

The quality of the airflow distribution in a steady state is scored with a dimensionless ratio, called Temperature Distribution Factor TDF:

$$TDF = \frac{\Delta T_{cargo}}{\Delta T_{unit}} = \frac{T_{warmest} - T_{coldest}}{|T_{ret} - T_{sup}|} \quad [-] \quad (3)$$

In case of ideal airflow distribution $\Delta T_{cargo} = \Delta T_{unit}$, resulting in TDF = 1. In practice the airflow distribution is usually non-ideal, and the maximal temperature range ΔT_{cargo} in the reefer is larger than ΔT_{unit}, resulting in TDF > 1.

Table 1 Key performance indicators used for different variables in the tests.

Variable	Key performance indicator (KPI)
Temperature uniformity	ΔT_{cargo}, warmest time-averaged cargo temperature minus coldest time-averaged cargo temperature during steady state.
Air flow distribution	Ratio TDF (eqn. 3) during steady state.
Pull down/up	Just visual presentation of temperature graphs
Power off	Just visual presentation of temperature graphs
Door opening	Just visual presentation of temperature graphs
Recovery	Just visual presentation of temperature graphs

3 Equipment specifications

3.1 Reefer container

Container identification number	PVDU380268[0]
Tare weight	7,495 kg
Max. gross weight	34,000 kg

3.1.1 Insulated body

Description	Value
Container box serial number	TL14076958
Date of construction insulated body	Oct. 2014
Box manufacturer	Yangzhou Tonglee Reefer Container Co. Ltd.
Box type	D45-NPGD-560-A-LASA
External dimension of insulated enclosure	L(@floor)xWxH(@door) = 13.37 x 2.55 x 2.82 m
External height at unit-end	1.81 m
External length at top	12.82 m
Inside dimensions of insulated enclosure	L(@floor, without return air duct)xWxH(@door) = 13.24 x 2.44 x 2.57 m
Internal height @ unit-end	1.59 m
Inside length @ ceiling	12.69 m
Thickness of doors	75 mm (note approx. 1/3rd of area has 26 mm recesses at door's outside)
Thickness of walls	55 mm
Thickness of roof	155 mm
Thickness of floor	95 mm
Thickness of front wall (@floor, calculated)	55 mm (not measured, calculated as L_{extern}(@floor) – L_{intern}(@floor) – door thickness)
Gooseneck dimensions (position, L, W, recess)	@ unit-end in center of container, L = 3.68 m, W = 1.03 m, recess = 0.07 m (i.e. in this area the floor is 7 cm thinner than in rest of floor)
Supply air outlet	W x H = 122 x 12.5 cm
Distance between top of supply air outlet and ceiling	20 cm
Distance between supply air outlet and front wall	68 cm

Note that the internal length at the floor is more than at the ceiling because at the unit-end the container has a cavity in the upper part. That cavity houses the refrigeration unit's external components like diesel engine, condenser and compressor (Fig. 2).

Figure 2 Refrigeration unit's external section.

Table 2 Calculated surface areas and internal volume.

Description	value
Total floor area	32.31 m^2
Usable internal volume	81.71 m^3
Total internal surface area S_i of body	144.13 m^2
Total external surface area S_e of body	156.87 m^2
Mean surface are S = $\sqrt{S_i \times S_e}$	150.36 m^2

3.1.2 Return air duct (bulkhead)

Description	value
Return air duct width @ bottom	244 cm
Return air duct width @ top	120 cm
Distance between floor and return air inlet	14 cm
Space between front wall and bulkhead, i.e. depth of return air duct	8 cm
Are there other return air entries to evaporator than at lower end of return air duct?	No

Fig. 3 shows a photo of the return air duct. It shows a 14 cm high open gap between the floor and the return air inlet. At the floor the return air duct spans the complete container width. Higher up it assumes the width of the evaporator and the supply air outlet. After a 90° turn forward and a 90° upward the return air duct connects to the evaporator.

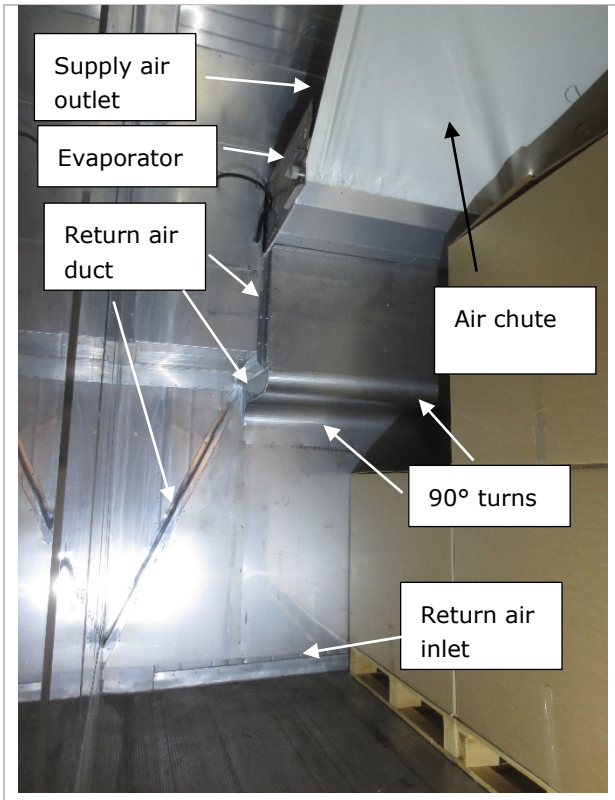

Figure 3 Photo of return air duct.

3.1.3 Supply air duct

Fig. 4 shows an overall photo of the supply air duct, also known as air chute. Fig. 3 already showed a close-up of how it connects to the evaporator. Two more photos are presented in Fig. 5 and Fig. 6. The supply air duct has a complex geometry. Both at the end and at the sides there is an opening between the air chute and the ceiling. The opening is widest at the unit-end and gradually narrows towards the door-end. Fig. 7 till Fig. 9 present some design drawings made based on our own measurements of the dimensions.

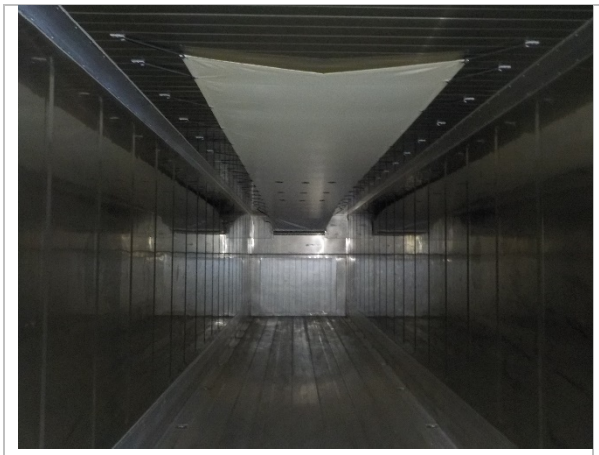

Figure 4 Container's supply air duct.

Figure 5 Dor-end opening of air chute.

Figure 6 ***Supply air outlet above air chute.***

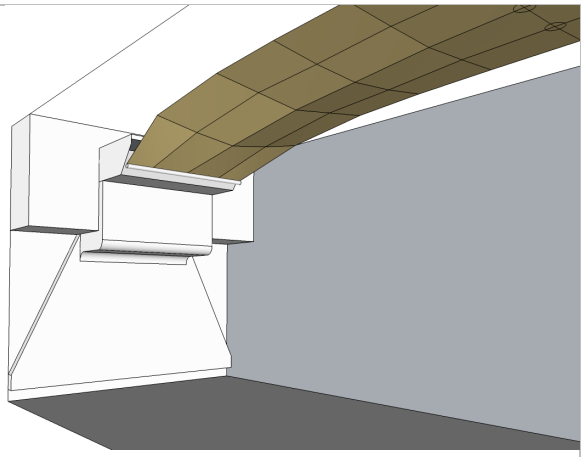

Figure 7 ***Close-up drawing of air chute (brown) connection to evaporator.***

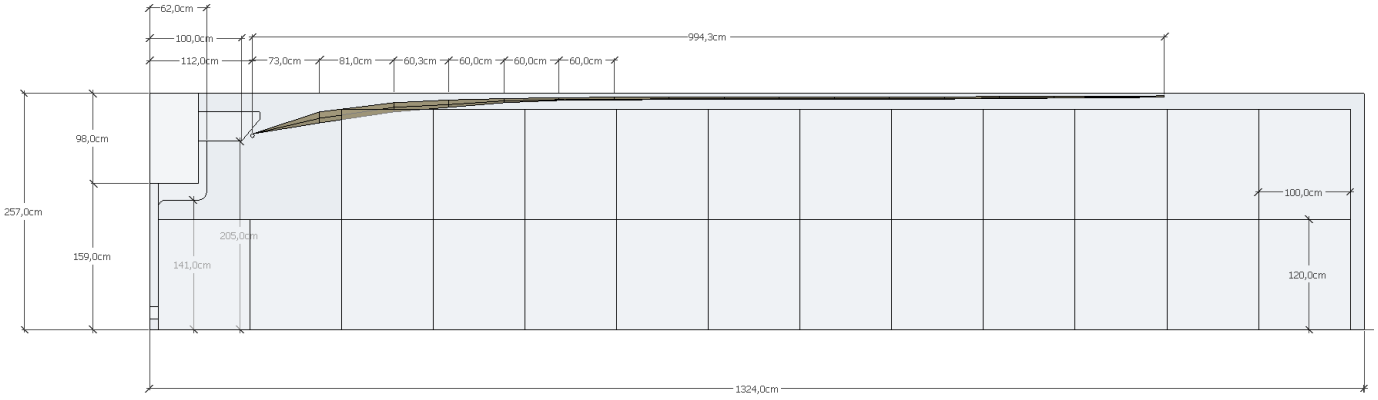

Figure 8 ***Side view drawing of air chute (brown).***

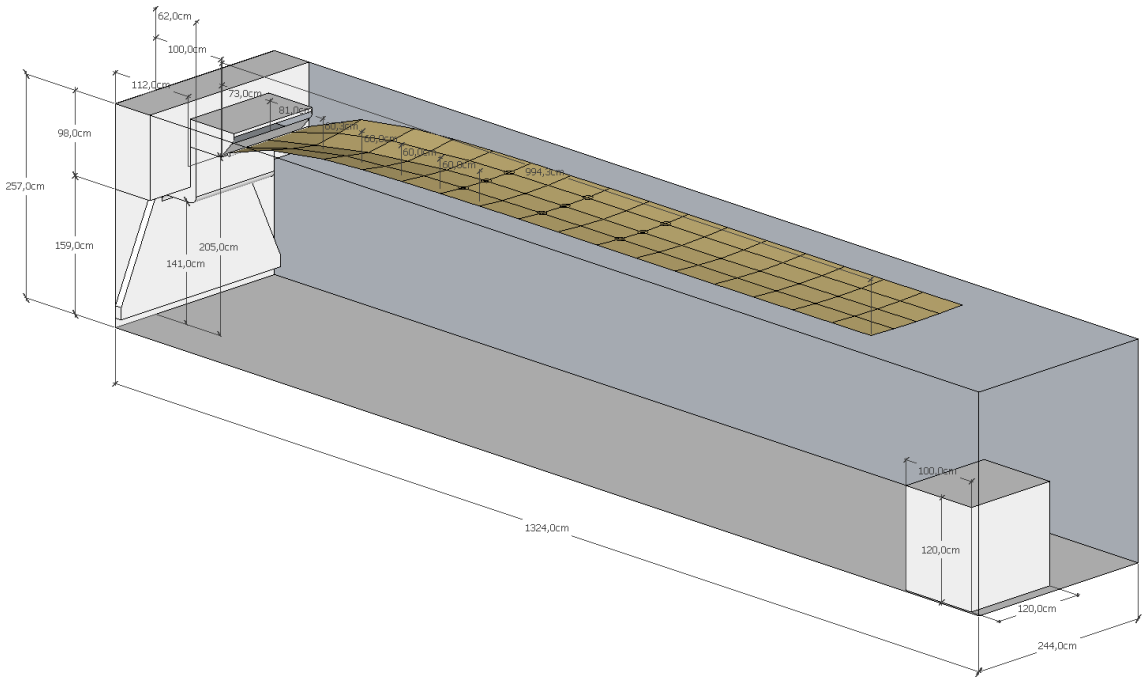

Figure 9 ***3D drawing of container geometry with air chute in brown.***

3.1.4 Refrigeration unit type and settings

Description	Value
Manufacturer	Thermo King
Type	T-1200R
Serial no.	GLW1022907
Manufacturing date	Unknown
Controller's software version	75B0
Date of last PTI	7-5-2020
Set defrost interval	12 h (maximum permitted)

Description of unit: the unit has a rigid coupling from engine to both the two evaporator fans and the compressor. Electric drive operation yields evaporator fan speed just below low speed diesel engine operation. In diesel drive the diesel engine can run at two speeds: high or low, and the controller automatically chooses which one is applied. The typical logic is to run high engine speed when control temperature is far from setpoint (during pull down / pull up), and low speed otherwise (in steady state). The unit has a turtle option that blocks the diesel engine to low speed regardless of operating conditions, that option was disabled during the tests.

3.2 Dummy load during testing

During tests on air flow distribution, static pressure distribution and temperature distribution the container was filled with a dummy load. The dummy load consisted of empty palletized pallet boxes. Table 3 lists all relevant parameters of the pallets and boxes.

Table 3 Dummy load parameters.

Description	Value
Dimensions of pallets	L x W x H = 120 x 100 x 16 cm
Weight of pallet	18.9 kg
Area of openings at 120 cm side of pallet	2 openings of 41.7 x 9.5 cm (= 396 cm^2)
Area of openings at 100 cm side of pallet	2 openings of 38.5 x 11.5 cm (=443 cm^2)
No. of slats on top of pallet	10 slats of approx. 8 cm wide
Distance between slats on top of pallet	6 openings of approx. 7 cm
All slat distances ± equal?	No, see Fig. 10 and Fig. 11.
Size of pallet boxes	L x W x H = 118.5 x 98.5 x 87.0 cm
Weight of one pallet box	6.0 kg
No. of pallet box layers	2.5 (see Fig. 12)
Height of pallet stacked with 2.5 tiers of pallet boxes	233 cm

The pallet boxes were specially purchased for this test from webshop.viv.nl/palletdozen-voor-blokpallet-dubbelgolf-1185-x-985-x-870-mm.

Figure 10 ***Pallet used for the experiment.***

Figure 11 ***Bottom view of the pallet***

Figure 12 ***2.5 boxes stacked on top of each pallet.***

Figure 13 ***Sensors mounted on the pallet box.***

3.3 Logger types and positions

This section briefly describes all measurement devices used during the tests.

Table 4 ***Used logger types.***

Logger type	Number	Measured parameter
ATP sensors	12	T [°C]
LogTags (Fig. 16)	42	T [°C]
Type T thermocouples connected to OM-CP-OCTPRO logger	4	T [°C]
Air pressure difference sensor	1	Pressure difference [Pa]
Hot wire anemometers, type EE65-VB5, range 0.2 till 20 m/s, log every 15 sec	12	Air velocity [m/s]
Hot wire anemometers, type EE576-V3B2, range 0.2 till 2 m/s, log every 15 sec	6	Air velocity [m/s]
Hot wire anemometers, type EE671, range 0.2 till 10 m/s, log every 30 sec, wireless.	16	Air velocity [m/s]

Hot wire anemometers type EE671 record till their batteries are flat, at the set log interval of 30 s. The batteries last approximately 5 hours. The two other types of hot wire anemometers are powered by the grid (230 V / 50 Hz).
Accuracy of hot wire anemometer EE65-VB5: ± (0.2 m/s + 3% of measured value)
Accuracy of hot wire anemometer EE576-V3B2: ± (0.08 m/s + 4% of measured value)
Accuracy of hot wire anemometer EE671: ± (0.3 m/s + 4% of measured value)

Figure 14 ***Hot wire anemometers EE576-V3B2 (left) and EE65-VB5 (right).***

Figure 15 ***EE671 hot wire anemometer.***

Figure 16 ***LogTag logger for temperature.***

Figure 17 ***ATP sensor (= 4-wire PT100 temperature sensors of IEC751 class A, manufacturer: Tempcontrol).***

Accuracy of all temperature sensors: ± 0.5°C

The log interval during the tests is 5 min. for the LogTags and 1 min. for the ATP sensors. Only the readings of the ATP temperature sensors are real-time available.

Figure 18 Testo 480 pressure difference sensor.

Accuracy of testo 480 pressure difference sensor: ± (0.3 Pa + 1 % of measurement value)

For assessing the supply air flow rate a handheld hot wire anemometer (testo 425) is used (Fig. 19, Fig. 20). Accuracy of testo 425: ± (0.03 m/s + 5% of measurement value) in the range of 0 till 20 m/s.

Figure 19 Handheld hot wire anemometer used to assess supply air flow rate.

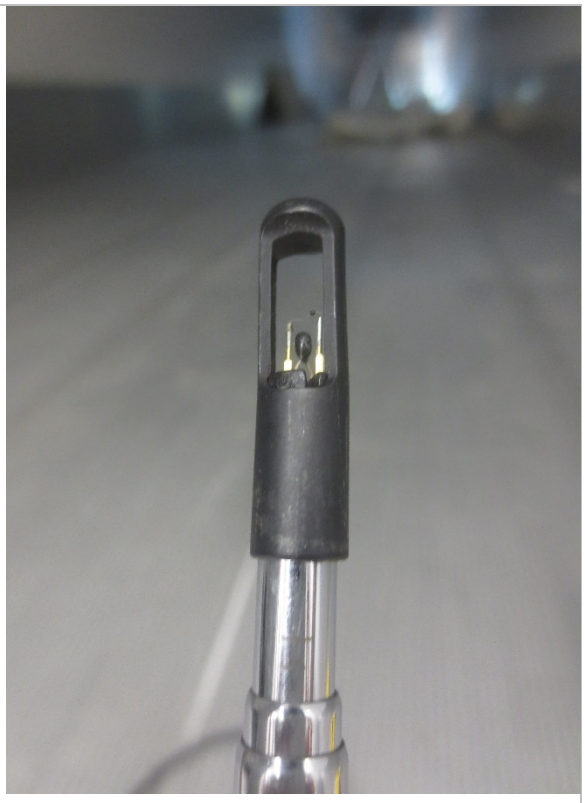

Figure 20 Close-up of hot wire sensor.

4 Test program

4.1 K-value

The K-value of the empty container was measured according to ATP procedures (ATP, 2020) by following the relevant steps in WFBR internal Standard Operating Procedure T-10006.

4.2 Supply air flow rate

The supply air flow rate was measured after completion of all other tests. The measurements were done in an empty container. The procedure was to measure the air velocity [m/s] averaged over the supply air outlet and multiply it by the area [m^2] of the supply air outlet. First the supply air duct was removed. Then the air velocity right in front of the supply air outlet was measured as an average over time and place. The average was assessed with the handheld anemometer's time-averaging function while slowly moving the handheld anemometer over the complete supply air outlet for a period of 30 till 50 seconds. That time- and space-averaged measurement was repeated at least thrice. If the mutual difference between largest and smallest measurement was more than 10% a fourth repetition was done after which the deviant measurement was discarded. The measurement was performed for the three possible evaporator fan speeds: electric drive, low engine speed diesel drive and high engine speed diesel drive. During these measurements the unit was running at a setpoint close to 20 °C. All tests were done within in a time frame of two hours.
This test procedure is less accurate than for example the test procedure described in ISO5801, but it is convenient and fast, and therefore adequate for roughly checking manufacturer specs and mutually comparing different situations.

4.3 Mapping of temperature, air velocity and static pressure difference

4.3.1 Tested configurations

Three configurations were tested:
1. Configuration 1 (reference): standard container with standard stowage
2. Configuration 2 (no air chute): reference + removed supply air duct
3. Configuration 3 (23 pallets): reference + right row of pallets 90° rotated to increase space between walls and cargo from 2 to 12 cm

Fig. 21 till Fig. 23 visualize the defined configurations. Note that L x W = 120 x 80 cm for the last row of pallets at the door-end, while all other pallets are 120 x 100 cm.

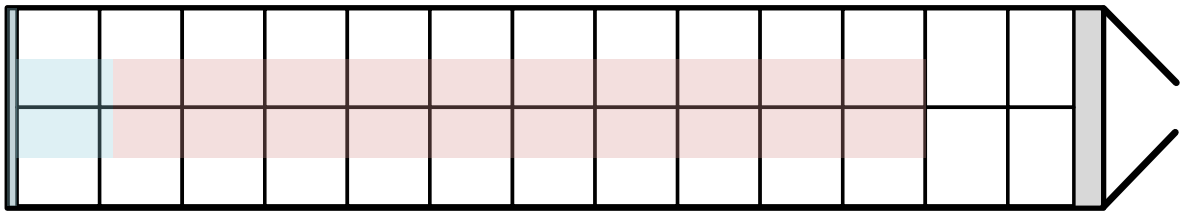

Fig. 21 ***Configuration 1 (reference) top view. Red indicates the air chute. Blue indicates the return air duct and evaporator above the first two pallets.***

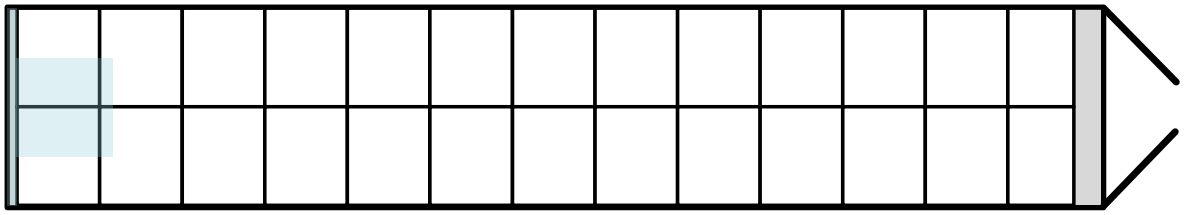

Figure 22 ***Configuration 2 (no air chute): reference + removed supply air duct. Blue indicates the return air duct and evaporator above the first two pallets.***

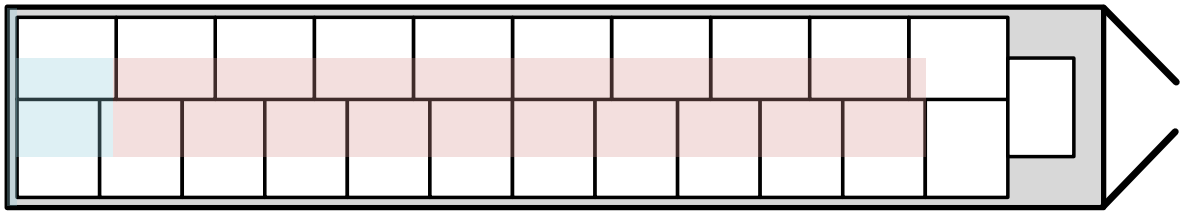

Figure 23 ***Configuration 3 (23 pallets): reference + right row of pallets 90° rotated to increase space between walls and cargo. Red indicates the air chute. Blue indicates the return air duct and evaporator above the first two pallets.***

Table 5 ***(measured) stowage parameters.***

Description	Value
Distance between last pallet and door	27 cm
Height of headspace (= distance between ceiling and top of cargo)	24 cm
Airflow blocking at door-end	none

In a climate chamber at WFBR the above listed configurations were subjected to a series of test conditions. In each test condition the objective is to gain insight in the distribution of temperature and airflow.

4.3.2 Sensor positions

Fig. 24 and Fig. 25 schematically depict the sensor locations for the reference configuration 1. The pallets in Fig. 24 are numbered 1 till 26 in the order in which they are placed in the container. The 3 yellow dots indicate LogTag sensors outside the container: one at the air inlet to the condenser, and two at 10 cm from the container walls at the center of both sides. The 2 yellow squares indicate 2 inside ATP sensors in pallets 4 and 22, these are placed inside the box at half height, and used to verify if inside temperatures have reached steady state. All LogTag temperature recorders are taped at the outside to the front or rear of boxes. Where applicable the recorder's sensor faces, but does not touch, the wall. Wherever there is red square, there are three LogTags positions above each other: at the bottom, middle and upper corner of the pallet load. The three red dots at the unit-end indicate positions of LogTags at the inlet of the return air duct (taped to the inside of return air duct at its lower-end). The two red dots above pallet 3 and 4 depict positions of LogTags at the supply air outlet. The orange squares indicate the position of the internal ATP sensors. Fig. 24 contains numbers adjacent to each temperature sensor position. These numbers are the unique serial numbers of the sensors, where the upper number is physically the upper sensor (e.g. at the unit-end pallet 1 contains ATP sensor number ATP1 at the top and ATP2 at the bottom). The side view in Fig. 25 especially helps to visualize the measurement locations for air velocity and pressure. Dark green dots indicate the positions for measurement of static pressure difference compared to the position of the purple dot: 0, 1, 3, 5, 7, 9, and 11 m from unit-end. The blue markers in Fig. 24 and Fig. 25 relate to the measurement of air velocity with hotwire anemometers. Blue dots indicate the hot wire anemometer positions in the center of pallet openings during measurement of air velocity in the longitudinal direction of the container. Blue squares indicate hot wire anemometer positions in the air slit between pallet load and container wall at half the container height for measurement of both vertical and horizontal air velocity. Blue triangles indicate the hot wire anemometer positions above the cargo: halfway between air chute and ceiling in configurations 1 and 3, and at the same position in configuration 2.

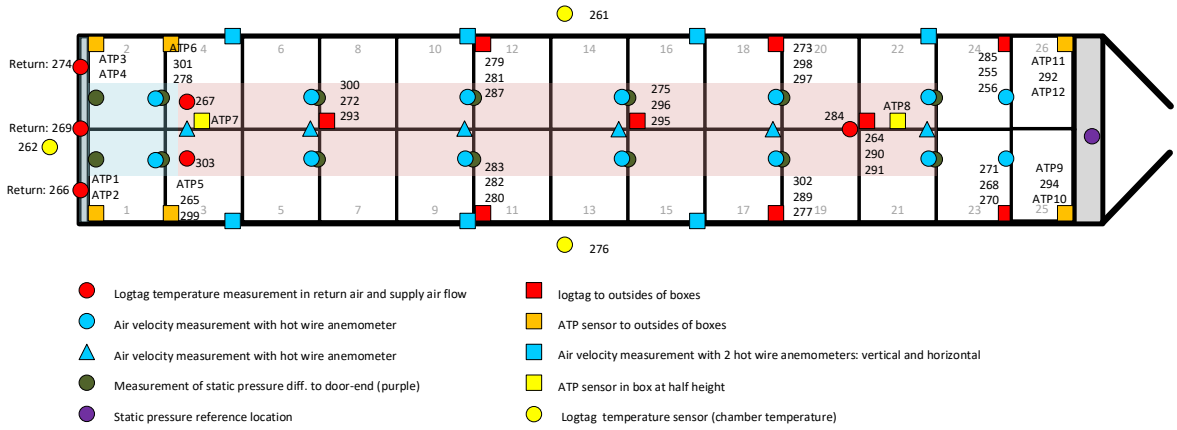

Figure 24 Schematic representation of sensor positions in configuration 1 and 2 (top view).

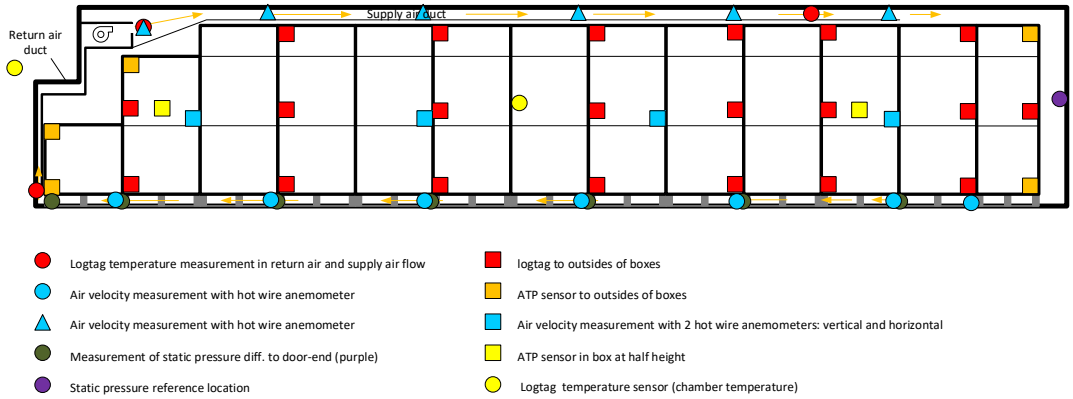

Figure 25 Schematic representation of sensor positions in configuration 1 and 2 (side view).

Fig. 26 and Fig. 27 visualize the sensor locations during configuration 3. After the preceding paragraph these figures need no further explanation.

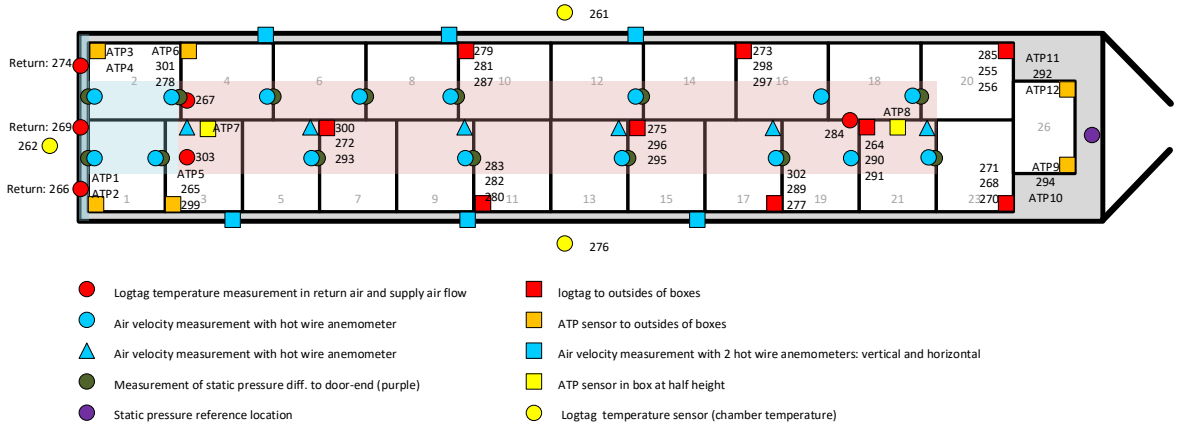

Figure 26: Schematic representation of sensor positions in configuration 3 (top view).

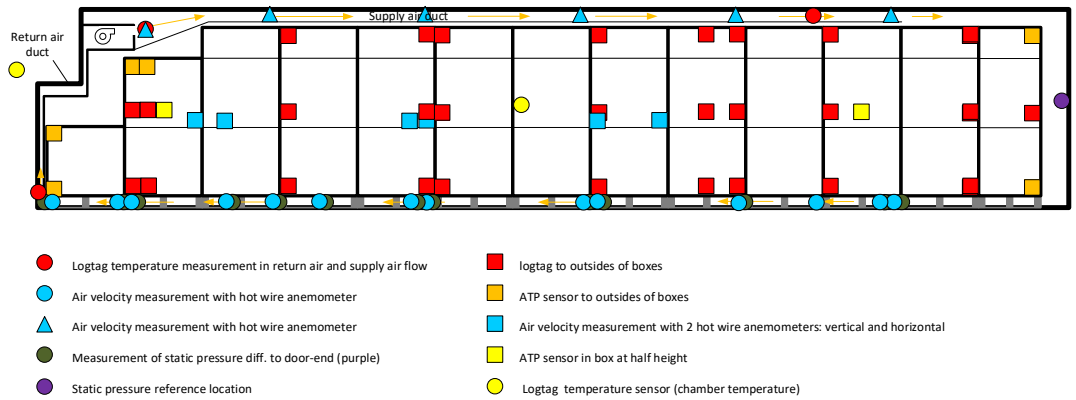

Figure 27 Schematic representation of sensor positions in configuration 3 (side view).

4.3.3 Temperature mapping tests

Table 6 till Table 8 list all conducted temperature mapping tests. The first column in each of these tables lists the unit's temperature setpoint T_{set} and the intended chamber temperature T_{amb} as measured by the two sensors at 10 cm from the container walls at the center of both sides (yellow dots in Fig. 24 till Fig. 27). Column 2 is the test number assigned to each test. The numbering was chronologically in the plan upfront. For many practical reasons the eventual work order deviated from the original plan. To avoid confusion in the data processing the original numbering has been kept in the report. Column 3 lists the run mode, as on virtually every trailer refrigeration unit there are two possible values: continuous or cycle-sentry. Column 4 lists the method of drive: diesel or electric (50 Hz / 400 V). Column 5 lists the configuration number: 1, 2 or 3 (see Fig. 21 till Fig. 23).

Table 6 Steady state tests in test programme.

T_{set} / T_{amb} [°C]	Test	Run mode	Method of drive	Configuration
6 / -15 [°C]	8	Continuous	Diesel	1 (reference)
6 / -19 [°C]	9	Continuous	Diesel	1 (reference)
22 / -17 [°C]	11	Continuous	Diesel	1 (reference)
22 / -17 [°C]	17	Cycle-Sentry	Diesel	1 (reference)
18 / 40 [°C]	20	Continuous	Electric	1 (reference)
18 / 40 [°C]	21	Cycle-Sentry	Electric	1 (reference)
18 / 45 [°C]	22	Continuous	Electric	1 (reference)
4 / 40 [°C]	25	Continuous	Electric	1 (reference)
4 / 40 [°C]	25B	Continuous	Diesel	1 (reference)
4 / 30 [°C]	25C	Continuous	Electric	1 (reference)
4 / 30 [°C]	25D	Continuous	Diesel	1 (reference)
4 / 40 [°C]	33	Continuous	Electric	2 (no air chute)
4 / 40 [°C]	38	Continuous	Electric	3 (23 pallets)

Table 7 Pull down and pull up tests in test programme.

T_{set} / T_{amb} [°C]	Test	Run mode	Method of drive	Configuration
6 / -15 [°C]	7	Continuous	Diesel	1 (reference)
18 / 40 [°C]	19	Continuous	Electric	1 (reference)
4 / 40 [°C]	24	Continuous	Electric	1 (reference)
4 / 40 [°C]	32	Continuous	Electric	2 (no air chute)
4 / 40 [°C]	37	Continuous	Electric	3 (23 pallets)

Table 8 contains a 6th column that briefly describes the purpose of that test. E.g. test 13 is a 12 hours power off test: just record how temperatures evolve after powering the unit off in steady state at T_{set} / T_{amb}. Test 14 is the recovery test, initiated directly after test 13 with the purpose to record how temperatures recover after a 12 hours power off period. Every recovery test in Table 8 directly follows the test mentioned in the row above. The first test (test 5B) in Table 8 is deviant: just record how temperatures evolve when T_{amb} gradually reduces from 30 to -15 °C, starting in steady state at T_{set} = 4 °C and maintaining the setpoint.

Table 8 Power off/ door opening / recovery tests in test programme.

T_{set} / T_{amb} [°C]	Test	Run mode	Method of drive	Configuration	Description
4 / (30 -> -15) [°C]	5B	Continuous	Diesel	1 (reference)	Decreasing T_{amb}
22 / -17 [°C]	13	N/A	N/A	1 (reference)	12 h. power off
22 / -17 [°C]	14	Continuous	Diesel	1 (reference)	Recovery after preceding power off
22 / -17 [°C]	15	N/A	N/A	1 (reference)	1 h. door opening
22 / -17 [°C]	16	Continuous	Diesel	1 (reference)	recovery after preceding door opening
4 / 40 [°C]	28	N/A	N/A	1 (reference)	1 h. door opening
4 / 40 [°C]	29	Continuous	Diesel	1 (reference)	recovery after preceding door opening
4 / 40 [°C]	34	N/A	N/A	2 (no air chute)	12 h. power off
4 / 40 [°C]	39	N/A	N/A	3 (23 pallets)	12 h. power off

4.4 Inner surface temperatures

In tests 37, 38 and 39 the inner surface temperature of the container has been measured in four locations near the door-end (see Table 9). These recordings will be compared to the recordings of nearby cargo temperature sensors. The inner surface temperatures T_{si} of the walls are measured by taping type T thermocouples to the walls with duct tape (Fig. 28, Fig. 29) and connecting the thermocouples to an Omega logger.

Table 9 Lcations for measurement of inner wall surface temperatures T_{si}.

Sensor	Location
Ch1	left side wall, 30 cm above floor (near logger 268)
Ch2	left side wall, 10 cm from door, 10 cm from roof (near sensor ATP9)
Ch3	ceiling, 40 cm from side wall (near logger 271)
Ch4	left door, half height, 80 cm from side wall (near logger 294)

Figure 28 ***Wall surface temperature measurement near sensor 268.***

Figure 29 ***Cceiling surface temperature measurement near sensor 271.***

5 Results

5.1 Measured K-value

Testing method	:	inside heating
Start of inner heating (yyyy-mm-dd hh:mm:ss)	:	2020-05-16 20:23:01
Start time of steady state conditions (yyyy-mm-dd hh:mm:ss)	:	2020-05-17 08:00:01
End time of steady state conditions (yyyy-mm-dd hh:mm:ss)	:	2020-05-17 20:35:01
Total duration of test (dd hh:mm:ss)	:	01 00:12:00
Duration of steady state conditions (hh:mm:ss)	:	12:35:00

5.1.1 Measuring results

Outside			
Mean outside temperature of body (θ_e)	:	7.53	°C
Max. difference between two mean outside temperatures	:	0.22	°C
Max. difference between two outside measurement locations	:	0.39	°C
Inside			
Mean inside temperature of body (θ_i)	:	32.63	°C
Max. difference between two mean inside temperatures	:	0.27	°C
Max. difference between two inside measurement locations	:	1.47	°C
Mean temperature difference achieved ($\Delta\theta = \theta_i - \theta_e$)	:	25.10	°C
Mean temperature of walls of the body achieved ($\frac{\theta_e + \theta_i}{2}$)	:	20.08	°C

Electric power consumption (heaters + fans) ,	Q =	1790.45	W
Total heat leakage rate ($Q/\Delta\theta$),	U =	71.32	W/°C
Total heat transfer coefficient $\left(K = \frac{Q}{\Delta\theta * S}\right)$,	**K =**	**0.474**	**W/m². °C**

Max. error in measured K in this test, : ± 5 %

5.2 Supply air flow rate

The supply air flow rate was measured for the three possible evaporator fan speeds: electric drive, low engine speed diesel drive and high engine speed diesel drive. Table 10 contains the results.

Table 10 Measured air flow rate for the three possibly occurring evaporator fan speeds.

Evaporator fan speed situation	Measured supply air flow rate φ_{air} [m³/h]
electric drive	2867
low engine speed diesel drive	3162
high engine speed diesel drive	4207

5.3 Air velocities and static pressure differences

Air velocities and static pressure differences have been measured for all three configurations at all three possible evaporator fan speeds.
For all combinations of configuration and evaporator fan speed the static pressure differences between the dark green dots and the purple dot in Fig. 24 till Fig. 27 are shown in Fig. 30 till Fig. 32. During the measurements the container doors were closed. The measurement was repeated three times consecutively: for electric drive, diesel low engine speed (LS), and diesel high engine speed (HS). For the measurements in electric drive and diesel low speed the unit setpoint was set equal to the chamber temperature of 22 °C. For the measurements in diesel high speed the unit setpoint was set to 0 °C to evoke high engine speed.

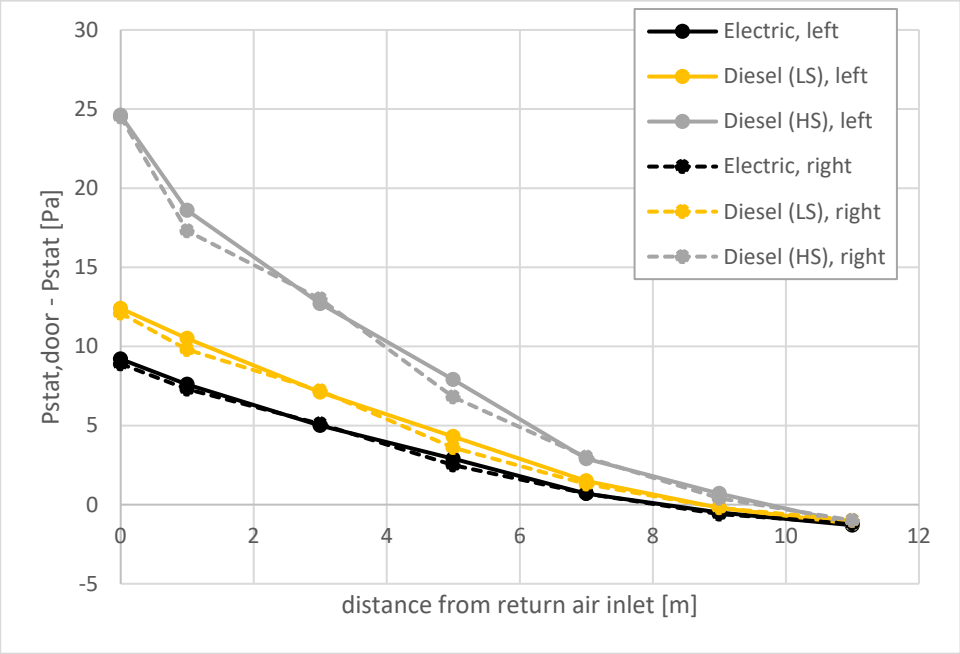

Figure 30 ***Configuration 1 (reference), static pressure difference between door-end and left (solid line), respectively right (dashed line) centre of pallet openings. Markers represent the measurements.***

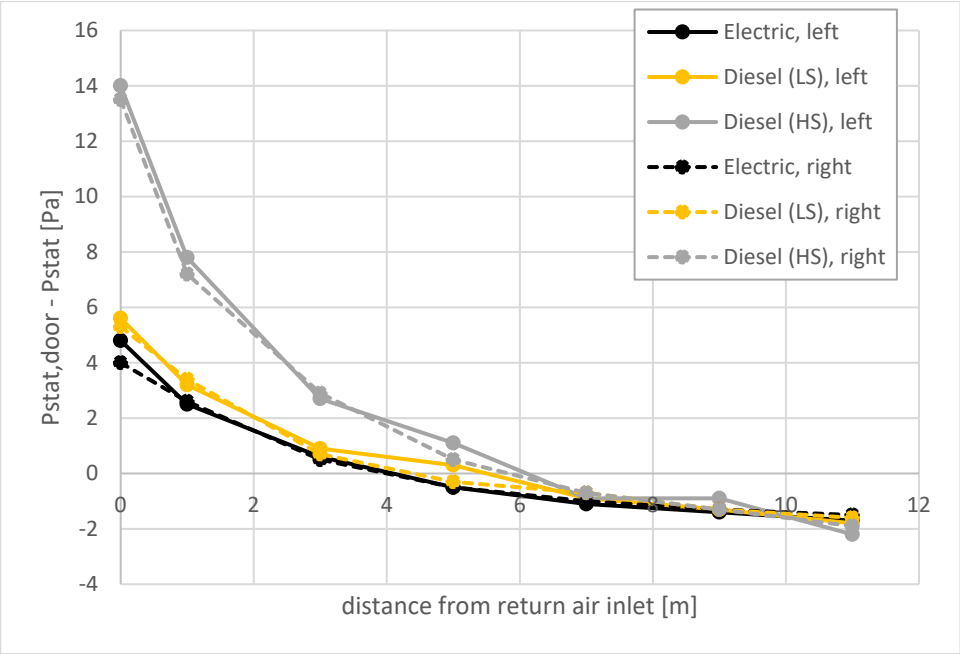

Figure 31 ***Configuration 2 (no air chute), static pressure difference between door-end and left (solid line), respectively right (dashed line) centre of pallet openings. Markers represent the measurements.***

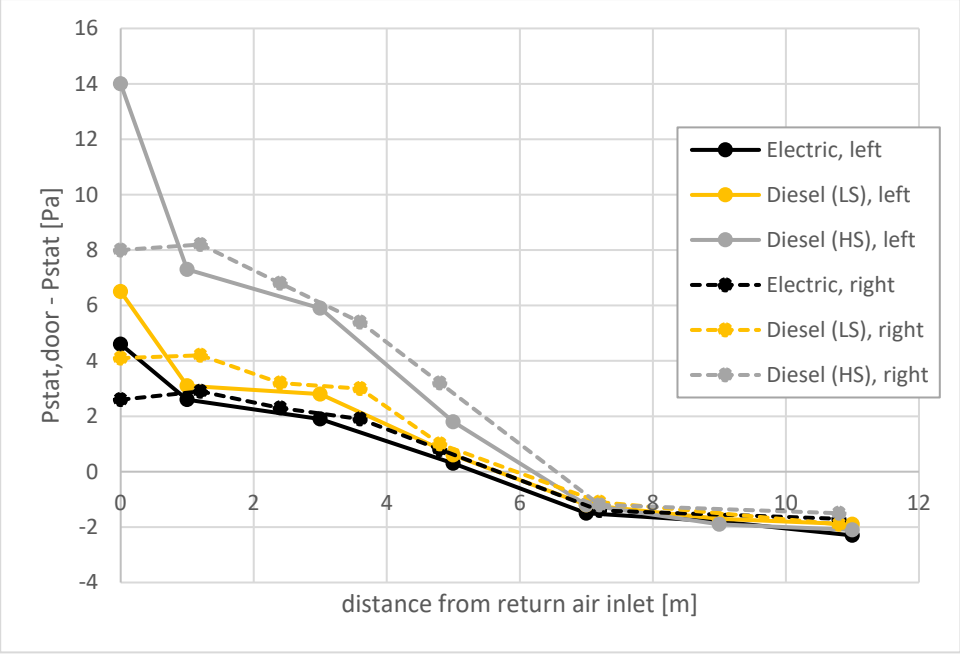

Figure 32 ***Configuration 3 (23 pallets), static pressure difference between door-end and left (solid line), respectively right (dashed line) centre of pallet openings. Markers represent the measurements.***

The tables in annex 3 (p. 59) contain the precise measurement data visualised in this section's Fig. 30 till Fig. 32.

For all combinations of configuration and evaporator fan speed also the air velocity was measured with anemometers in the locations of blue dots and triangles in Fig. 25 till Fig. 28. The measurement results are shown in Fig. 33 till Fig. 38 below. During the measurements the container doors were closed. The measurement was repeated three times consecutively: for electric drive, diesel low engine speed (LS), and diesel high engine speed (HS). For the measurements in electric drive and diesel low speed the unit setpoint was set equal to the chamber temperature of 22 °C. For the measurements in diesel high speed the unit setpoint was set to 0 °C to evoke high engine speed.

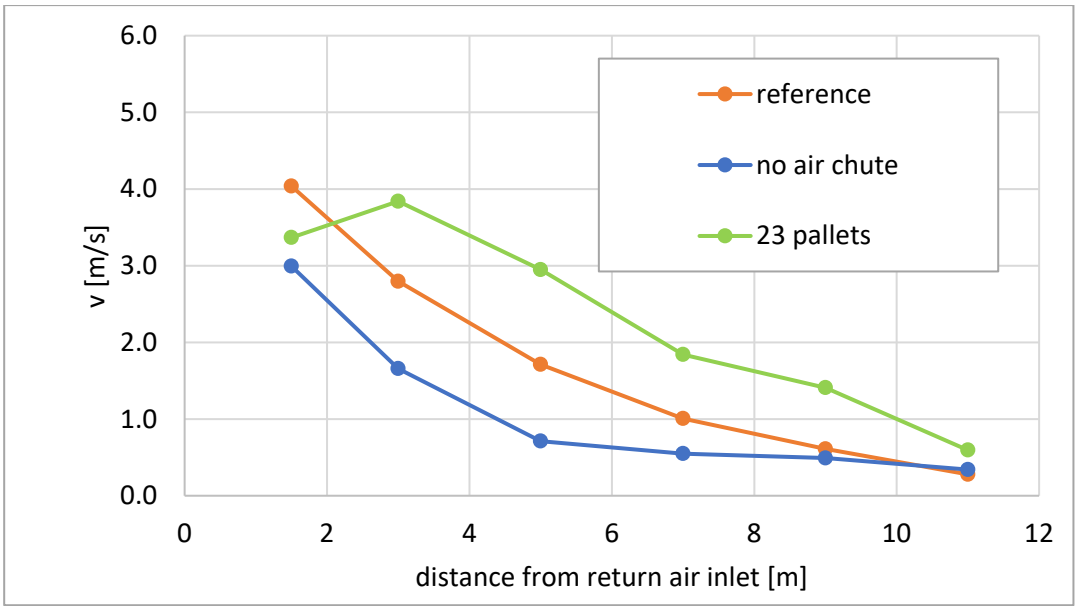

Figure 33 ***Air velocities measured above cargo (blue triangles in Fig. 24 till Fig. 27) in electric drive. Markers indicate measurements.***

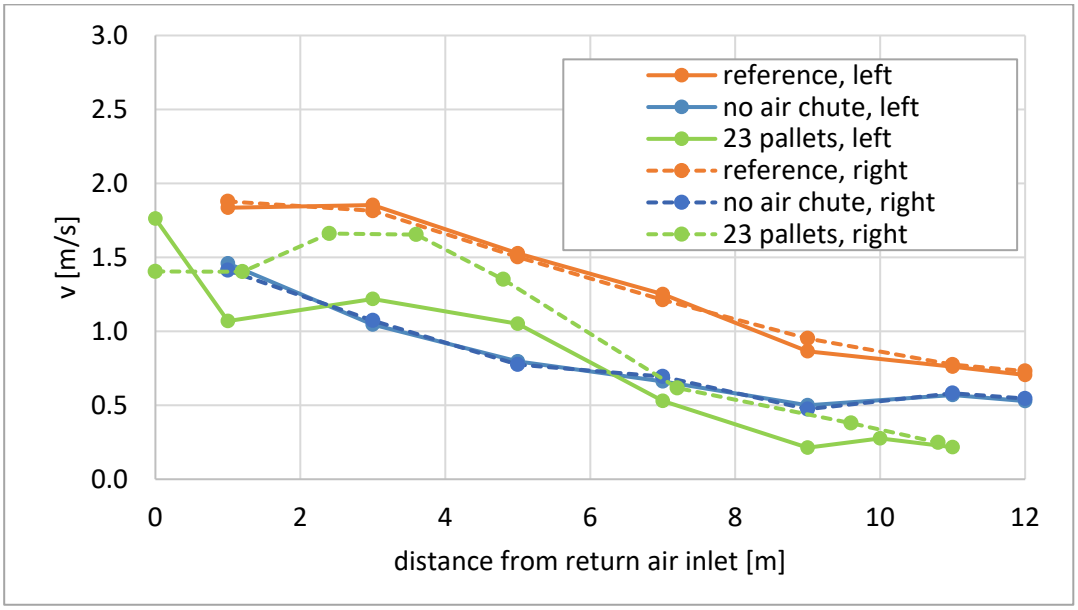

Figure 34 ***Air velocities measured in centre of pallet openings (blue dots in Fig. 24 till Fig. 27) in electric drive. Markers indicate measurements.***

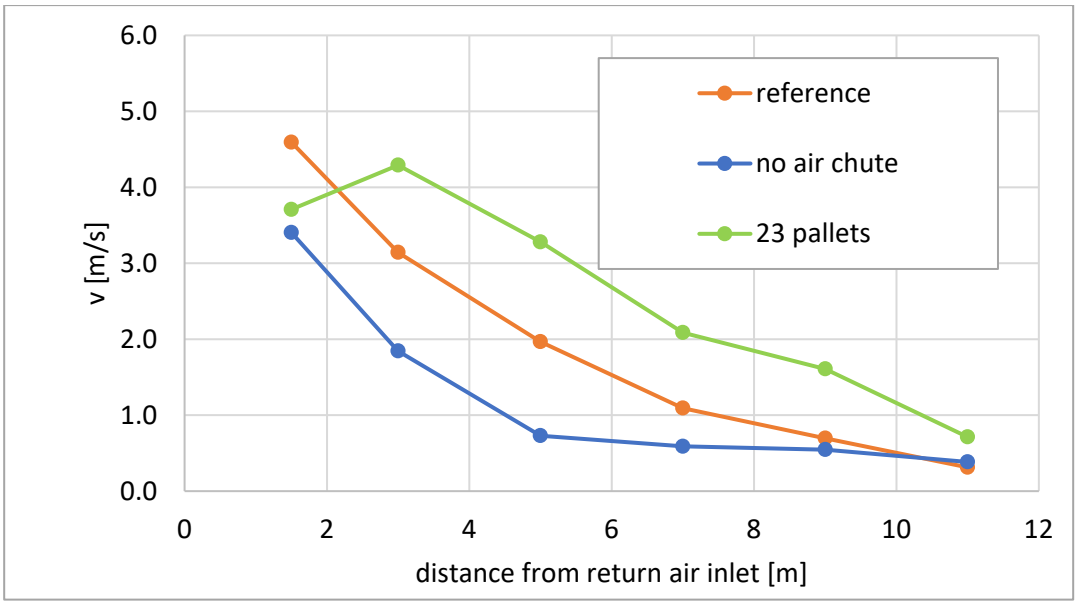

Figure 35 ***Air velocities measured above cargo (blue triangles in Fig. 25 till Fig. 28) in diesel (Low Speed engine) drive. Markers indicate measurements.***

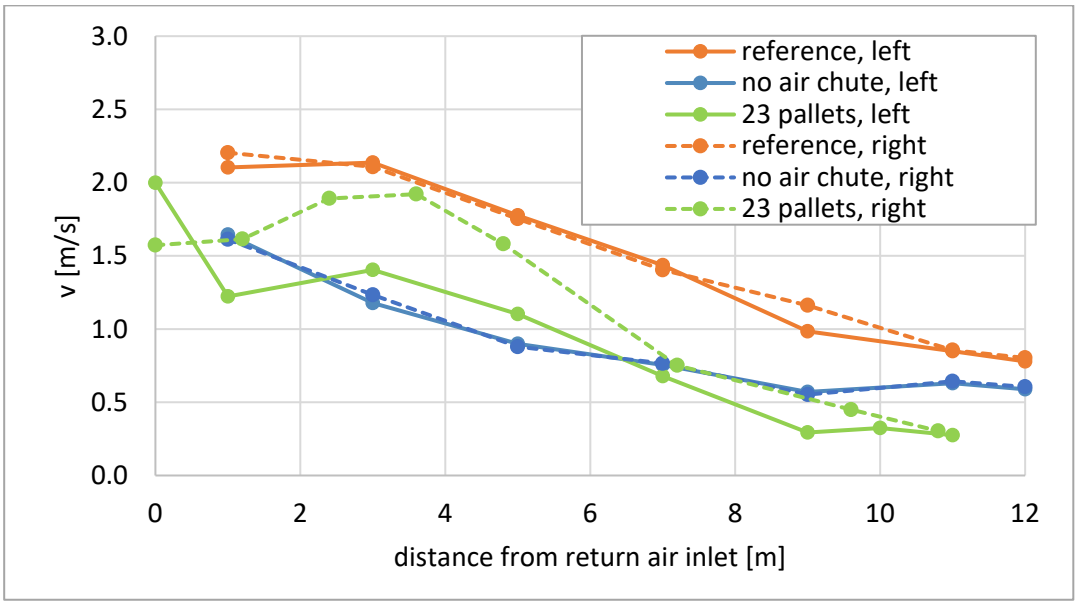

Figure 36 ***Air velocities measured in centre of pallet openings (blue dots in Fig. 25 till Fig. 28) in diesel (Low Speed engine) drive. Markers indicate measurements.***

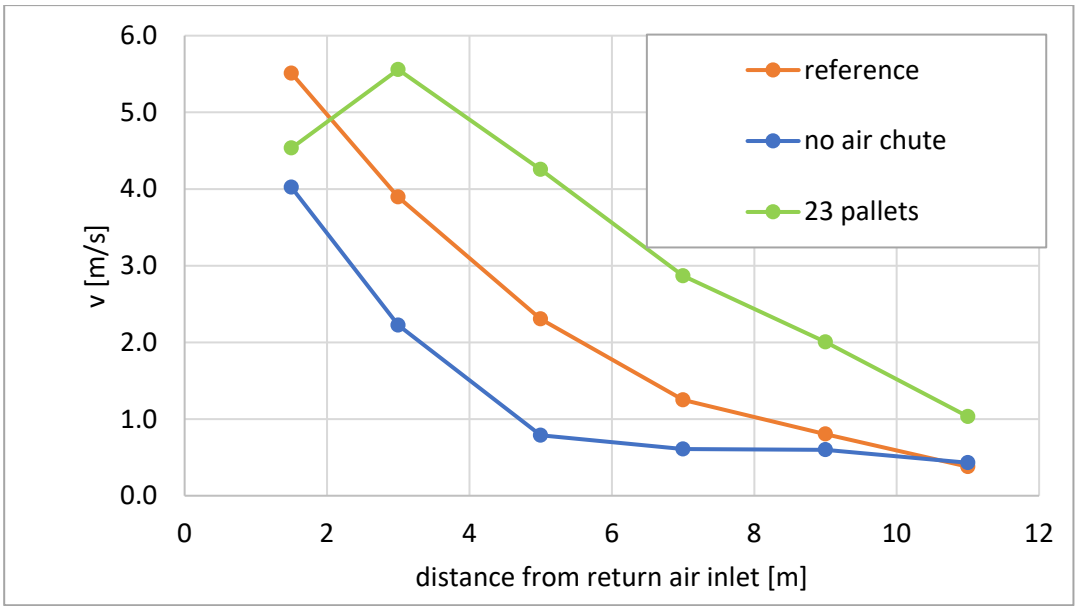

Figure 37 ***Air velocities measured above cargo (blue triangles in Fig. 25 till Fig. 28) in diesel (High Speed engine) drive. Markers indicate measurements.***

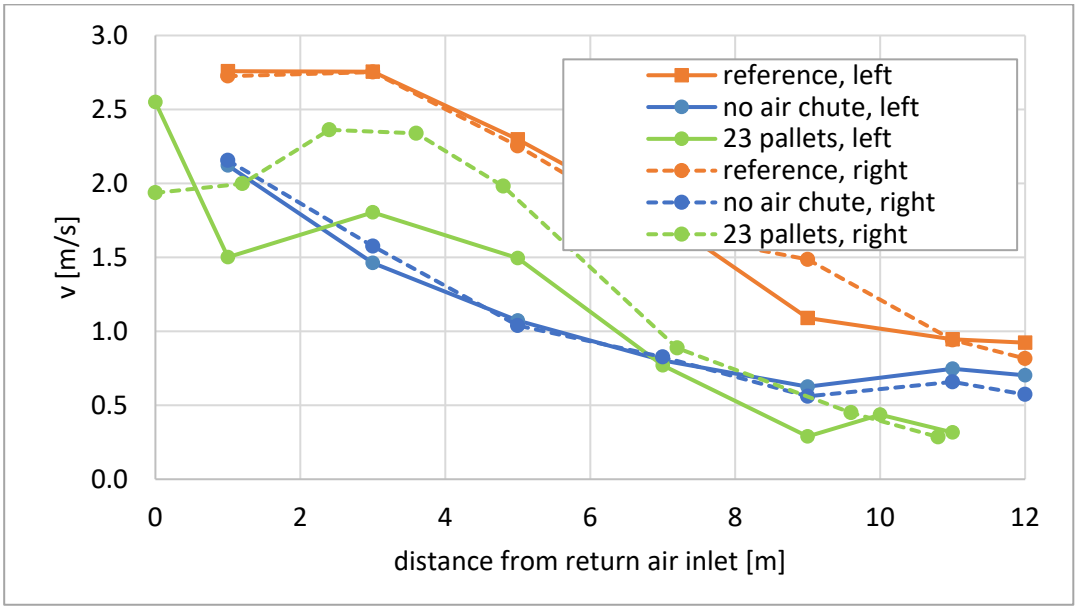

Figure 38 ***Air velocities measured in centre of pallet openings (blue dots in Fig. 25 till Fig. 28) in diesel (High Speed engine) drive. Markers indicate measurements.***

Table 20 till Table 28 in annex 4 (p. 61) contain the precise air velocity measurement data visualised in this section's Fig. 33 till Fig. 38.

At up to seven positions in the air slit between pallet load and container wall the air velocity was measured in both horizontal and vertical direction (blue squares in Fig. 25 till Fig. 28).The measurement was done simultaneously with the other air velocity measurements reported in Fig. 33 till Fig. 38. The measured values are reported in Table 29 till Table 31 (Annex 4, p. 63). Note that the direction of the measured horizontal air velocities is presumably towards the unit.

5.4 Temperature mapping

Table 11 presents the steady state temperatures measured in the different test conditions. Column 1 till 5 repeat Table 6, and have been explained there. Column 6 lists the duration of the steady state. All temperatures reported in Table 11 are time-averaged readings over the mentioned steady state period. Column 7 (coldest cargo temperature) reports the coldest temperature recorded by any of the

sensors taped to the cartons. Column 8 (coldest cargo temperature sensor) indicates which sensor was the coldest. Column 9 (warmest cargo temperature) reports the highest temperature recorded by any of the sensors taped to the cartons. Column 10 (warmest cargo temperature sensor) indicates which sensor was the warmest. Column 11 (warmest – coldest cargo temp.) reports the highest minus the lowest temperature recorded by the sensors taped to the cartons. Column 12 is the return air temperature, taken as the average of the time-averaged readings of sensors sn266, sn269 and sn274 mounted at the entry of the return air duct (see Fig. 24). Column 13 is the supply air temperature, taken as the average of the time-averaged readings of sensors sn267 and sn303, mounted right in front of at the unit's supply air outlet (see Fig. 24). Column 14 reports the absolute value of difference T_{ret}-T_{sup}. Finally the last column contains the ratio TDF, (warmest – coldest cargo temp.) / abs(T_{ret}-T_{sup}), as explained in eqn. 3 on p. 8.

Probably the last two columns are the most interesting: when is $T_{ret} - T_{sup}$ largest (worst)? And what is then the ratio TDF? The results are discussed in further detail in section 6.4.

Just as an illustration the recorded steady state temperatures for a few tests are shown in Fig. 43 (p. 42) till Fig. 47 (p. 44) in Annex 1.

Table 11 Steady state temperatures observed during tests.

1. Tset / T_{amb} [°C]	2. test	3. Run mode	4. Method of drive	5. Configuration	6. steady state duration [h:mm]	7. coldest cargo temperature [°C]	8. coldest cargo temperature sensor	9. warmest cargo temperature [°C]	10. warmest cargo temperature sensor	11. warmest - coldest cargo temperature [°C]	12. T_{ret} [°C]	13. T_{sup} [°C]	14. abs(T_{ret}-T_{sup}) [°C]	15. (Twarmest - Tcoldest) / abs(T_{ret} - T_{sup})
6 / -15 [°C]	8	Continuous	Diesel	1 (reference)	16:30	3.0	sn255	6.6	sn300	3.6	4.7	6.5	1.8	2.0
6 / -19 [°C]	9	Continuous	Diesel	1 (reference)	08:00	2.5	sn255	6.8	sn300	4.3	4.5	6.8	2.3	1.9
22 / -17 [°C]	11	Continuous	Diesel	1 (reference)	12:30	16.7	sn255	23.4	sn300	6.7	19.1	23.6	4.5	1.5
22 / -17 [°C]	17	Cycle-Sentry	Diesel	1 (reference)	12:00	12.5	ATP4	21.4	sn300	9.0	15.6	22.1	6.5	1.4
18 / 40 [°C]	20	Continuous	Electric	1 (reference)	13:40	17.6	sn283	23.0	ATP11	5.3	20.1	17.3	2.8	1.9
18 / 40 [°C]	21	Cycle-Sentry	Electric	1 (reference)	12:00	18.9	sn300	30.3	sn271	11.4	22.9	15.7	7.1	1.6
18 / 45 [°C]	22	Continuous	Electric	1 (reference)	13:16	17.4	sn283	24.2	ATP11	6.7	20.5	16.6	3.9	1.7
4 / 40 [°C]	25	Continuous	Electric	1 (reference)	12:00	3.2	sn283	12.0	sn255	8.8	7.0	2.3	4.6	1.9
4 / 40 [°C]	25B	Continuous	Diesel	1 (reference)	12:00	3.2	sn283	11.0	ATP11	7.7	6.6	2.3	4.3	1.8
4 / 30 [°C]	25C	Continuous	Electric	1 (reference)	12:04	3.6	sn283	10.0	sn255	6.4	6.5	3.0	3.5	1.8
4 / 30 [°C]	25D	Continuous	Diesel	1 (reference)	10:20	3.7	sn283	9.7	sn255	6.0	6.4	3.0	3.4	1.8
4 / 40 [°C]	33	Continuous	Electric	2 (no air chute)	03:27	4.0	sn283	23.6	sn292	19.5	7.3	3.1	4.2	4.7
4 / 40 [°C]	38	Continuous	Electric	3 (23 pallets)	12:00	3.3	sn283	15.6	ATP11	12.3	6.2	1.8	4.4	2.8

A note on the T_{sup} values in test 25 and further: during the data analysis peculiar values for time-average T_{sup} values were noticed. Analysis showed that this was due to the set 10 minutes log interval of the LogTag recorders in combination with an oscillating T_{sup} with 5 minutes period time. Fortunately, the unit's own T_{sup} recording is available at a 1 minute log interval, and it corresponds perfectly with the WFBR loggings in all preceding tests. Therefore, it was decided to show the unit's time-averaged T_{sup} readings for tests 25 and further in Table 11.

Pull down and pull up tests (Table 7) and power off / door opening / recovery tests (Table 8) are reported in temperature graphs without further comments (Fig. 48 till Fig. 58 in annex 1, p. 45).

5.5 Inner surface temperatures

Table 12 till Table 14 present the measurements of the inner surface temperature T_{si} of the walls. In these tables column 1 describes the position of the inner surface temperature sensors. Column 2 and column 3 give the identification number of respectively the wall sensor and the nearby cargo sensor. Column 4 and column 5 give the temperature recorded by the wall sensor and the nearby cargo sensor. Finally, for ease of comparison, the last column contains the difference between the wall surface temperature T_{si} and the nearby cargo temperature T_{cargo}.

Table 12 Steady state temperatures during test 38 (see Table 6 for test conditions).

Position	Wall sensor no.	Nearby cargo sensor no.	T_{si} [°C]	T_{cargo} [°C]	T_{si} - T_{cargo} [°C]
Wall: left side wall, 30 cm above floor	Ch1	sn268	15.6	14.3	1.3
Corner: left side wall, 10 cm from door, 10 cm from roof	Ch2	ATP9	20.1	15.6	**4.5**
Ceiling: 40 cm from side wall	Ch3	sn271	15.8	14.7	1.1
Door: left door, half height, 80 cm from side wall	Ch4	sn294	20.0	14.7	**5.3**

Table 13 Steady state temperatures 1 hour after start of test 39 (12 h power off), i.e. at 21-7-2020 10:10. See Table 8 for test conditions.

Position	Wall sensor no.	Nearby cargo sensor no.	T_{si} [°C]	T_{cargo} [°C]	T_{si} - T_{cargo} [°C]
Wall: left side wall, 30 cm above floor	Ch1	sn268	16.0	14.7	1.3
Corner: left side wall, 10 cm from door, 10 cm from roof	Ch2	ATP9	20.4	15.6	**4.8**
Ceiling: 40 cm from side wall	Ch3	sn271	16.6	15.7	0.9
Door: left door, half height, 80 cm from side wall	Ch4	sn294	20.3	14.9	**5.4**

Table 14 Steady state temperatures 6 hours after start of test 39 (12 h power off), i.e. at 21-7-2020 15:10. See Table 8 for test conditions.

Position	Wall sensor no.	Nearby cargo sensor no.	T_{si} [°C]	T_{cargo} [°C]	T_{si} - T_{cargo} [°C]
Wall: left side wall, 30 cm above floor	Ch1	sn268	25.5	24.5	1.0
Corner: left side wall, 10 cm from door, 10 cm from roof	Ch2	ATP9	29.9	25.8	**4.1**
Ceiling: 40 cm from side wall	Ch3	sn271	26	25.9	0.1
Door: left door, half height, 80 cm from side wall	Ch4	sn294	30.3	24.3	**6.0**

6 Discussion

6.1 K-value

How to appreciate the measured K-value of 0.474 W/m^2.°C? A slightly further analysis was done. The K-value was calculated. In the calculation the measured wall thicknesses were used (section 3.1.1). Based on that the thicknesses of the insulation in all panels were estimated using assumed thickness for claddings and reinforcements, while the insulation material's heat conduction coefficient was assumed to be 0.024 W/m.K. The K-value calculated in this way was 0.346 W/m^2.°C. The measured K-value is 37% worse than the calculated one. The container was six years old at the time of measurement. With an assumed ageing of 5% per year after 6 years the insulation would have increased by a factor $(1.05)^6 = 1.34$, i.e. a 34% gap between measurement and calculation could be explained by 5% ageing per year. As Lawton et al. (2019) illustrate the number of 5% ageing per year is a bit pessimistic, but not unrealistic. All in all the measured K-value of 0.474 W/m^2.°C for this six years old container is a little worse than expected based on measured panel thicknesses and six years of ageing.

Table 15 K-value analysis

Variable	Value
Measured K-value (section 5.1)	0.474 W/m^2.°C
Calculated K-value	0.346 W/m^2.°C
$K_{measured}$ / $K_{calculated}$	1.37
Manufacturing date	2014
Aging (5%) loss factor	1.34

6.2 Supply air flow rate

Table 16 repeats the results presented in Table 10, with added to that the manufacturer specs. The manufacture spec reported in Table 16 is the air flow rate measured at a static pressure drop of 0 Pa.

Table 16 Supply air flow rate measurement and manufacturer spec. (source: ATP test report)

Evaporator fan speed situation	measured φ_{air} [m^3/h]	Manufacturer spec. φ_{air} [m^3/h]	Difference [%]
electric drive	2867	2250	27%
low engine speed diesel drive	3162	2400	32%
high engine speed diesel drive	4207	3300	27%

The measurement procedure is not very accurate. Yet it is remarkable to see a measurement of around 30% more than manufacturer spec in all three situations.

6.3 Air velocities and static pressure differences

It is to be expected that measured air velocities in the pallet openings decrease when the distance from the return air inlet increases. However, this is not the case in the first four meters in configuration '23 pallets' (Fig. 34, Fig. 36, Fig. 38). Without exactly understanding the mechanism involved, this must somehow relate to the 12 cm gap between walls and cargo in configuration '23 pallets'.
Fig. 34, Fig. 36 and Fig. 38 present measured air velocities in the left and right pallet openings. In the configuration with 23 pallets the pallet openings also differ between left and right. For a comparison

between left and right in that configuration it is therefore better to compare the calculated left and right air flow rates. This is calculated as

$$air\ flow\ rate\ = \frac{1}{3600} \times velocity\ \times area \qquad [m3/h] \quad (4)$$

Note that this calculation assumes an equal air velocity everywhere in the pallet opening. The figure below presents this calculated flow rate. Looking at air flow rate instead of velocities basically enlarges the left-right difference in the configuration with 23 pallets, because pallet openings at the 1 meter side are larger than at the 1.2 meter side of pallets (Table 3).

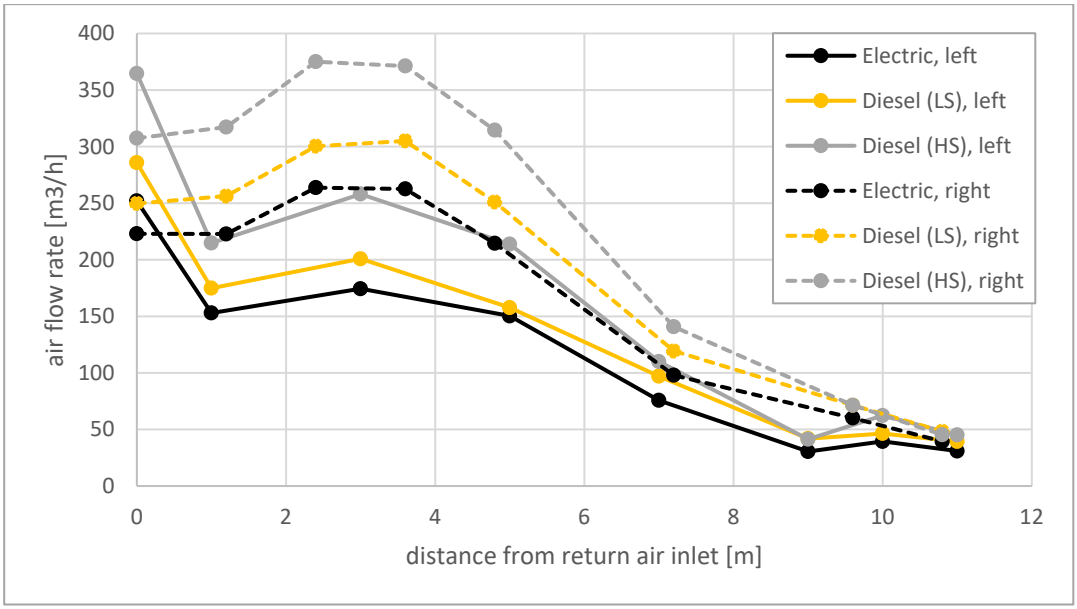

Figure 39 Calculated air flow rates in left (solid line) and right (dashed line) centre of pallet openings (blue dots in Fig. 25 till Fig. 28) for configuration'23 pallets'. The markers represent the air velocity measurement locations.

6.4 Temperature mapping

6.4.1 General temperature distribution patterns

For each steady state test a 3D contour plot of temperature distribution is included in annex 2 (p. 51). In heating mode (winter conditions) the coldest temperatures occur at the floor near the door-end (see e.g. Fig. 59 on p. 51). In cooling mode (summer conditions) the highest temperatures occur at the door-end, where the temperature gradient in vertical direction is limited (Fig. 66 on p. 55).

6.4.2 Maximal cargo temperature difference ΔT_{cargo}

Column 11 in Table 11 shows that the maximal temperature difference in the container exceeds the maximally acceptable 3°C by far in all steady state tested. Let's first analyze the heating and cooling mode for the situation which is most relevant to practice: method of drive = diesel, run mode = continuous, and configuration = reference. In heating mode (test 11, T_{set} / T_{amb} = 22 / -17 °C) ΔT_{cargo} = 6.7 °C. In cooling mode (test 25B, T_{set} / T_{amb} = 4 / 40 °C) ΔT_{cargo} = 7.7 °C. This is much worse than the desired situation of ΔT_{cargo} < 3 °C.
The four tests with biggest ΔT_{cargo} are the two tests with cycle-sentry operation and the tests for configuration 2 (no air chute) and 3 (23 pallets).

6.4.3 ΔT_{cargo} in heating mode vs. cooling mode

When is the temperature distribution worse, in heating or cooling mode? In cooling mode, though the difference is limited. Compare e.g. test 11 (heating mode) to test 25B (cooling mode). The only

difference is T_{set} / T_{amb}: T_{set} / T_{amb} = 22 / -17 °C in test 11, and 4/ 40 °C in test 25B. ΔT_{cargo} (6.7 °C vs. 7.7 °C) is a little larger in the cooling mode test 25B.
The explanation lies in the effect of top-air delivery in combination with natural convection (warm air is lighter and therefore rises up, cold air is heavier and therefore falls down). It is always a challenge to carry enough air to the door-end, but in systems with top-air delivery the cooling mode is most challenging. Towards the door-end the air velocity reduces, but in heating mode natural convection supports the forced air convection by making the warm supply air stay on top and proceed towards the door-end (Fig. 40). In cooling mode when the cold supply air loses velocity on its way towards the door-end natural convection tends to make the cold supply air fall down before reaching the door-end, resulting in a secondary warmer vortex towards the door-end (Fig. 41). If the forced air convection is weak due to limited amounts of air reaching the door-end the effect can be surprisingly large. The effect is also a little bit visible in the 3D contour plots in annex 2: in heating mode the isotherms are nearly horizontal (e.g. Fig. 61 on p. 52 for test 11), while in cooling mode the isotherms tend to be more vertical towards the door-end (e.g. Fig. 67 on p. 55 for test 25B).

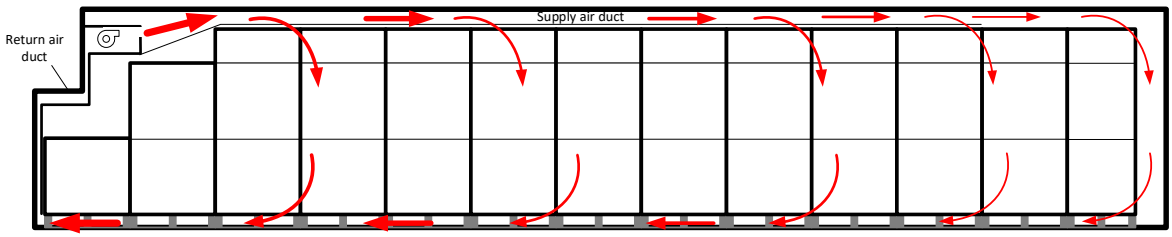

Figure 40 ***Assumed air circulation pattern in heating mode (thicker arrows indicate higher air velocities).***

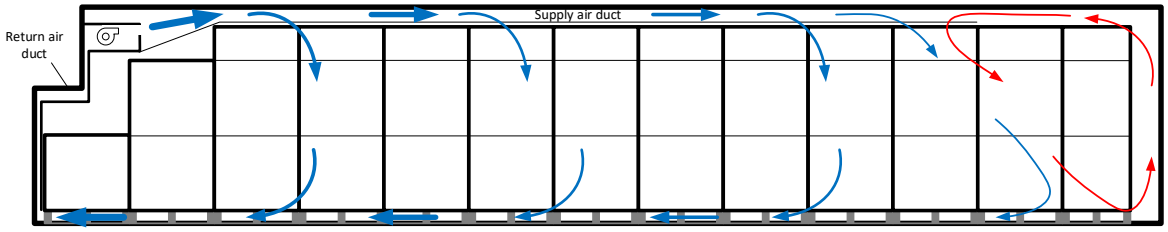

Figure 41 ***Assumed air circulation pattern in cooling mode (thicker arrows indicate higher air velocities).***

6.4.4 Effect of supply air duct

Does the supply air duct improve temperature uniformity? Yes. To assess the effect of the supply air duct mutually compare test 25 and 33. In both tests T_{set} / T_{amb} = 4 / 40 °C, method of drive = electric and run mode = continuous. The only difference is the supply air duct: present in test 25 (configuration 1) and not present in test 33 (configuration 2). Column 11 in Table 11 shows the effect: with air chute ΔT_{cargo} = 8.8 °C in test 25, after removing the air chute ΔT_{cargo} = 19.5 °C in test 33. The worst temperatures occur in the door-end area. Also compare Fig. 70 (configuration 1) on p. 57 to Fig. 66 (configuration 2) on p. 55.
Clearly this supply air duct contributes significantly to making the temperatures more uniform. Probably the effect is so big because the cargo, apart from pallet 1 till 4, reaches higher than the supply air outlet (Fig. 41). Without supply air duct the supply air clashes against pallet 5 and 6. The supply air duct gently guides most supply air to the space above pallets 5 till 26. Note that this is in a test with airtight cargo and only a 2 cm air slit between cargo and side walls. So the cargo itself creates kind of an air duct between top of cargo and ceiling. Many cargos will have less resistance against vertical air flow through or along the cargo. In those situations expect an even stronger positive effect of the air chute.
Also note that even with this supply air duct (test 25) the highest temperatures occur at the door-end. This indicates that the shape of this supply air duct can be optimized, such that it directs a larger share of the supply air towards the door-end, which should improve temperature uniformity.

6.4.5 Effect of distance between cargo and walls (23 or 26 pallets)

Does temperature uniformity improve when the distance between cargo and wall increases from 2 to 12 cm improve? No. In configuration 3 the distance between cargo and side walls is 12 cm. In the reference configuration (configuration 1) the distance between cargo and side walls is only 2 cm. Because the cartons are not 100% straight this very small air slit is in fact 0 cm in some locations and maybe 4 cm in other locations. To assess the effect of the increased width of the air slit between cargo and walls compare test 25 and 38. In both tests T_{set} / T_{amb} = 4 / 40 °C, method of drive = electric and run mode = continuous. The only difference is the distance between cargo and walls: 2 cm in test 25 and 12 cm in test 38. Column 11 in Table 11 shows the effect: ΔT_{cargo} = 8.8 °C in test 25, after increasing the air slit from 2 to 12 cm ΔT_{cargo} = 12.3 °C in test 38. As in all test conditions, the worst temperatures occur in the door-end area. Also compare Fig. 66 on p. 55 (configuration 1) to Fig. 72 on p. 58 (configuration 3).
Apparently increasing the distance between cargo and wall from 2 to 12 cm adversely affects the door-end temperatures, and hence temperature uniformity. Why? Lots of supply air escapes from the supply air duct to the sides. Then a narrower slit between cargo and walls inhibits vertical air flow between cargo and walls and hence supports the carriage of some of this 'escaped' air further towards the doors. Increasing the spacing between walls and cargo enables more air flow between walls and cargo and should hence yield cargo temperatures closer to setpoint in the regions near the walls. This positive effect is visible in the first meters (unit-end temperatures in Fig. 72 are closer to set point than in Fig. 66). However, the downside outweighs this upside: even less air reaches the door-end, resulting in even higher door-end temperatures. This explanation corresponds with the observed slight decrease of ΔT_{unit} from 4.6 °C in test 25 to 4.4 °C in test 38: in test 38 the cargo has less air flow resistance therefore the airflow rate increases and hence ΔT_{unit} decreases. In test 38 ΔT_{cargo} is larger and ΔT_{unit} is smaller than in test 25. This of course results in a significantly increased TDF: from 1.9 in test 25 to 2.8 in test 38.
This observation illustrates the complexity of air flow distribution problems: the narrower 2 cm slit outperforms the wider 12 cm slit. Yet an air slit of 0 cm is not recommendable. If the air slit between cargo and walls was 0 cm along the complete side walls the cargo would be in direct touch with the wall and cargo temperatures against the wall would rise.

6.4.6 Air flow distribution

Could a better air flow distribution improve temperature uniformity? Yes, even in the reference configuration. In all tests for the reference configuration and continuous run the ratio TDF, i.e. ΔT_{cargo} / $|\Delta T_{unit}|$, is between 1.5 and 2.0, which is significantly higher than the optimal situation of TDF =1 (section 2). The observed large ratio TDF corresponds with the very low air flow rate at the door-end observed during measurement of air velocities (section 5.3).

6.4.7 Return air temperature control

It looks like the unit uses return air temperature control. That is probably why for all cooling tests at T_{set} = 4 °C the average T_{sup} is between 1.8 and 3.1 °C. Return air temperature control causes cargo temperatures below setpoint. How much below setpoint is uncertain, because it depends on heat load. Therefore return air temperature control is a recipe for freezing injury in chilled range (T_{set} > -10 °C). It is a good common practice in marine containers in chilled range (T_{set} > -10 °C) and cooling mode to use supply air temperature control, as opposed to return air temperature control. Supply air temperature control yields tight control over the coldest cargo temperatures, avoids cargo temperatures colder than setpoint, and hence reduces the risk of freezing injury. Also for chilled range cargo in this 45ft container supply air temperature control would be preferable in cooling mode.

6.4.8 Effect of method of drive

When are the temperatures more uniform: in diesel drive or in electric drive? In diesel drive. Compare e.g. cooling mode test 25 to test 25B. The only difference between these two tests is the method of drive. By switching to diesel drive ΔT_{cargo} improves from 8.8 °C in test 25 to 7.7 °C in test 25B. This matches with the observed higher airflow rate in diesel drive, also at low engine speed (Table 10 on p. 24).

6.4.9 Effect of run mode

When are the temperatures more uniform: in continuous run mode or in cycle-sentry run mode? In continuous run mode. However, in the tested conditions the difference is limited. Compare e.g. heating mode test 11 to test 17. The only difference is run mode. By switching to cycle-sentry run mode ΔT_{cargo} deteriorates from 6.7 °C in test 11 to 9.0 °C in test 17. Also the oscillations in instantaneous T_{sup} during cycle-sentry run mode are reasonably limited to 4 °C (see the two coldest temperatures in Fig. 45 on p. 43).

6.5 Inner surface temperatures

For four positions at the door-end of the container Table 12 shows the inner surface temperature T_{si} of the walls and the nearby cargo temperature T_{cargo} during the steady state situation of test 38. The cargo temperatures in the four positions are all about 15 °C. The difference T_{si} - T_{cargo} is about 1°C for the side wall and ceiling, and about 5°C in the corner and at the door. The larger difference in T_{si} - T_{cargo} in the corner and at the door can be caused by three local factors: 1) diminished air flow velocity, 2) less insulation, or 3) the simple fact that the distance between wall and cargo is a bit larger in those two positions.

Let's analyse what determines $T_{si} - T_{cargo}$. The heat flow resistance from outside to inside the container can be viewed as a series connection of three resistances (schematically presented in Fig. 42):

1. Heat transfer from ambient air to the external wall surface through a boundary layer of air ($\frac{1}{\alpha_{ext}}$. in Fig. 42)
2. Heat conduction through the multiple layers in the wall ($\sum_{i=1}^{n} \frac{d_i}{\lambda_i}$ in Fig. 42), dominated by the layer of insulation material with large thickness d_i and low heat conduction coefficient λ_i.
3. Heat transfer from the internal wall surface to the air inside the container through a boundary layer of air ($\frac{1}{\alpha_{int}}$. in Fig. 42)

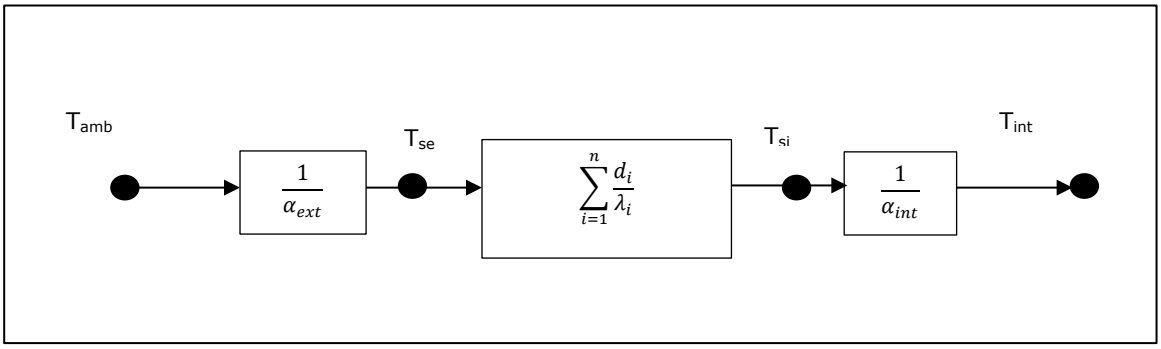

Figure 42 Schematic representation of heat flow through container wall.

During test 38 T_{amb} = 40 °C and internal temperature T_{int} near the door-end is around 15 °C. In a heavily insulated container the heat flow resistance of the walls ($\sum_{i=1}^{n} \frac{d_i}{\lambda_i}$ in Fig. 42) is far larger than the two other heat transfer resistances. Therefore external surface temperature T_{se} is usually close to T_{amb}, and internal surface temperature T_{si} is usually close to T_{int}, while the main temperature gradient occurs over the wall ($T_{se} - T_{si}$). The heat transfer resistances $\frac{1}{\alpha_{ext}}$ and $\frac{1}{\alpha_{int}}$ depend on air movement around the wall surface: the less air movement the bigger the heat transfer resistance. Hence there are two ways to reduce the difference $T_{si} - T_{int}$:

1. Increase internal air flow along the wall surface to decrease $\frac{1}{\alpha_{int}}$.
2. Increase the wall insulation, i.e. increase $\sum_{i=1}^{n} \frac{d_i}{\lambda_i}$.

Stopping the air circulation in the container stops the internal air movement and hence should increase $\frac{1}{\alpha_{int}}$, as explained above. However, after 1 hour power off not much has changed (Table 13) as compared to the steady state condition with running evaporator fans (Table 12). This means that the air flow velocity in all four measurement positions is not affected by the evaporator fans, hence very low, and hence air flow velocity cannot be the factor explaining the larger difference in T_{si} - T_{cargo}

in the corner and at the door. This leaves two options open: 1) less insulation, or 2) the simple fact that the distance between wall and cargo is a bit larger in those two positions.
In view of the preceding background information the mutual differences between the four positions in Table 12 are a surprise. As mentioned in section 3.1.1 in this container the roof (155 mm) is thicker than the doors (75 mm), which are thicker than the walls (55 mm). In the door-end area the air movement is small, let us assume it is equal in all measurement locations in Table 12. Then it is to be expected that in steady state $T_{si} - T_{int}$ (called T_{cargo} in Table 12) at the roof (Ch3 in Table 12) is smaller than at the doors (Ch4 in Table 12), which in turn is smaller than at the walls (Ch1 in Table 12). The observed $T_{si} - T_{cargo}$ for roof, doors and walls is respectively 1.1, 5.3 and 1.3 °C. Clearly, $T_{si} - T_{cargo}$ at the doors breaks the pattern. It remains to be explained what the cause is: 1) less insulation, or 2) the simple fact that the distance between wall and cargo is a bit larger in those two positions.

7 Conclusions

1. The measured K-value of 0.474 W/m^2.°C for this six years old container is a little worse than expected based on measured panel thicknesses and six years of ageing.
2. The measured supply air flow rate exceeds the manufacturer's specs by about 30%.
3. Too little supply air reaches the door-end, illustrated by a ratio TDF (warmest – coldest cargo temp.) / abs(T_{ret} – T_{sup}) which was above 1.4 for all tests.
4. The temperature differences inside the container are too large, especially in cooling mode. In cooling mode at T_{set} / T_{amb} = 4 / 40 °C, method of drive = diesel, and run mode = continuous, even in the favorable reference configuration the difference between the warmest and the coldest cargo temperature is 7.7 °C. This is worse than the desired situation of (warmest – coldest cargo temp.) < 3 °C.
5. This supply air duct contributes significantly to making the temperatures more uniform.
6. The shape of this supply air duct can be optimized, such that it directs more air towards the door-end, which should improve temperature uniformity.
7. Increasing the distance between cargo and walls from 2 to 12 cm in this container adversely affects door-end temperatures, and hence temperature uniformity.
8. In diesel drive temperatures are more uniform than in electric drive.
9. Cycle-sentry mode deteriorates temperature uniformity.
10. The three measured inner wall surface temperatures near the door-end are 1.1 till 5.3 °C warmer than the cargo temperature measured nearby.
11. A complete dataset of temperatures, air velocities, and static pressure differences has been collected. These data should suffice for accurate CFD model calibration.

Literature

ATP (2020). Agreement on the international carriage of perishable foodstuffs and the special equipment to be used for such carriage. Available from https://www.unece.org/trans/main/wp11/atp.html.

Lawton R., Rhodes C. Mynott T. (2019). Ageing of insulated marine containers. *Proc. of 25th int.'l conf. of refrigeration*, Montreal, Canada, paper ID 1695. DOI: 10.18462/iir.icr.2019.1695.

Acknowledgements

We thank all partners for their financial support and their kind cooperation in facilitating this large test series. Anthos provided the dummy load. Thermo King taught us how to operate the unit, enabled us to collect the unit data, and was always quick in assistance whenever needed. Essers kindly made its container available for many weeks of testing and participated in defining the test plan. Unit45 participated in defining the test plan.

Annex 1 Temperature graphs

Fig. 43 till Fig. 47 show the recorded temperatures during an arbitrary selection of steady state temperature tests (Table 11). The legends correspond with the naming of temperature sensors in Fig. 24 and Fig. 26. Basically the recorded temperatures are clustered in two bundles: a small bundle of three recordings outside the container, and all others inside the container. The internal recordings with the biggest fluctuation are the ones most directly exposed to the refrigeration unit's supply air flow, which is not perfectly stable.

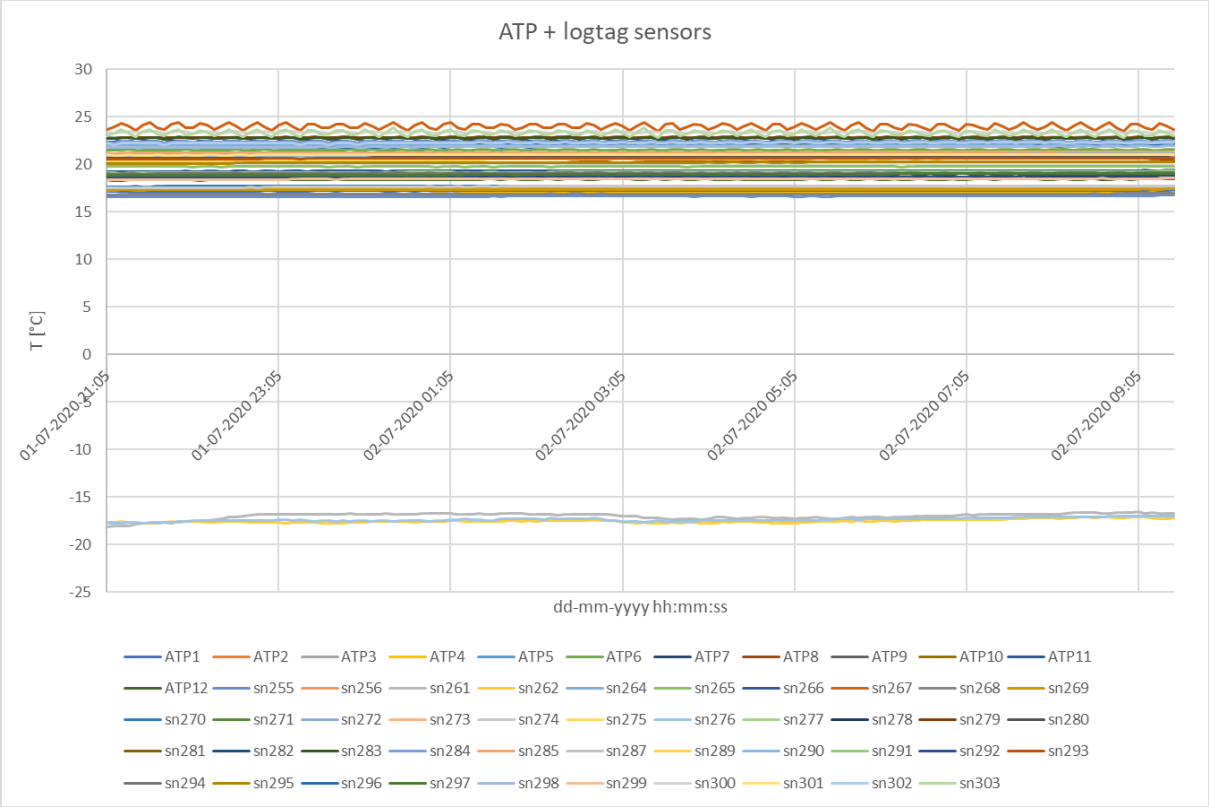

Figure 43 Recorded steady state temperatures for test 11.

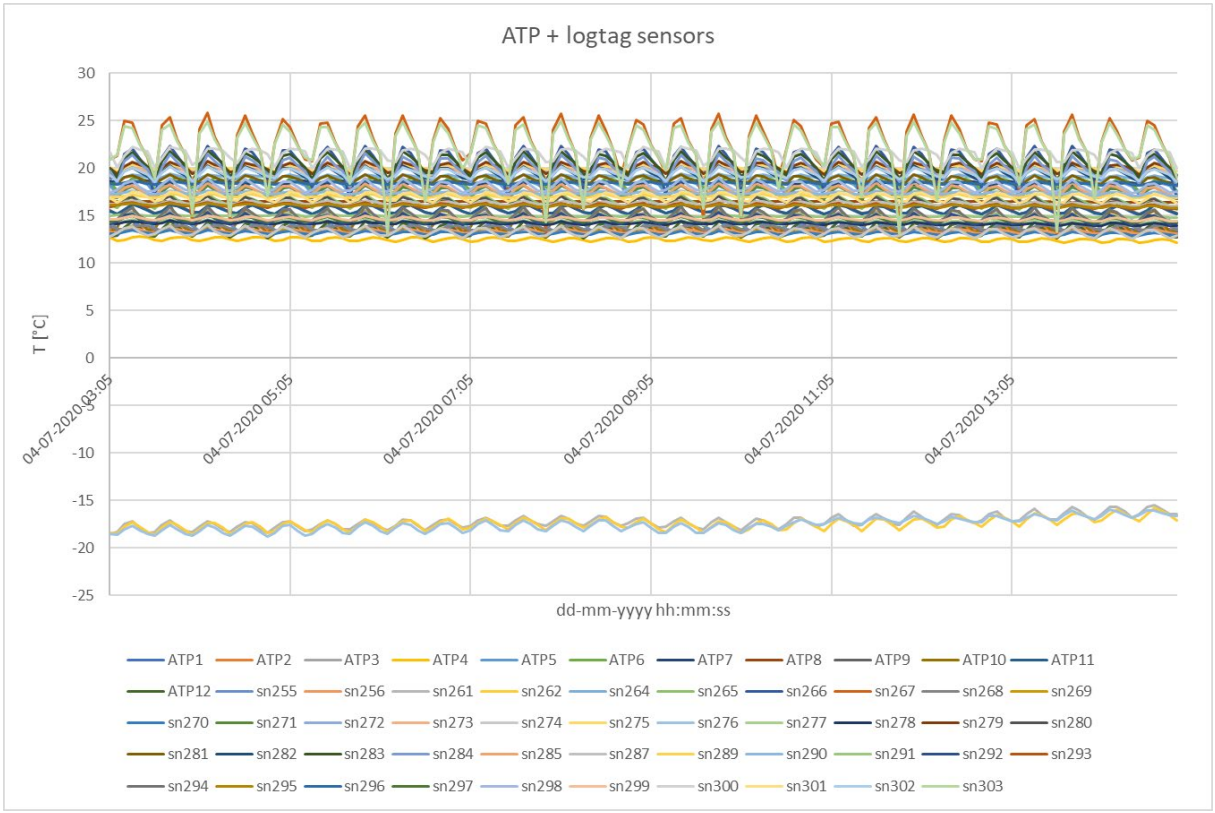

Figure 44 Recorded steady state temperatures for test 17.

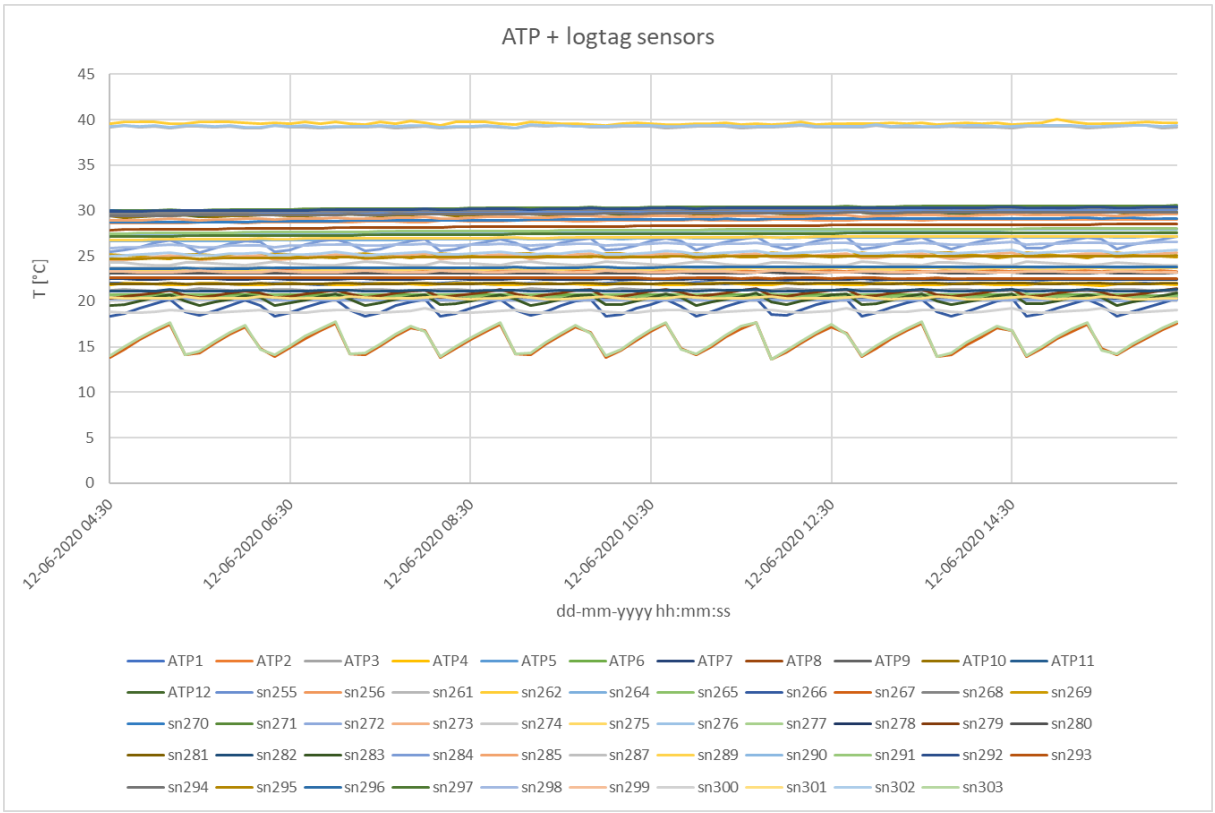

Figure 45 Recorded steady state temperatures for test 21.

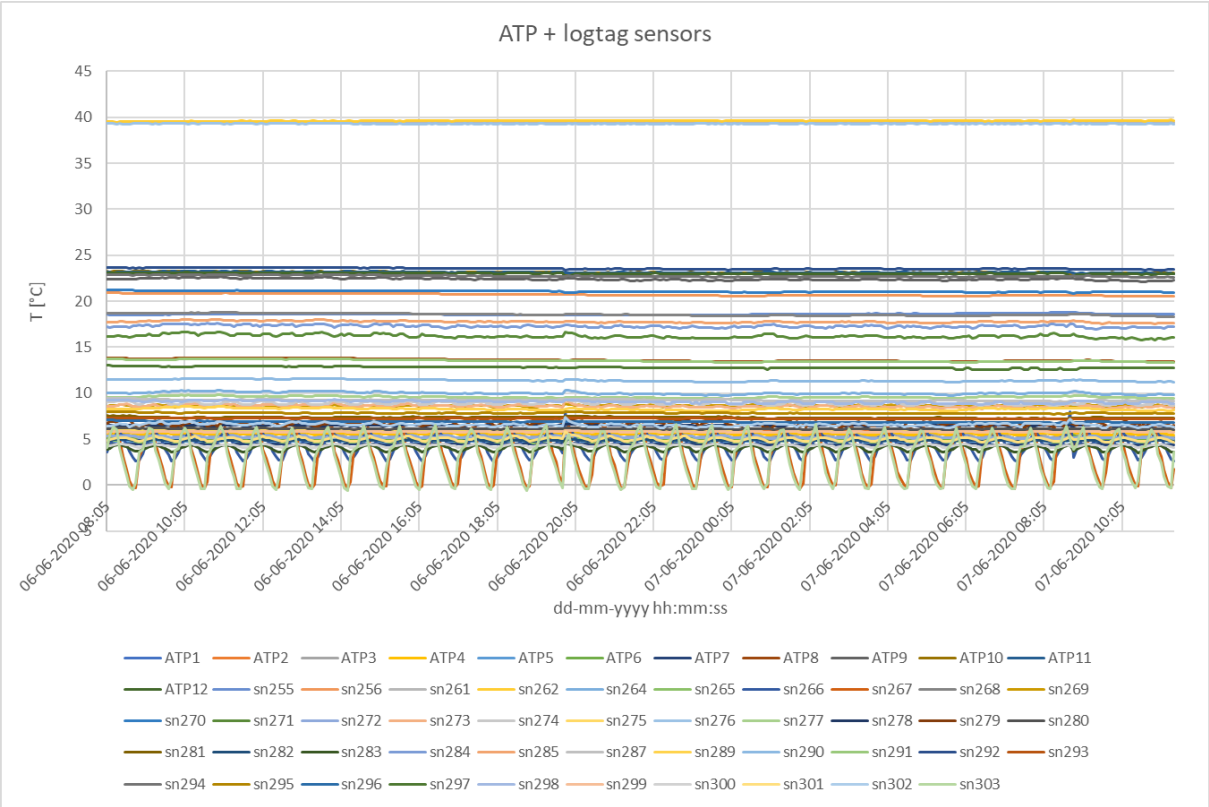

Figure 46 Recorded steady state temperatures for test 33.

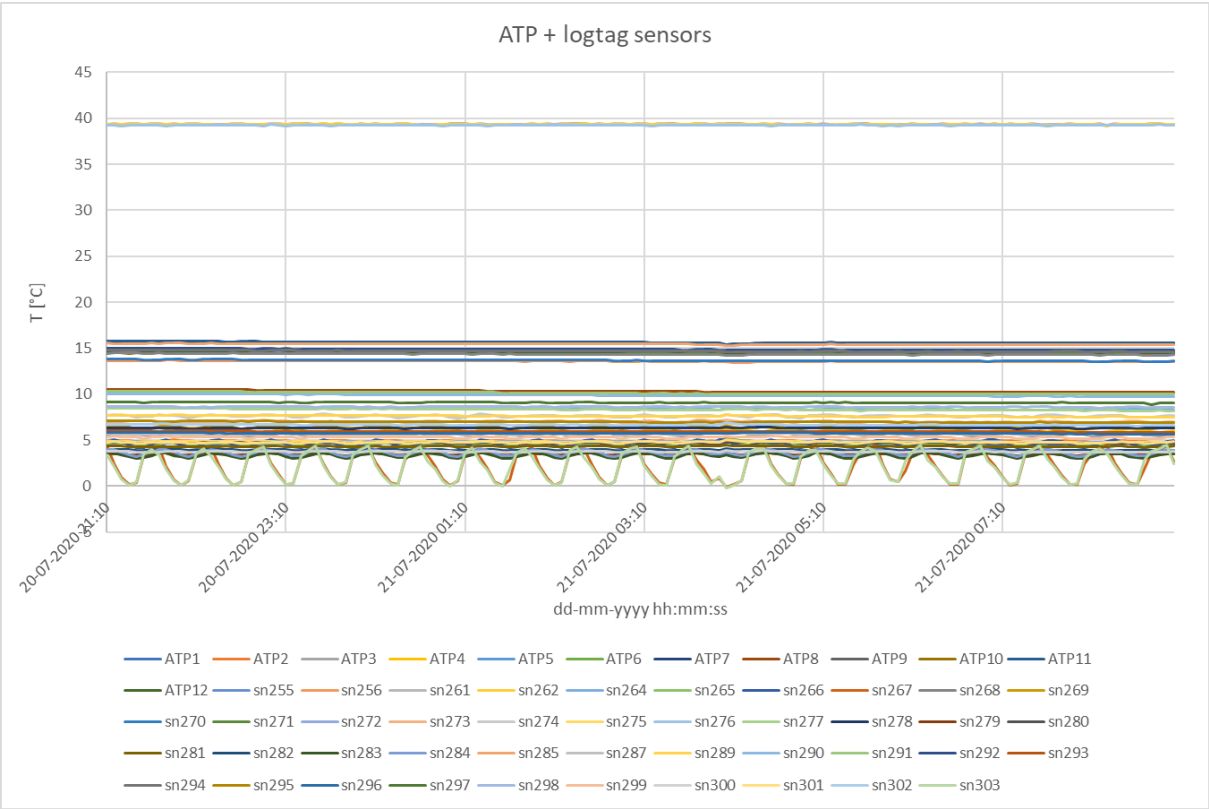

Figure 47 Recorded steady state temperatures for test 38.

Fig. 48 till Fig. 52 show the recorded temperatures during all pull down and pull up tests (Table 7). The legends correspond with the naming of temperature sensors in Fig. 24 and Fig. 26. Basically the recorded temperatures are clustered in two bundles: a small bundle of three recordings outside the container, and all others inside the container. The internal recordings with the fastest response are the ones most directly exposed to the refrigeration unit's supply air flow.

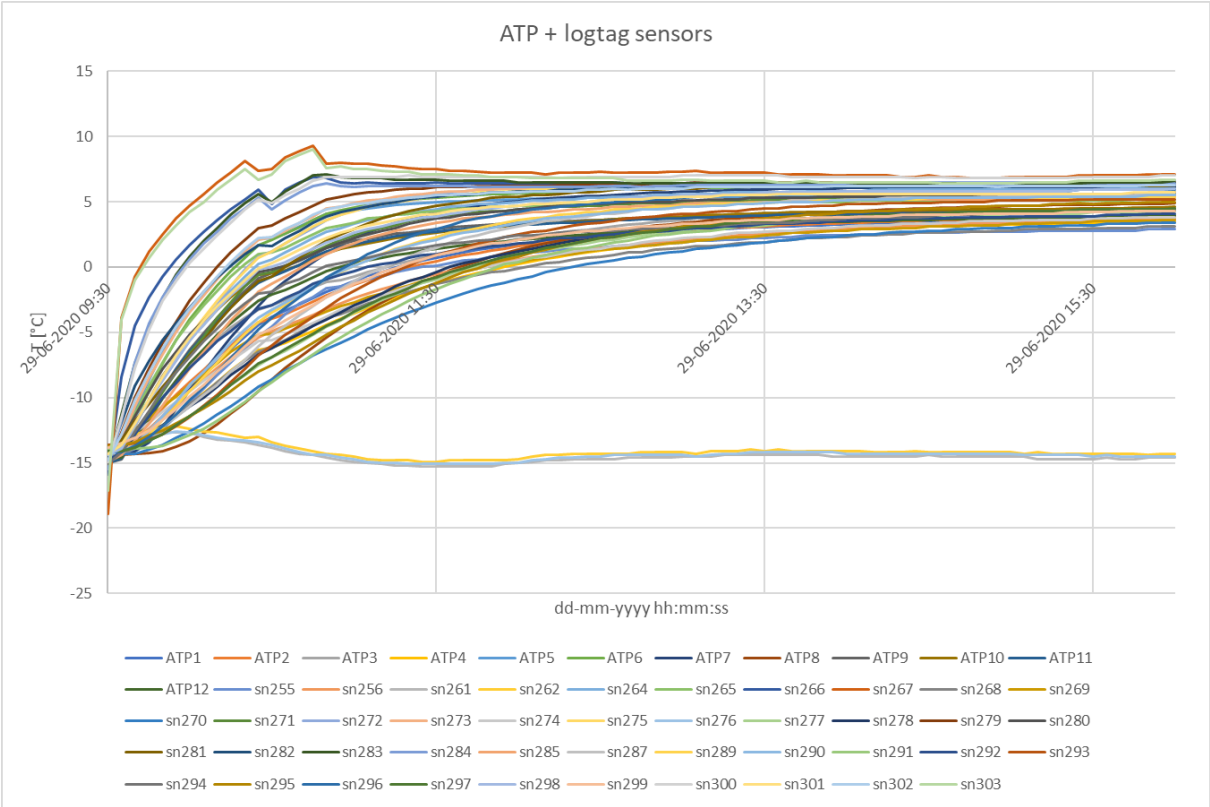

Figure 48 All temperatures recorded during pull up test 7.

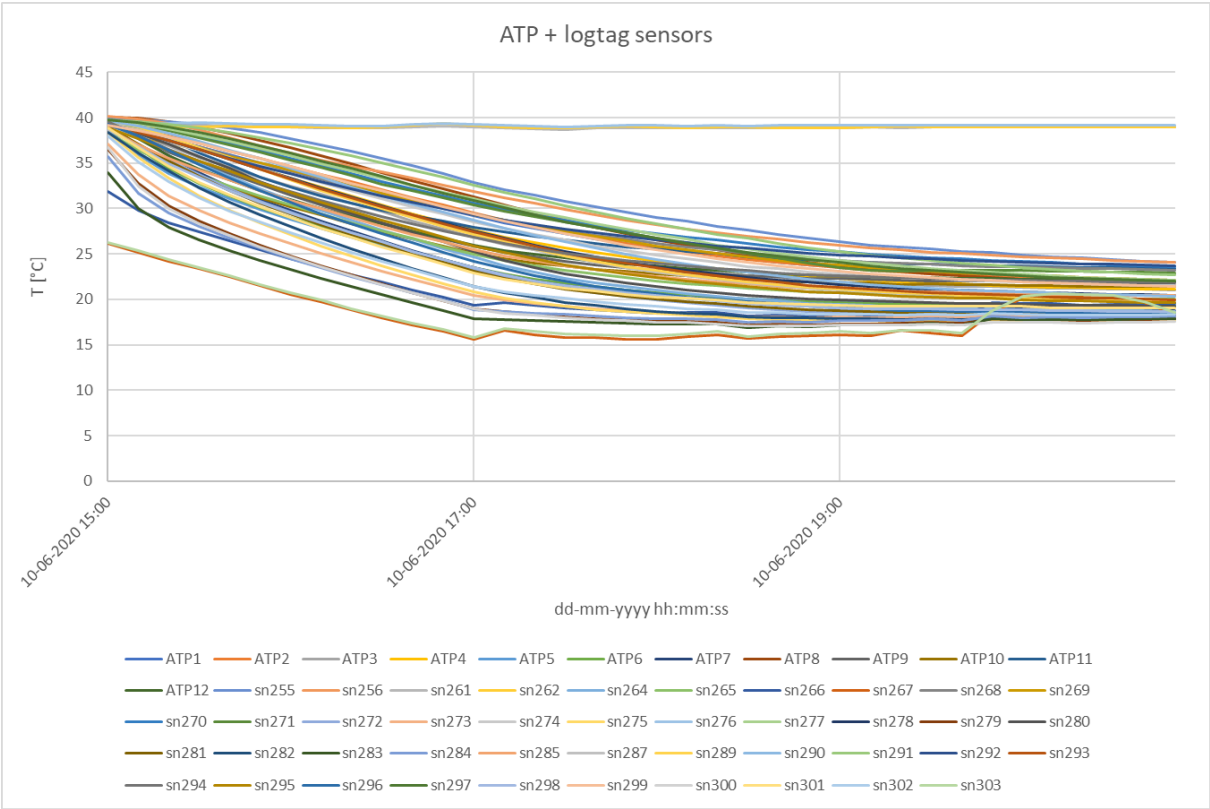

Figure 49 All temperatures recorded during pull down test 19.

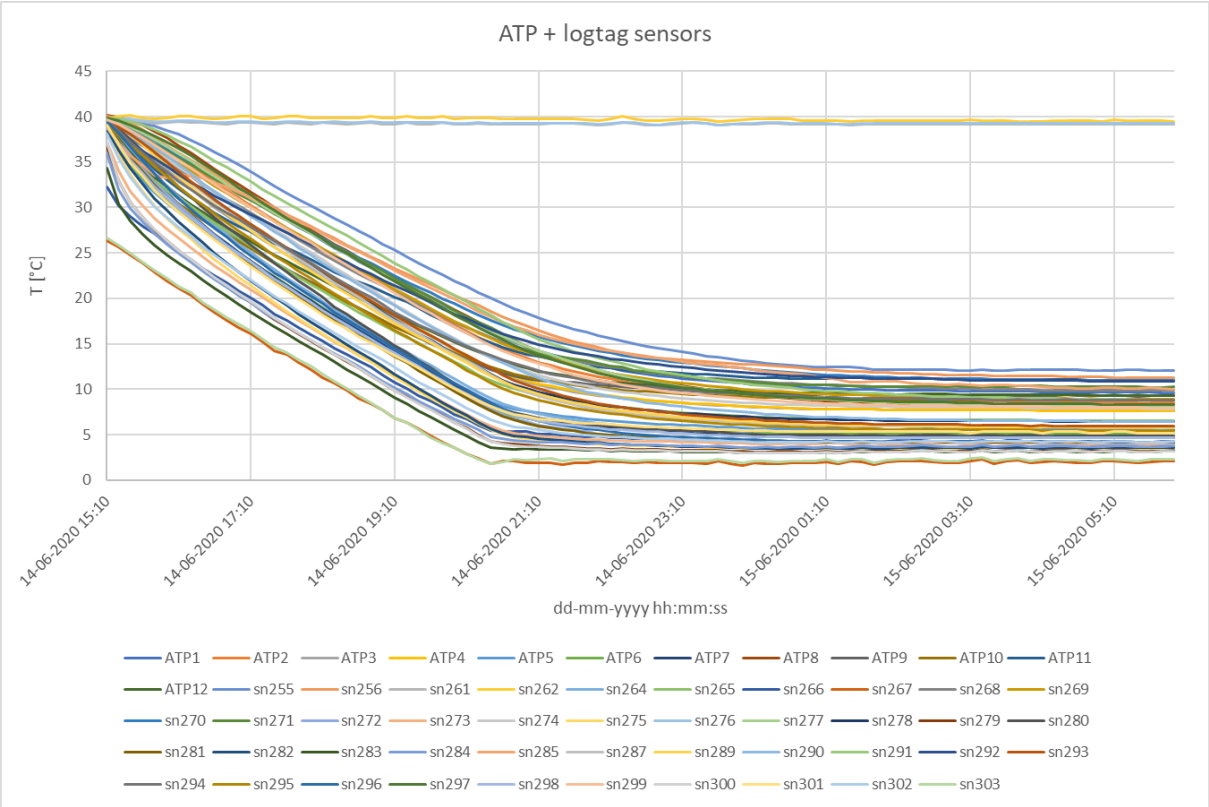

Figure 50 All temperatures recorded during pull down test 24.

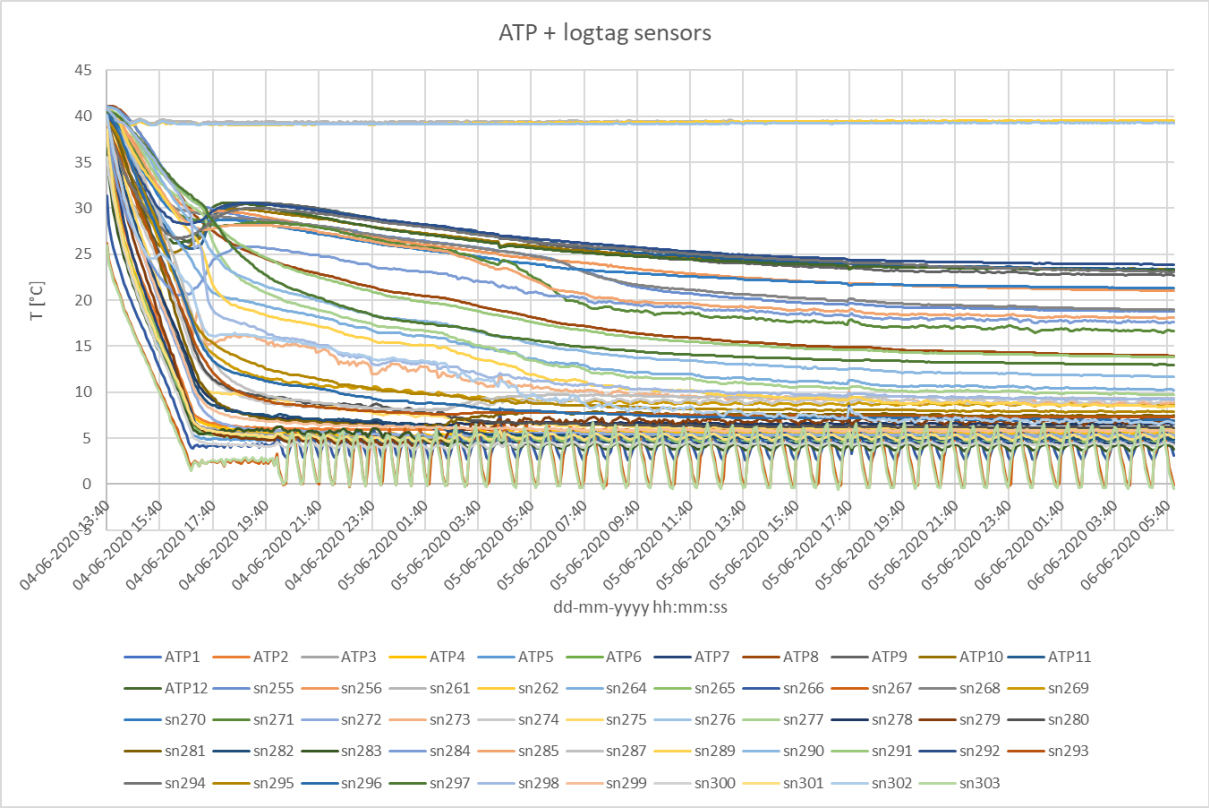

Figure 51 All temperatures recorded during pull down test 32.

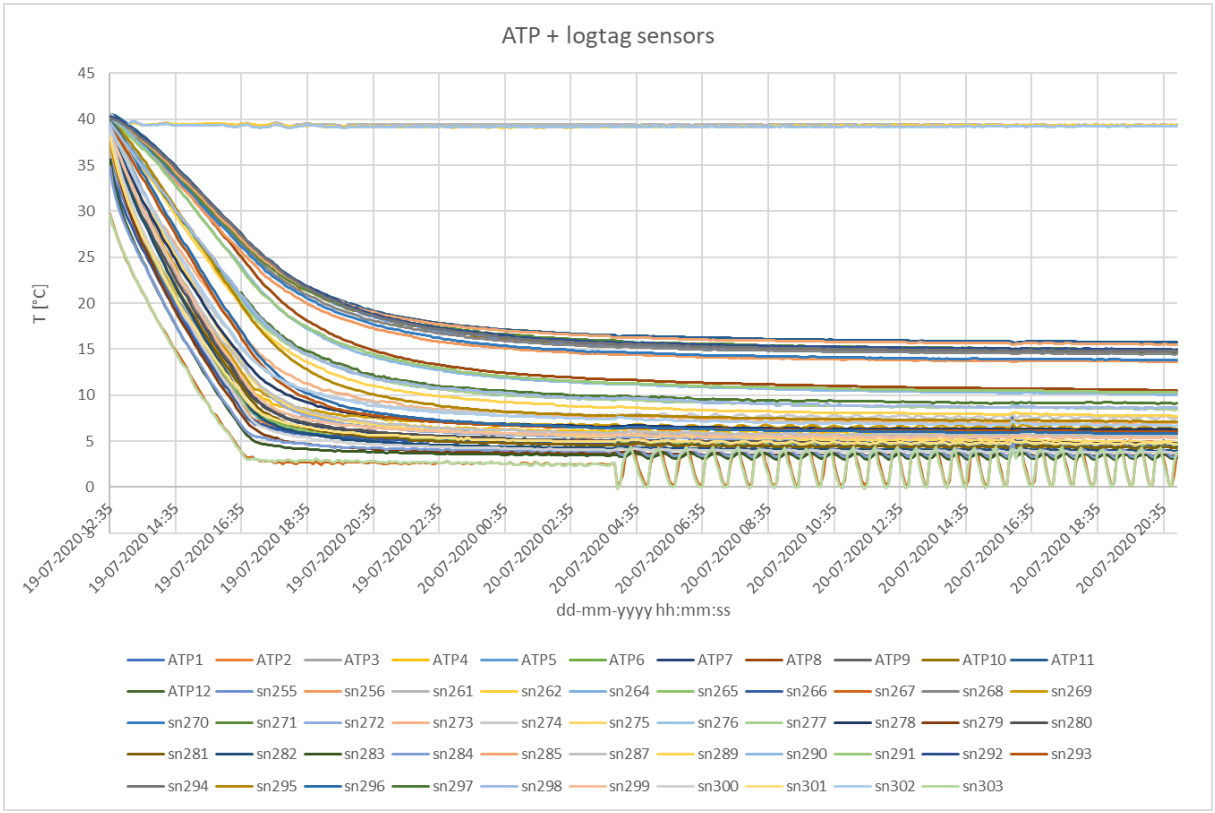

Figure 52 All temperatures recorded during pull down test 37.

Fig. 53 till Fig. 58 show the recorded temperatures during all power off, door opening and recovery tests (Table 8). The legends correspond with the naming of temperature sensors in Fig. 24 and Fig. 26. Basically the recorded temperatures are clustered in two bundles: a small bundle of three recordings outside the container, and all others inside the container. Not all tests are exactly identical. Most figures show the same pattern: internal temperatures starting in steady state and moving towards the outside temperatures due to power off / door opening, followed by a recovery stage after unit was turned on.

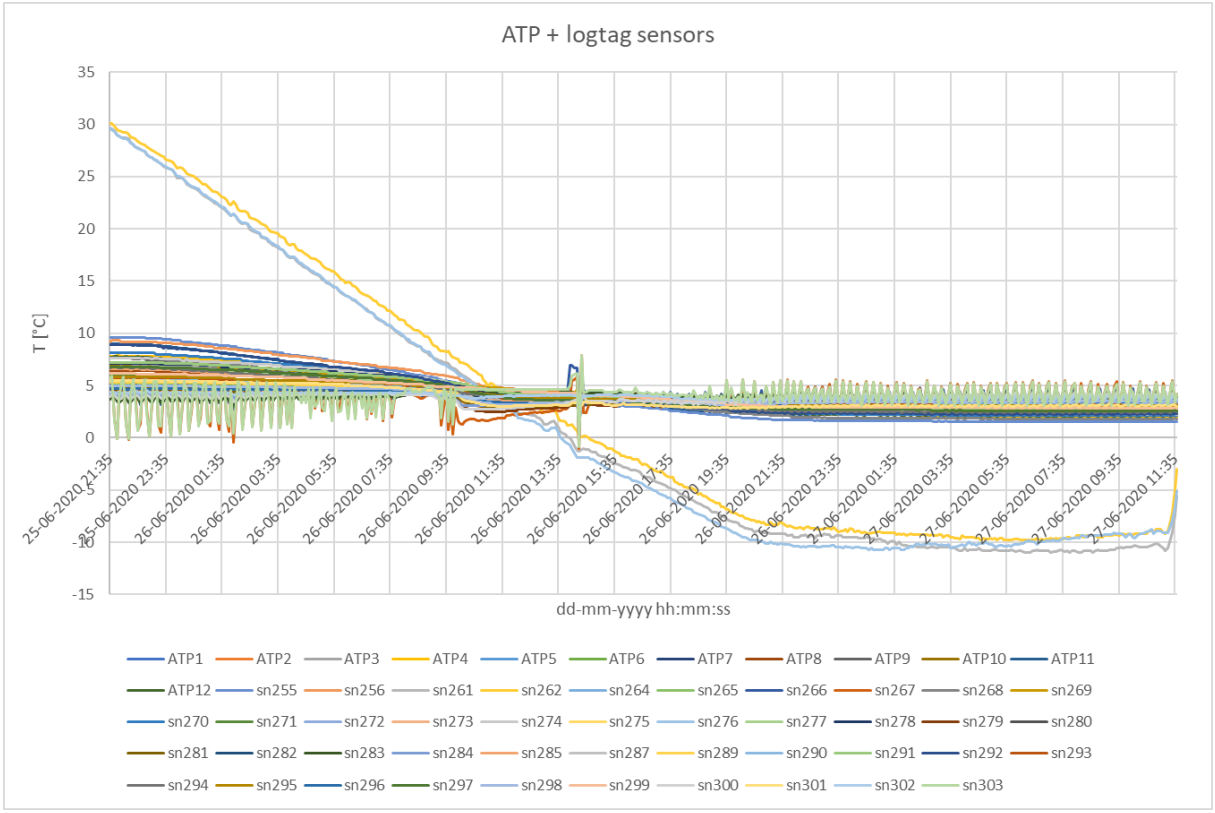

Figure 53 All temperatures recorded during test 5B (decreasing Tamb).

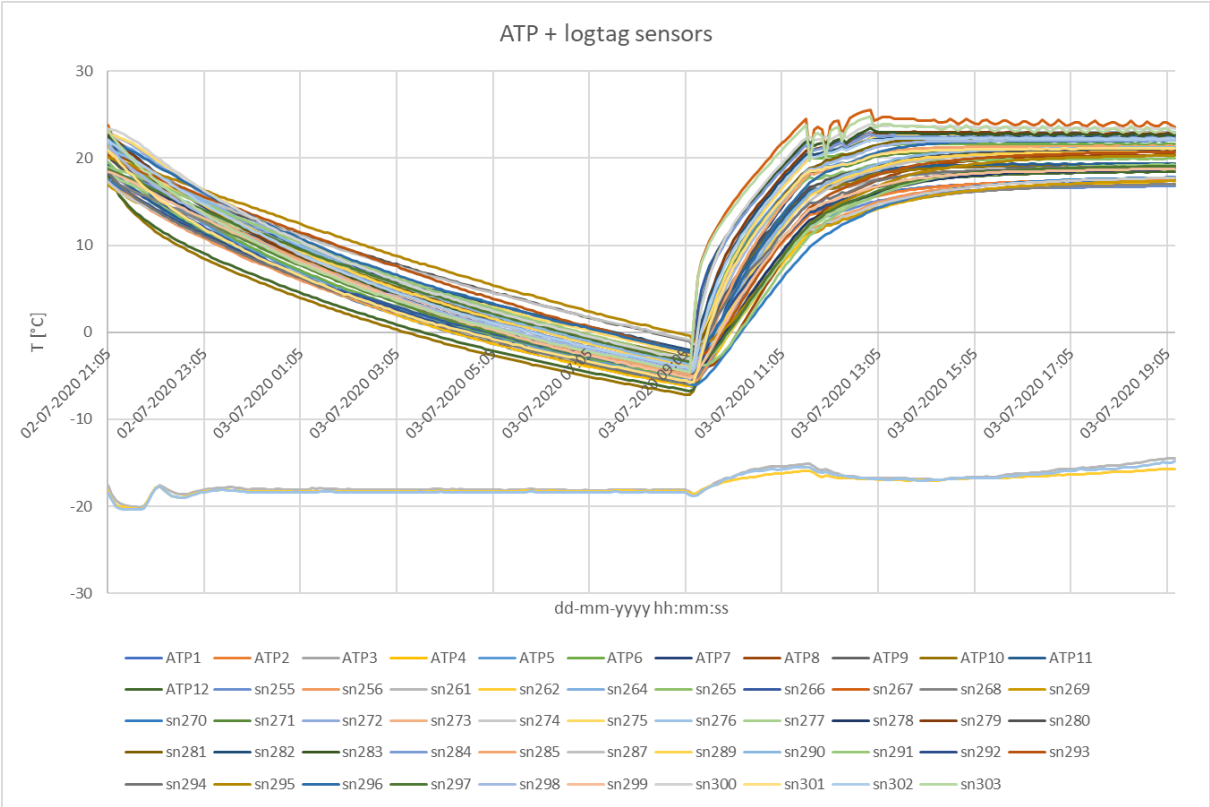

Figure 54 ***All temperatures recorded during tests 13 and 14 (power off and recovery).***

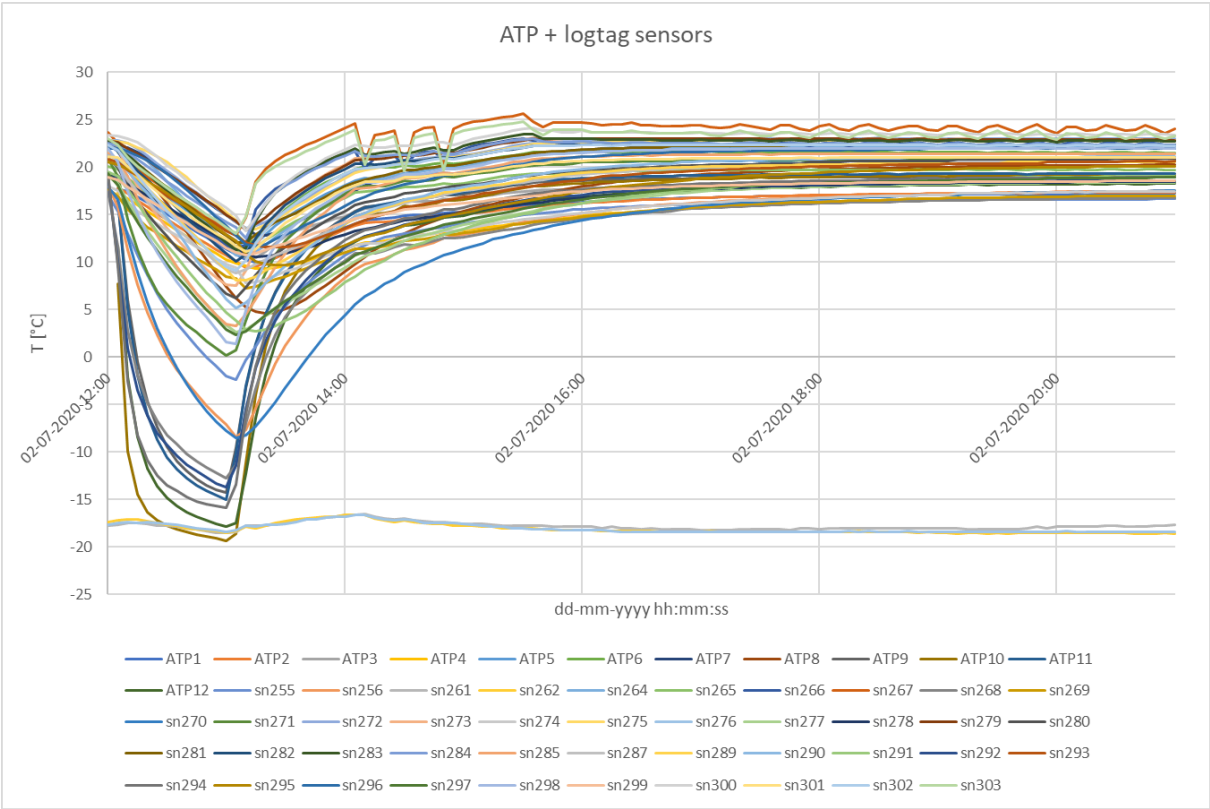

Figure 55 ***All temperatures recorded during tests 15 and 16 (door opening and recovery).***

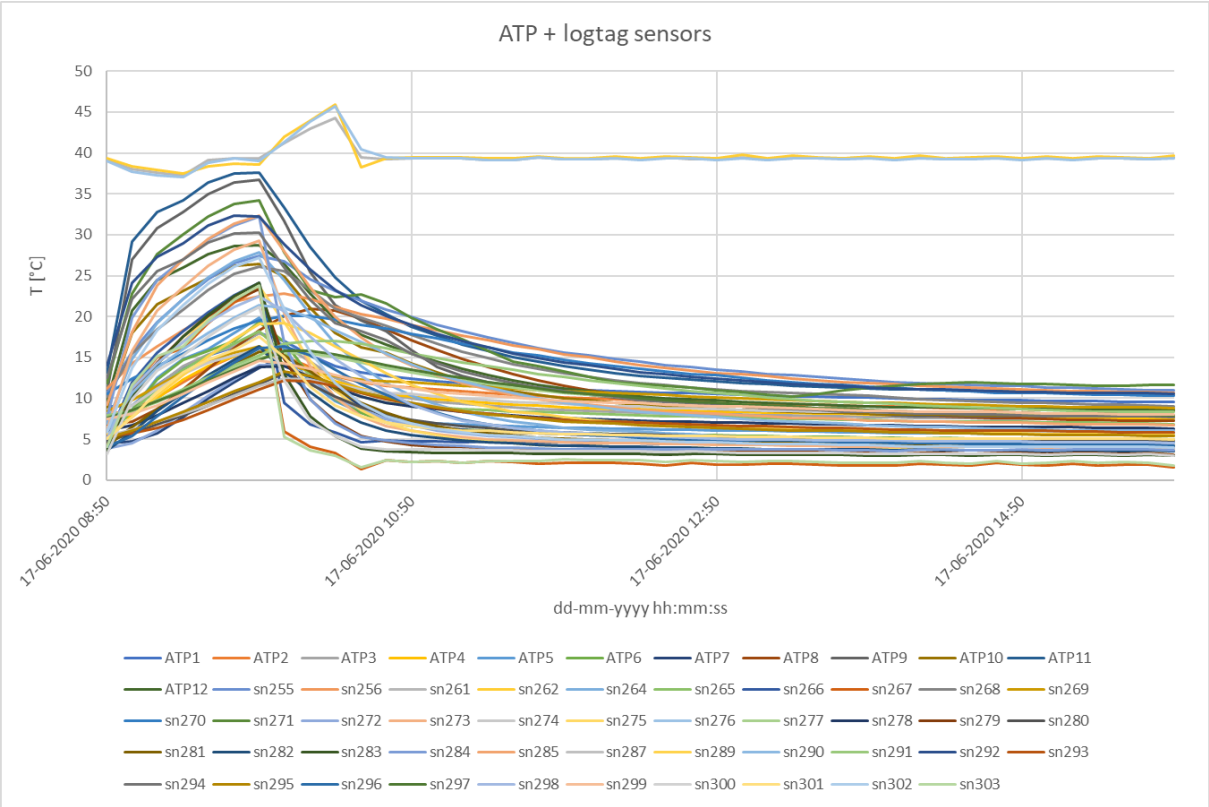

Figure 56 ***All temperatures recorded during tests 28 and 29 (door opening and recovery).***

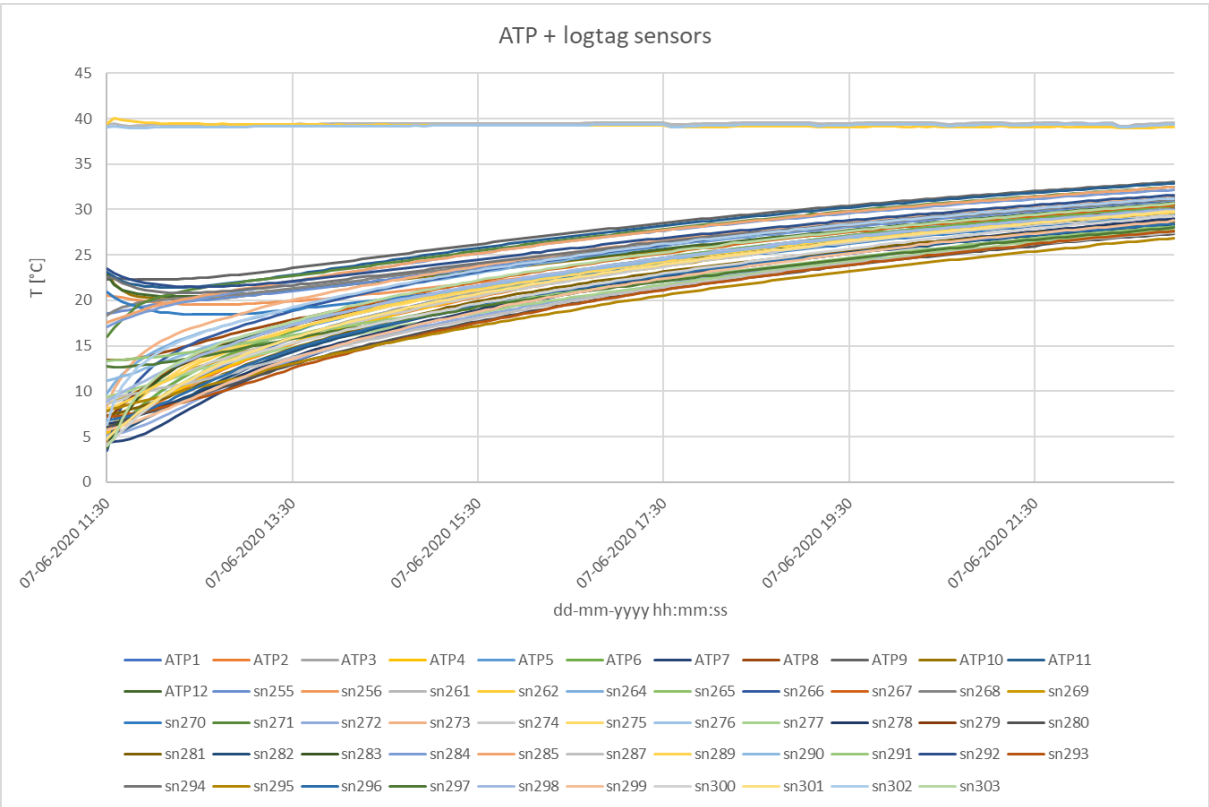

Figure 57 ***All temperatures recorded during test 34 (power off).***

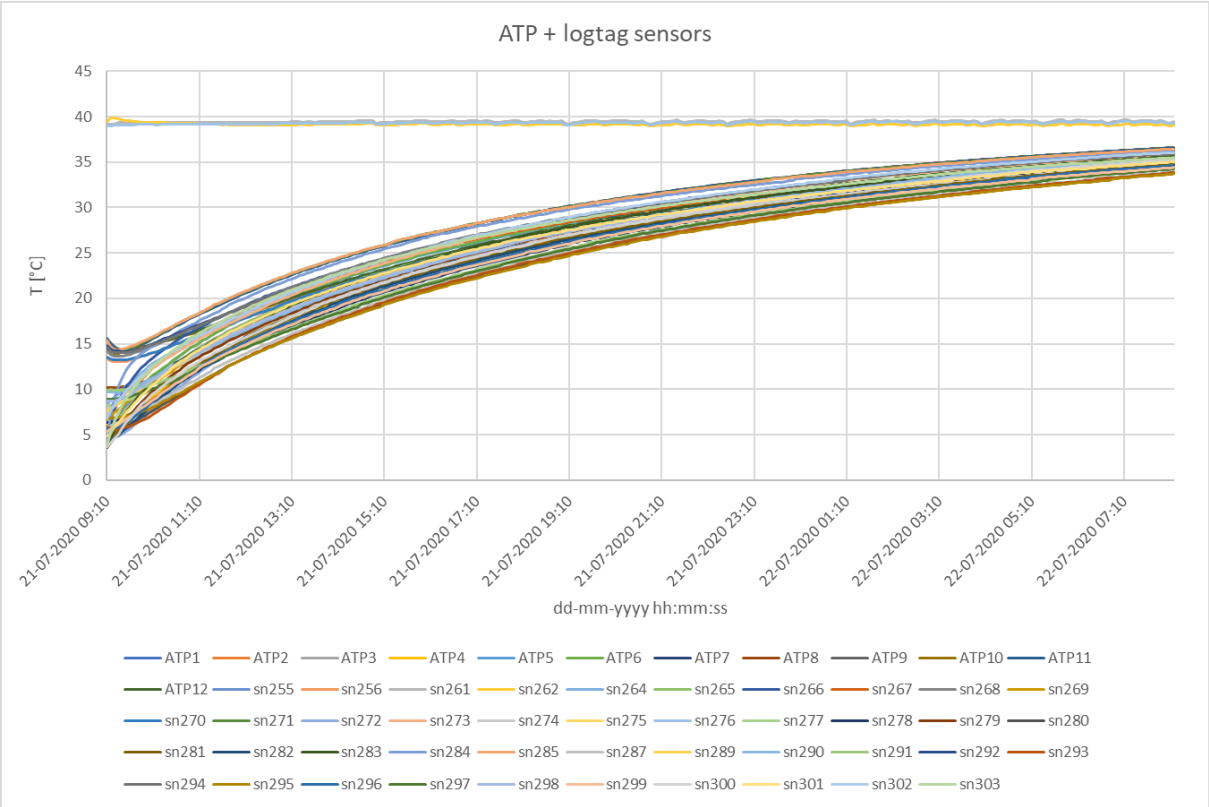

Figure 58 All temperatures recorded during test 39 (power off).

Annex 2 steady state temperatures in 3D

All figures in this annex are 3D contour plots of temperatures measured during the steady state tests listed in Table 6, and based on the temperature sensors shown in Fig. 24 till Fig. 27. Above each figure is a short description linking to the descriptions in Table 6. In the figures the refrigeration unit (not shown) is on the left, and the doors (not shown) are on the right.

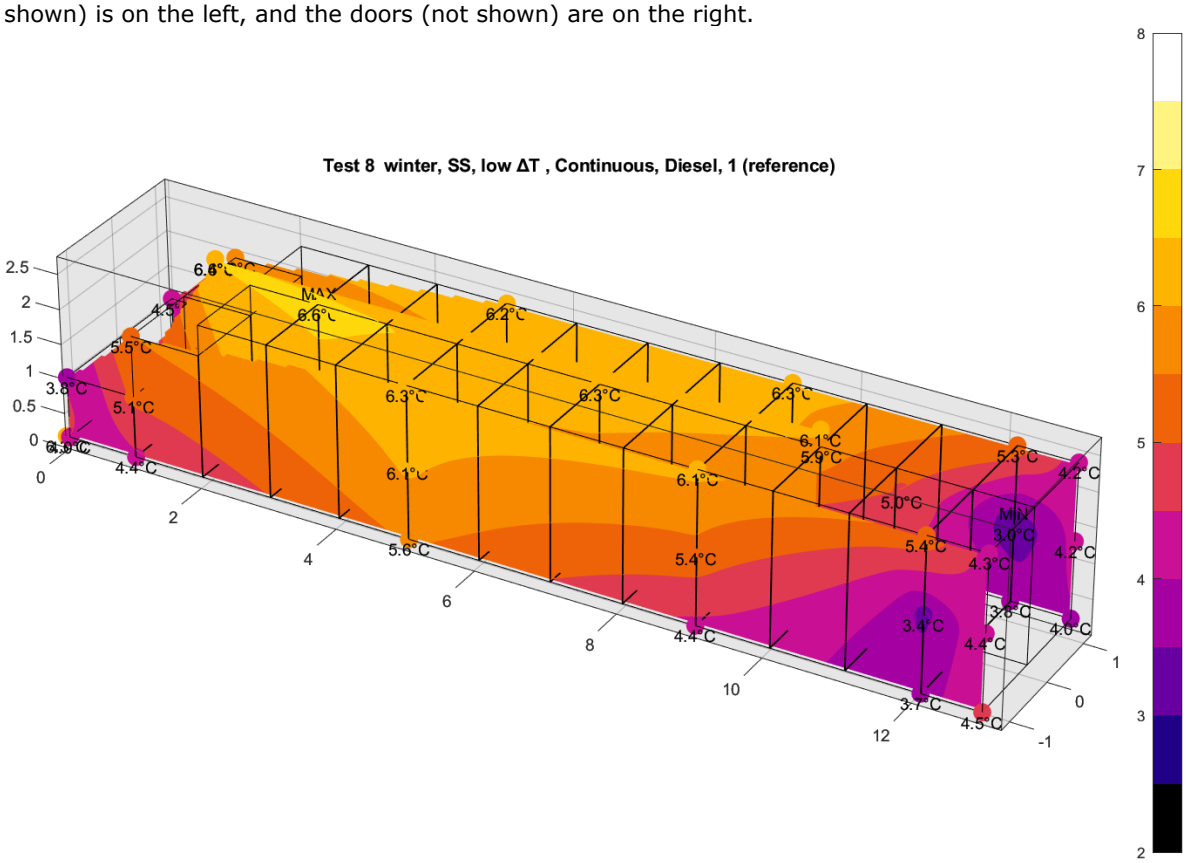

Figure 59 3D contour plots of steady state temperatures during test 8.

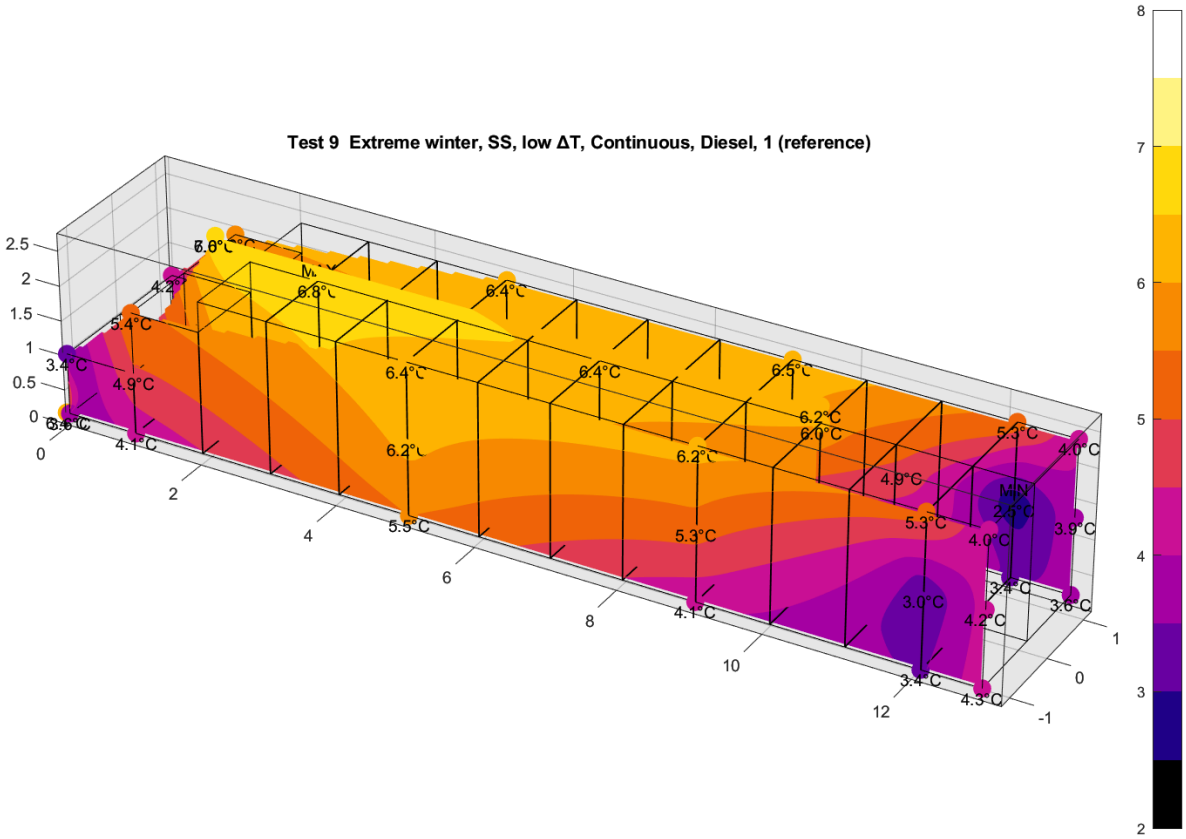

Figure 60 ***3D contour plots of steady state temperatures during test 9.***

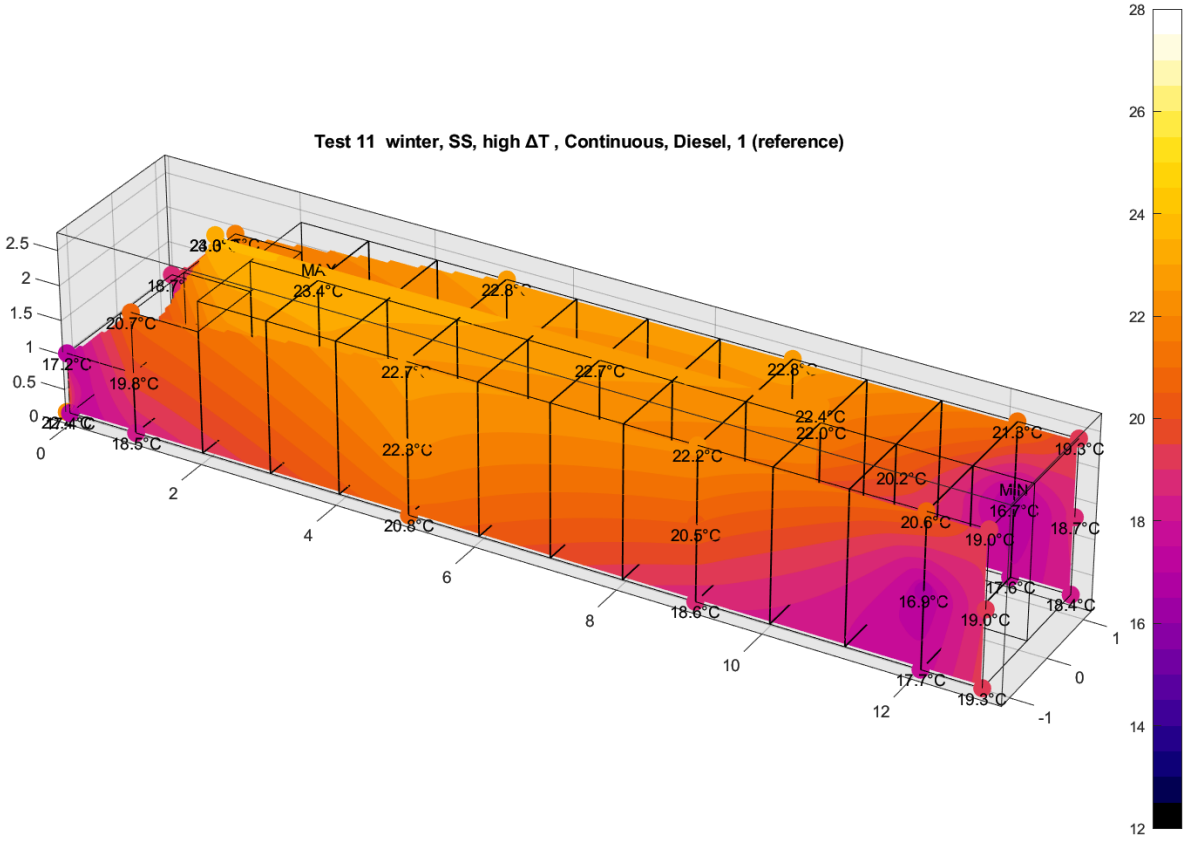

Figure 61 ***3D contour plots of steady state temperatures during test 11.***

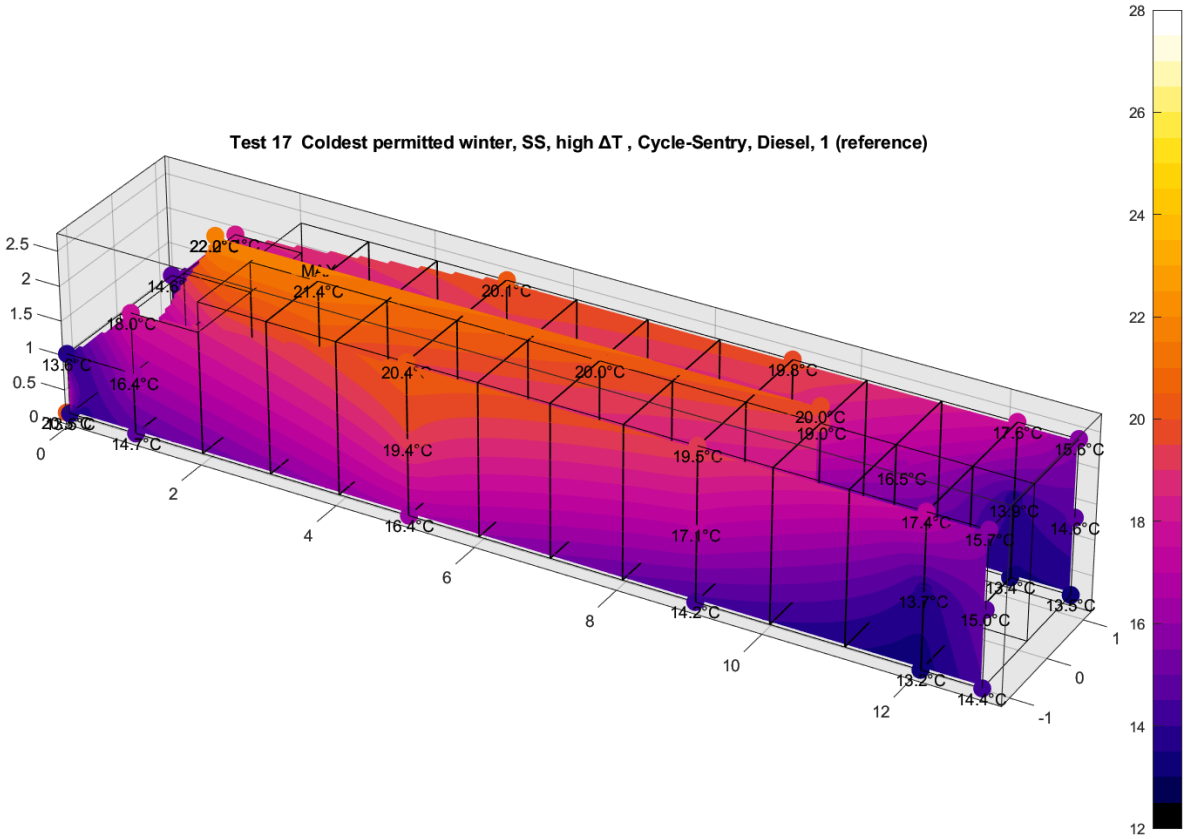

Figure 62 3D contour plots of steady state temperatures during test 17.

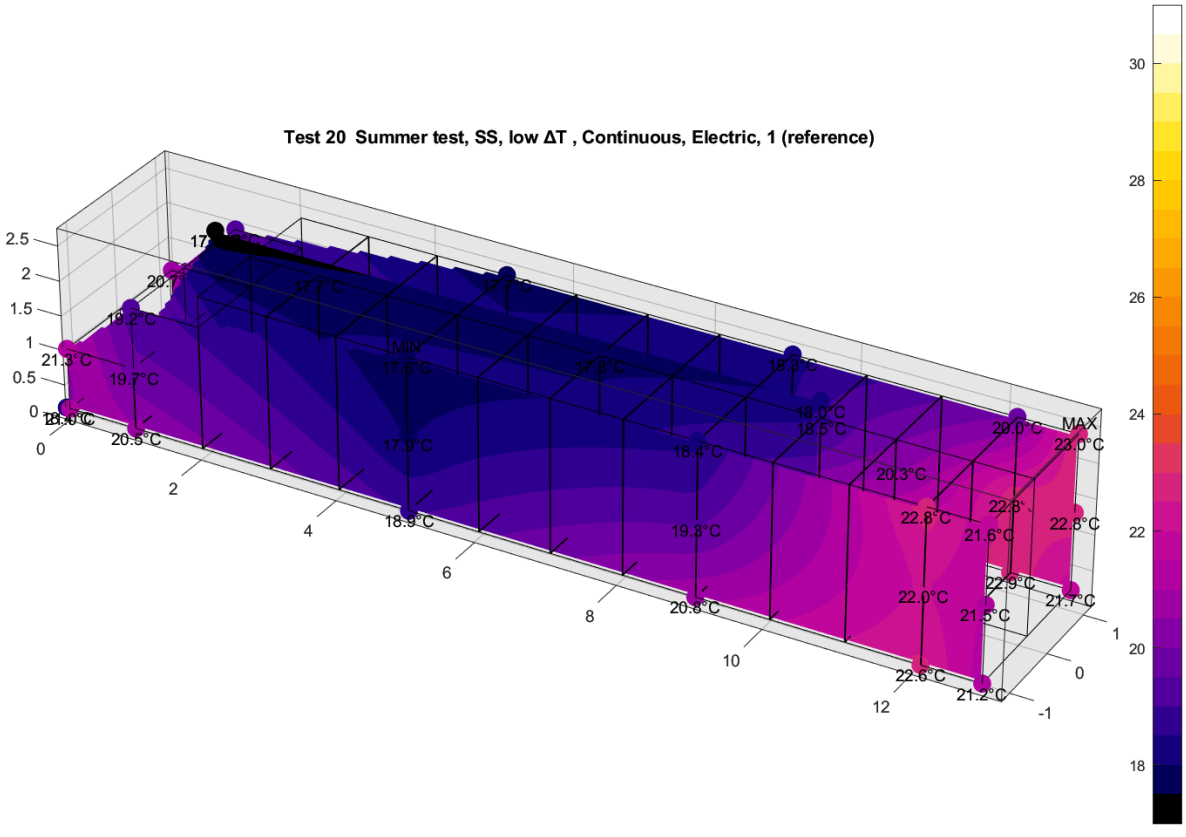

Figure 63 3D contour plots of steady state temperatures during test 20.

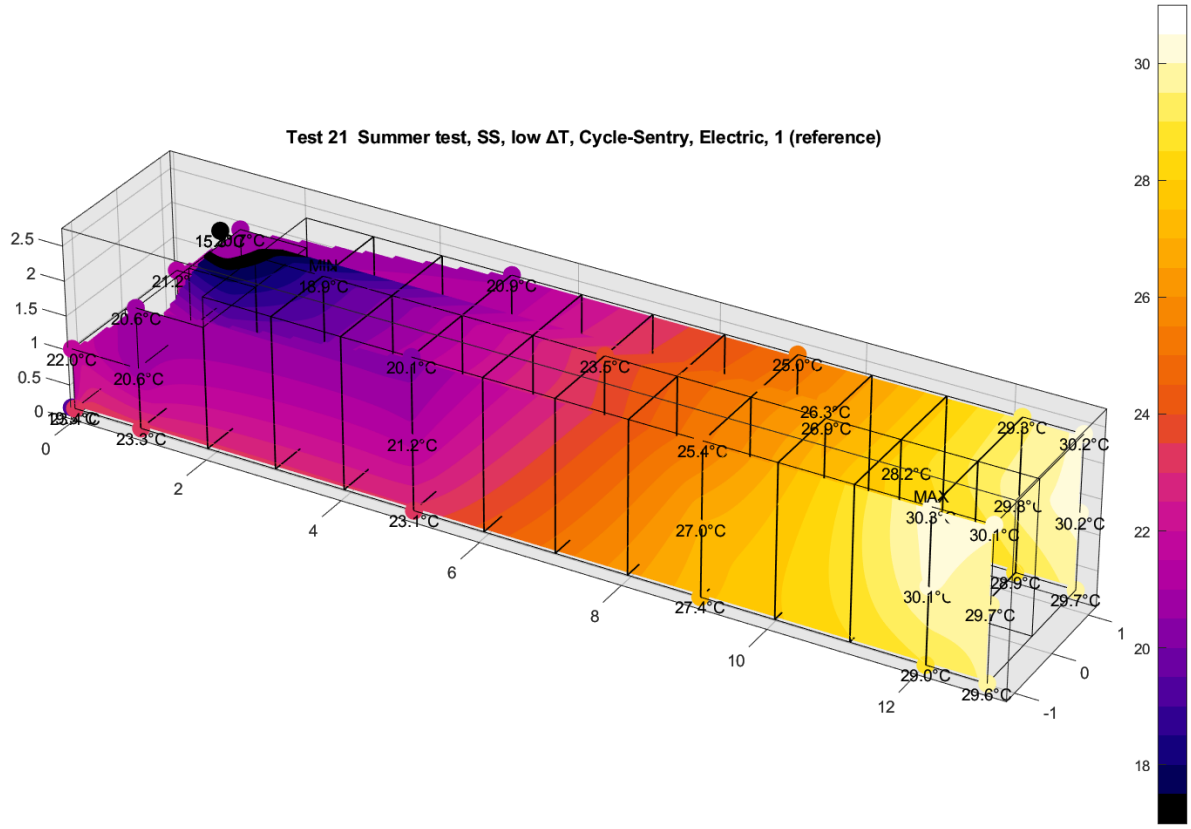

Figure 64 3D contour plots of steady state temperatures during test 21.

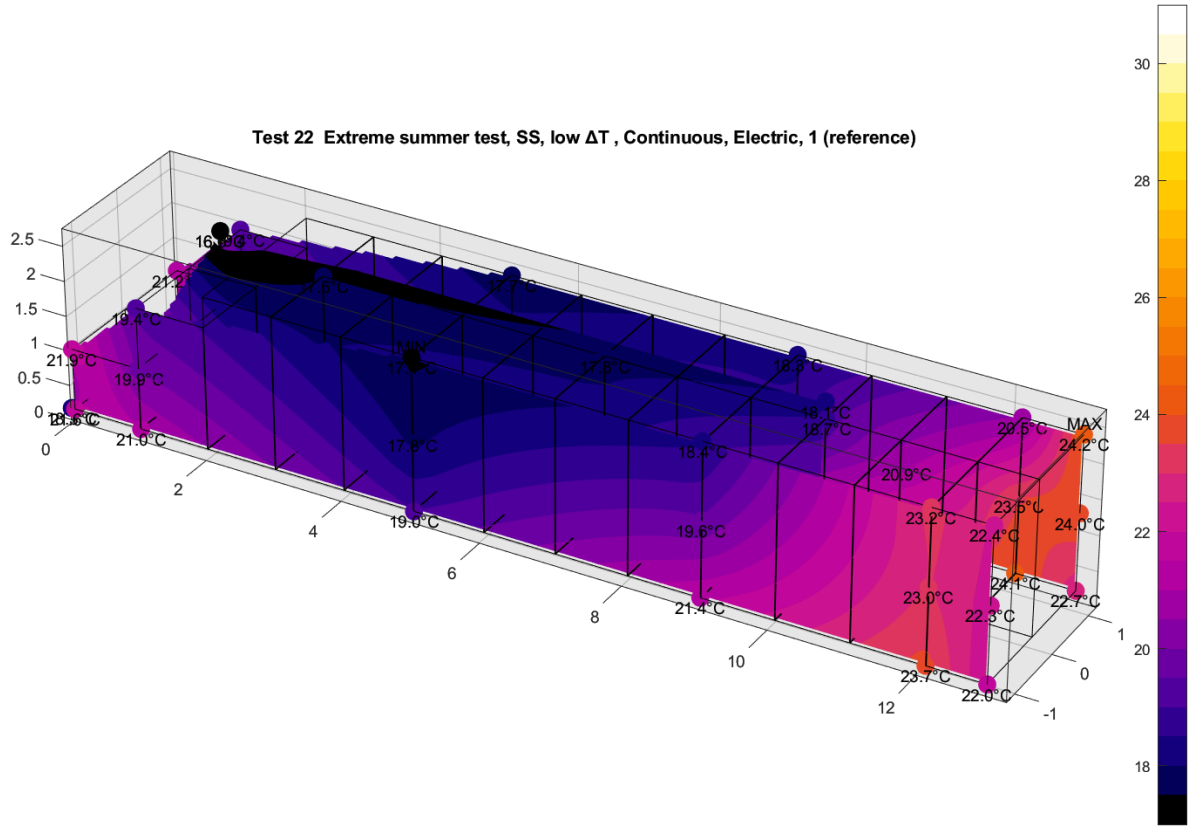

Figure 65 3D contour plots of steady state temperatures during test 22.

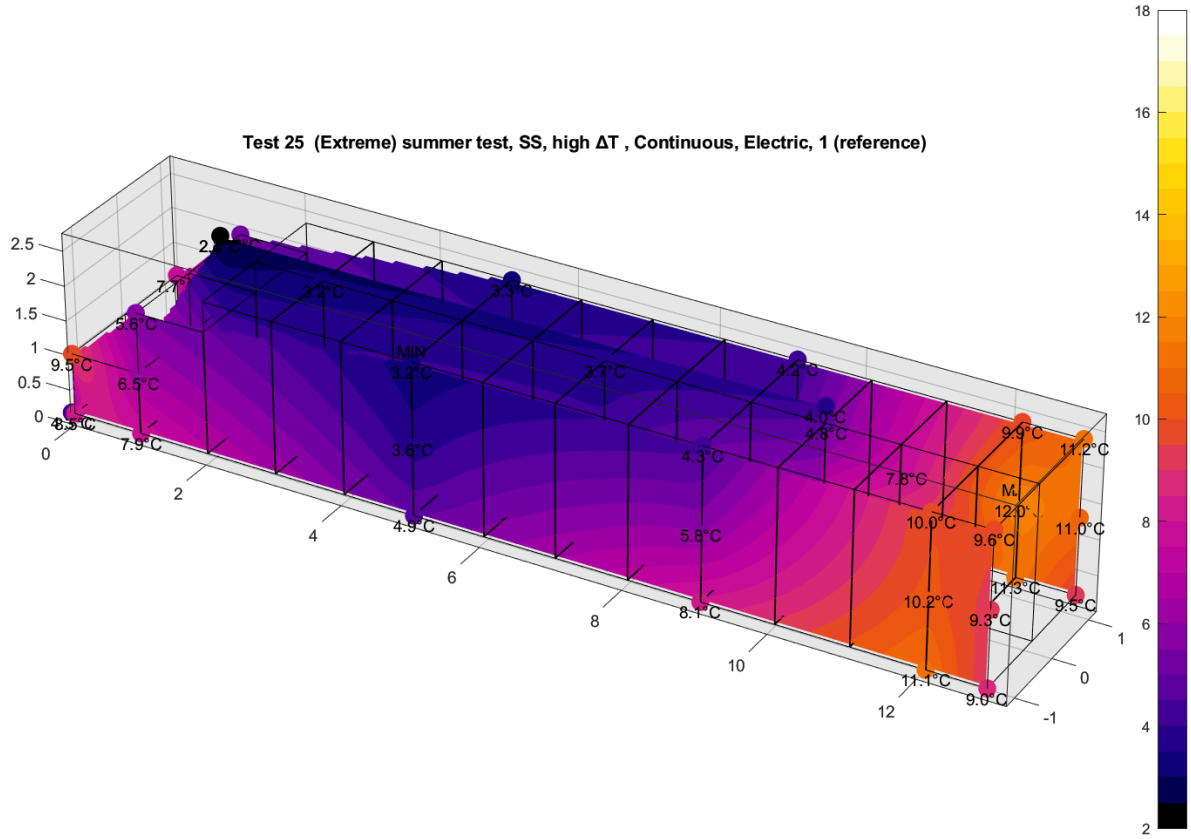

Figure 66 3D contour plots of steady state temperatures during test 25.

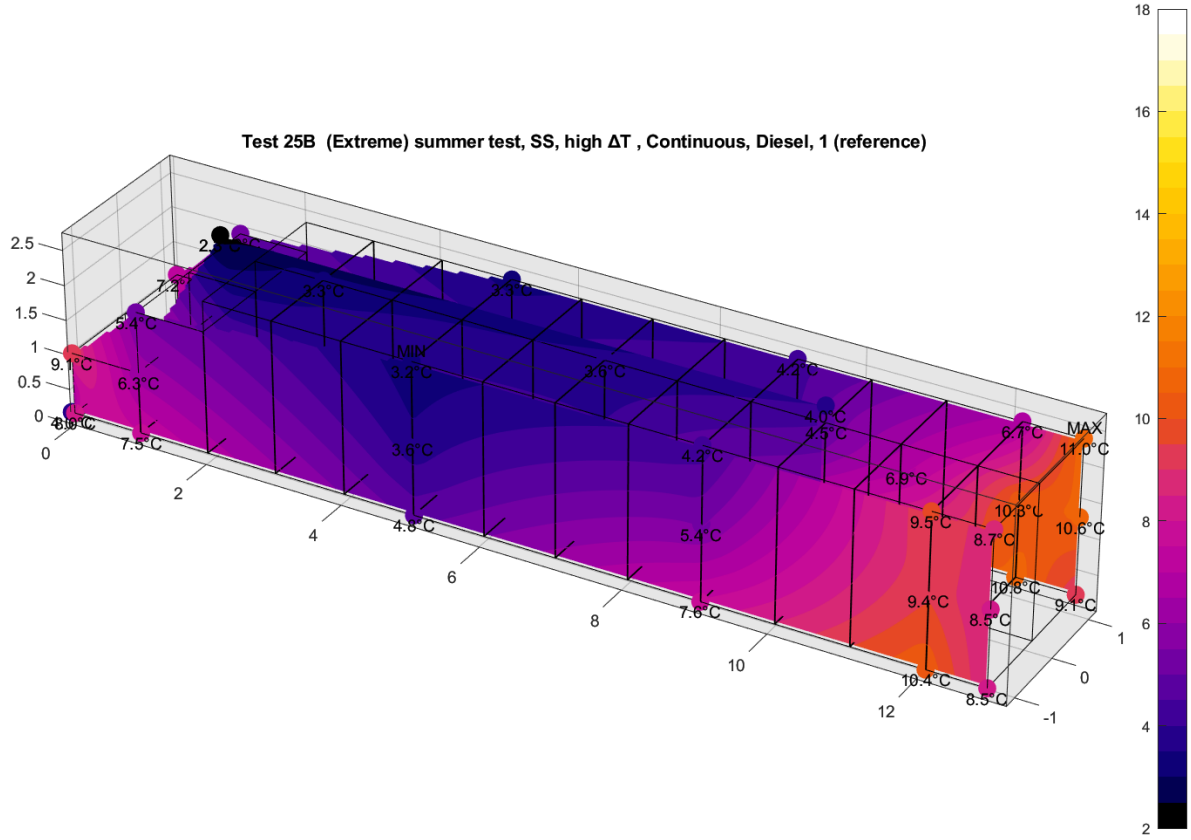

Figure 67 3D contour plots of steady state temperatures during test 25B.

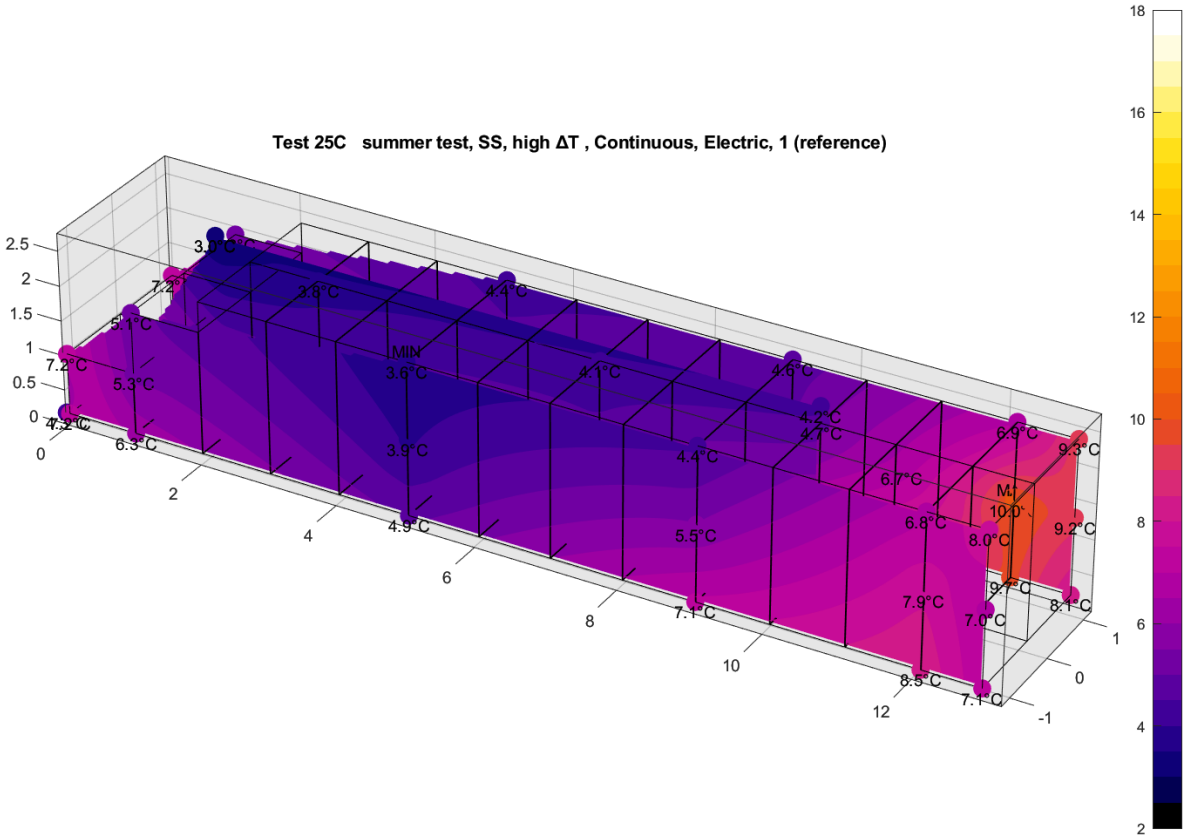

Figure 68 3D contour plots of steady state temperatures during test 25C.

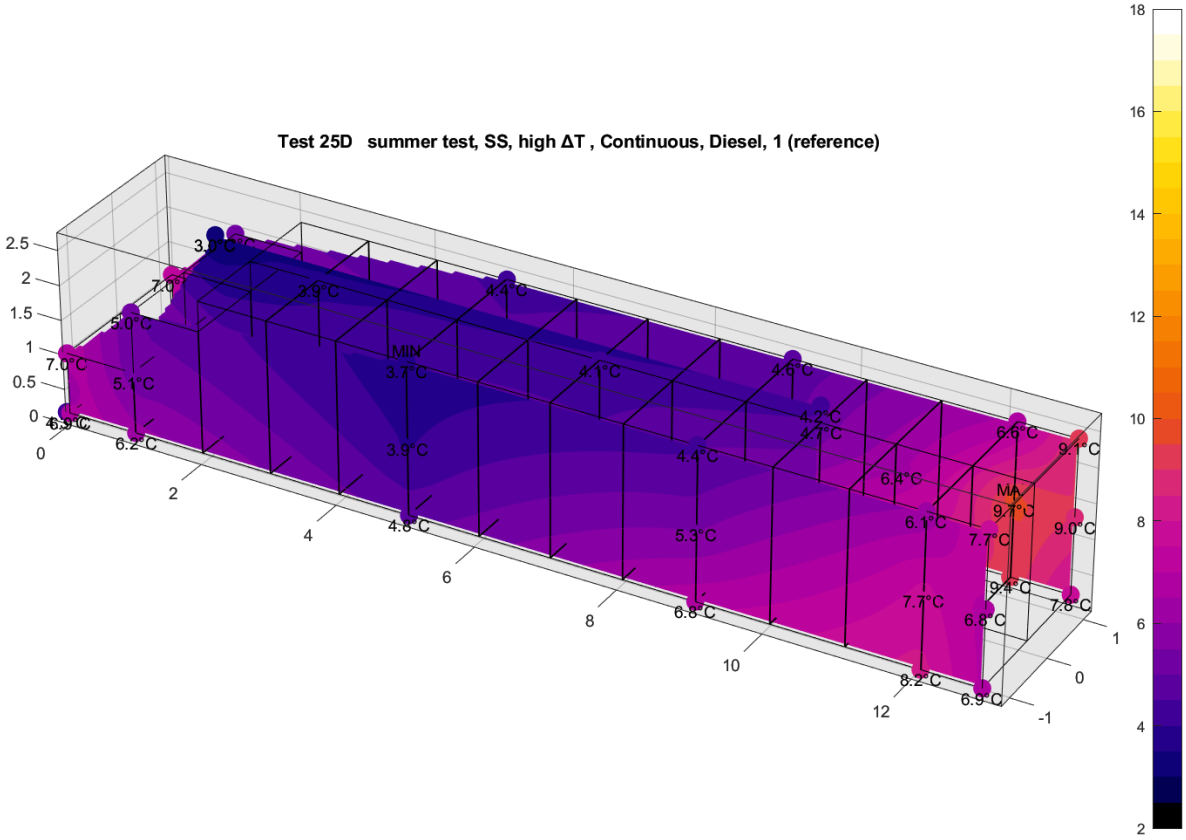

Figure 69 3D contour plots of steady state temperatures during test 25D.

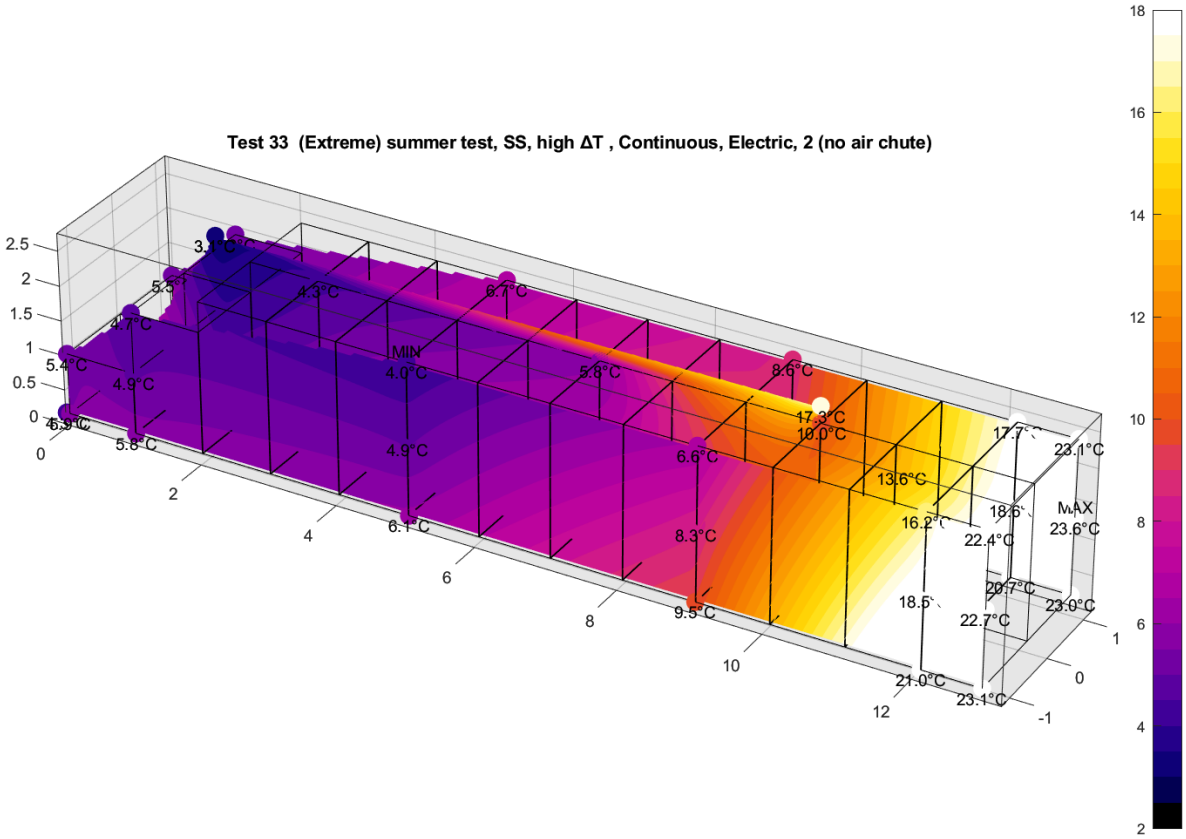

Figure 70 ***3D contour plots of steady state temperatures during test 33.***

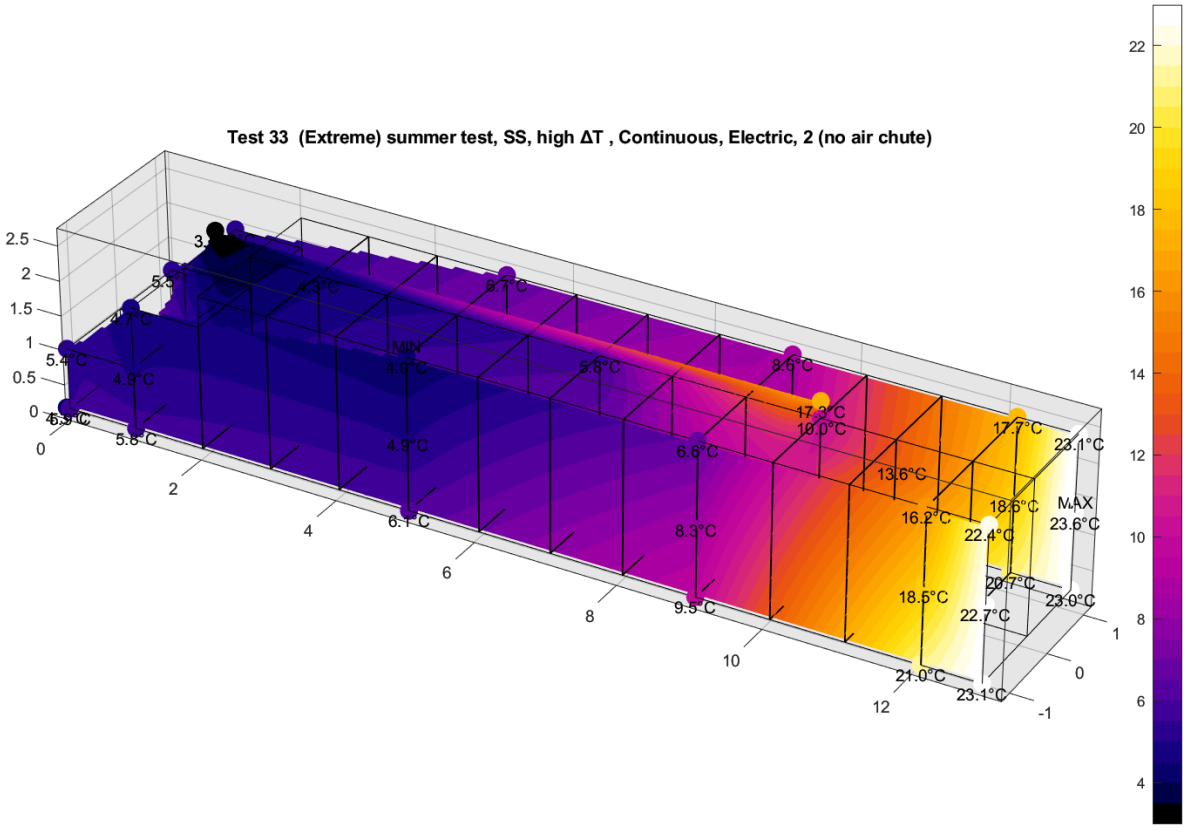

Figure 71 ***3D contour plots of steady state temperatures during test 33 (wider colour scale).***

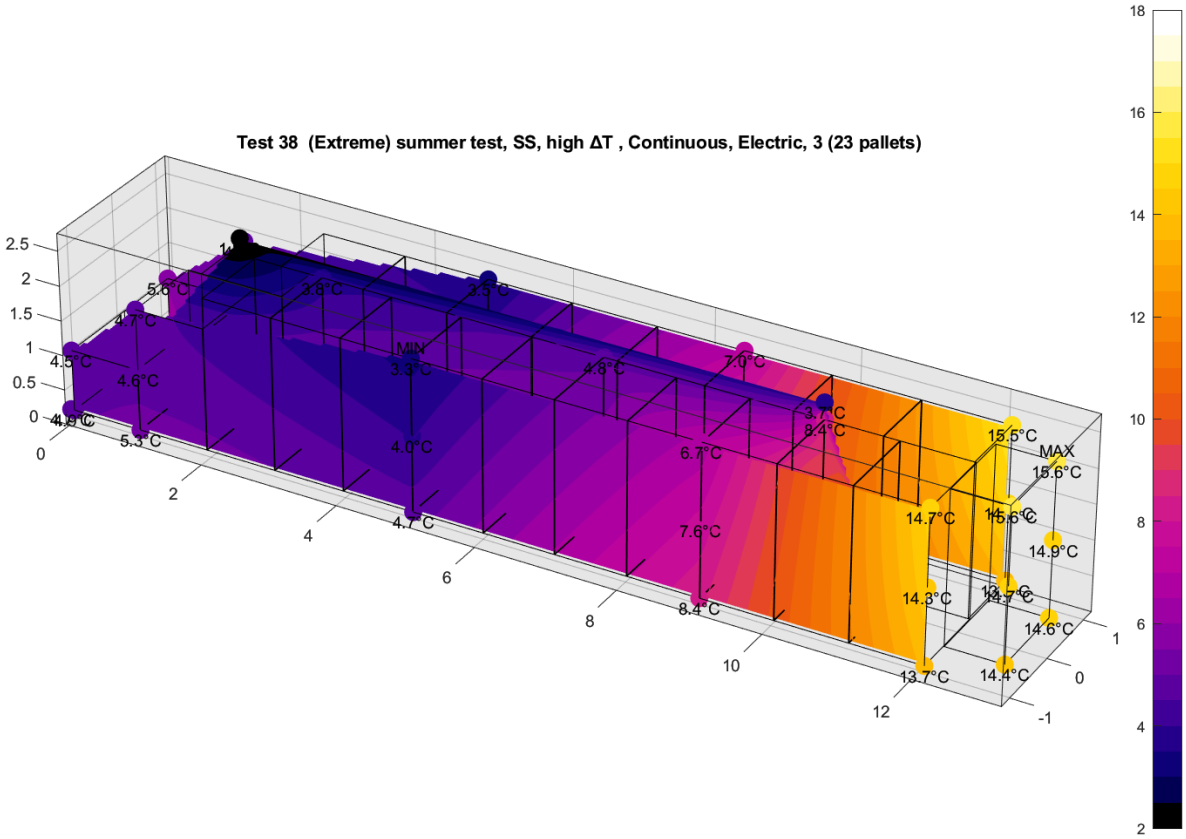

Figure 72 3D contour plots of steady state temperatures during test 38.

Annex 3 Static pressure differences

Table 17 ***Configuration 1 (reference) static pressure difference $P_{stat,door}$ - P_{stat} [Pa] between door-end (purple dot in Fig. 24 and Fig. 25) and left (solid line), respectively right (dashed line) centre of pallet openings (dark green dots in Fig. 24 and Fig. 25).***

Distance from return air inlet [m]	left/right	Electric, left	Diesel (LS), left	Diesel (HS), left
0	left	9.2	12.4	24.6
1	left	7.6	10.5	18.6
3	left	5	7.1	12.7
5	left	2.9	4.3	7.9
7	left	0.7	1.5	2.9
9	left	-0.5	-0.2	0.7
11	left	-1.3	-1.2	-1.2
0	right	8.9	12.1	24.5
1	right	7.3	9.8	17.3
3	right	5.1	7.2	13
5	right	2.5	3.6	6.8
7	right	0.7	1.3	3
9	right	-0.6	-0.2	0.4
11	right	-1.2	-1	-1

Table 18 ***Configuration 2 (no air chute) static pressure difference $P_{stat,door}$ - P_{stat} [Pa] between door-end (purple dot in Fig. 24 and Fig. 25) and left (solid line), respectively right (dashed line) centre of pallet openings (dark green dots in Fig. 24 and Fig. 25).***

Distance from return air inlet [m]	left/right	Electric, left	Diesel (LS), left	Diesel (HS), left
0	left	4.8	5.6	14
1	left	2.5	3.2	7.8
3	left	0.6	0.9	2.7
5	left	-0.5	0.3	1.1
7	left	-1.1	-0.9	-0.9
9	left	-1.4	-1.3	-0.9
11	left	-1.7	-1.8	-2.2
0	right	4	5.3	13.5
1	right	2.6	3.4	7.2
3	right	0.5	0.7	2.9
5	right	-0.5	-0.3	0.5
7	right	-1	-0.7	-0.7
9	right	-1.3	-1.3	-1.3
11	right	-1.5	-1.6	-1.9

Table 19 ***Configuration 3 (23 pallets) static pressure difference $P_{stat,door}$ - P_{stat} [Pa] between door-end (purple dot in Fig. 26 and Fig. 27) and left (solid line), respectively right (dashed line) centre of pallet openings (dark green dots in Fig. 26 and Fig. 27).***

Distance from return air inlet [m]	left/right	Electric, left	Diesel (LS), left	Diesel (HS), left
0	left	4.6	6.5	14
1	left	2.6	3.1	7.3
3	left	1.9	2.8	5.9
5	left	0.3	0.6	1.8
7	left	-1.5	-1.2	-1.2
9	left	-1.8	-1.7	-1.9
11	left	-2.3	-1.9	-2.1
0	right	2.6	4.1	8
1.2	right	2.9	4.2	8.2
2.4	right	2.3	3.2	6.8
3.6	right	1.9	3	5.4
4.8	right	0.8	1	3.2
7.2	right	-1.4	-1.1	-1.2
10.8	right	-1.7	-1.9	-1.5

Annex 4 Air velocities measured with anemometers

Table 20 Air velocities (m/s) measured above cargo (Fig. 33) with method of drive = electric.

distance from return air inlet	1.5 m	3.0 m	5.0 m	7.0 m	9.0 m	11.0 m
reference	4.04	2.80	1.71	1.01	0.61	0.28
no air chute	2.99	1.66	0.71	0.55	0.49	0.34
23 pallets	3.37	3.84	2.95	1.84	1.41	0.59

Table 21 Air velocities (m/s) measured above cargo (Fig. 35) with method of drive = diesel (Low Speed engine).

distance from return air inlet	1.5 m	3.0 m	5.0 m	7.0 m	9.0 m	11.0 m
reference	4.59	3.14	1.97	1.09	0.70	0.31
no air chute	3.40	1.84	0.73	0.59	0.55	0.38
23 pallets	3.71	4.29	3.28	2.09	1.61	0.71

Table 22 Air velocities (m/s) measured above cargo (Fig. 37) with method of drive = diesel (High Speed engine).

distance from return air inlet	1.5 m	3.0 m	5.0 m	7.0 m	9.0 m	11.0 m
reference	5.51	3.90	2.30	1.25	0.80	0.38
no air chute	4.02	2.22	0.79	0.61	0.60	0.43
23 pallets	4.53	5.56	4.25	2.87	2.01	1.03

Table 23 Air velocities (m/s) measured in pallet openings on the right side with method of drive = electric (Fig. 34).

distance from return air inlet	0.0 m	1.0 m	3.0 m	5.0 m	7.0 m	9.0 m	11.0 m	12.0 m
reference		1.88	1.81	1.50	1.21	0.95	0.77	0.73
no air chute		1.41	1.07	0.78	0.69	0.47	0.58	0.55
distance from return air inlet	0.0 m	1.2 m	2.4 m	3.6 m	4.8 m	7.2 m	9.6 m	10.8 m
23 pallets	1.40	1.40	1.66	1.65	1.35	0.62	0.38	0.25

Table 24 Air velocities (m/s) measured in pallet openings on the left side with method of drive = electric (Fig. 34).

distance from return air inlet	0.0 m	1.0 m	3.0 m	5.0 m	7.0 m	9.0 m	11.0 m	12.0 m
reference		1.84	1.85	1.53	1.25	0.86	0.76	0.71
no air chute		1.46	1.05	0.80	0.66	0.50	0.57	0.53
distance from return air inlet	0.0 m	1.0 m	3.0 m	5.0 m	7.0 m	9.0 m	10.0 m	11.0 m
23 pallets	1.76	1.07	1.22	1.05	0.53	0.21	0.28	0.22

Table 25 Air velocities (m/s) measured in pallet openings on the right side with method of drive = diesel (Low Speed engine) (see Fig. 36).

distance from return air inlet	0.0 m	1.0 m	3.0 m	5.0 m	7.0 m	9.0 m	11.0 m	12.0 m
reference		2.20	2.11	1.75	1.40	1.16	0.86	0.80
no air chute		1.61	1.23	0.88	0.77	0.55	0.64	0.61
distance from return air inlet	0.0 m	1.2 m	2.4 m	3.6 m	4.8 m	7.2 m	9.6 m	10.8 m
23 pallets	1.57	1.61	1.89	1.92	1.58	0.75	0.45	0.30

Table 26 Air velocities (m/s) measured in pallet openings on the left side with method of drive = diesel (Low Speed engine) (see Fig. 36).

distance from return air inlet	0.0 m	1.0 m	3.0 m	5.0 m	7.0 m	9.0 m	11.0 m	12.0 m
reference		2.10	2.14	1.78	1.44	0.98	0.85	0.78
no air chute		1.64	1.18	0.90	0.75	0.57	0.63	0.59
distance from return air inlet	0.0 m	1.0 m	3.0 m	5.0 m	7.0 m	9.0 m	10.0 m	11.0 m
23 pallets	2.00	1.22	1.40	1.10	0.68	0.29	0.32	0.28

Table 27 Air velocities (m/s) measured in pallet openings on the right side with method of drive = diesel (High Speed engine) (see Fig. 38).

distance from return air inlet	0.0 m	1.0 m	3.0 m	5.0 m	7.0 m	9.0 m	11.0 m	12.0 m
reference		2.73	2.75	2.25	1.67	1.49	0.94	0.82
no air chute		2.16	1.58	1.04	0.83	0.56	0.66	0.57
distance from return air inlet	0.0 m	1.2 m	2.4 m	3.6 m	4.8 m	7.2 m	9.6 m	10.8 m
23 pallets	1.94	2.00	2.36	2.34	1.98	0.89	0.45	0.29

Table 28 Air velocities (m/s) measured in pallet openings on the left side with method of drive = diesel (High Speed engine) (see Fig. 38).

distance from return air inlet	0.0 m	1.0 m	3.0 m	5.0 m	7.0 m	9.0 m	11.0 m	12.0 m
reference		2.76	2.76	2.30	1.77	1.09	0.95	0.92
no air chute		2.12	1.46	1.07	0.80	0.63	0.75	0.70
distance from return air inlet	0.0 m	1.0 m	3.0 m	5.0 m	7.0 m	9.0 m	10.0 m	11.0 m
23 pallets	2.55	1.50	1.80	1.49	0.77	0.29	0.44	0.32

Table 29 Air velocities (m/s) measured in the air slit between pallet load and container wall at half the container height (blue squares in Fig. 24 till Fig. 27) with method of drive = electric.

Container side:	**left**	**left**	**left**	**left**	**left**	**left**	**left**	**left**	**right**	**right**	**right**	**right**	**right**	**right**	**right**	**right**
flow direction (horizontal / vertical)	**vert.**	**vert.**	**vert.**	**vert.**	**hor.**	**hor.**	**hor.**	**hor.**	**vert.**	**vert.**	**vert.**	**vert.**	**hor.**	**hor.**	**hor.**	**hor.**
distance from return air inlet	**2.0 m**	**5.0 m**	**8.0 m**	**11.0 m**	**2.0 m**	**5.0 m**	**8.0 m**	**11.0 m**	**2.0 m**	**5.0 m**	**8.0 m**	**11.0 m**	**2.0 m**	**5.0 m**	**8.0 m**	**11.0 m**
reference	0.02	1.58	0.77	-	0.95	0.28	-	-	0.02	0.50	0.79	0.35	1.17	0.11	0.16	0.06
no air chute	0.27	0.98	0.35	-	0.06	0.25	-	-	0.71	0.39	0.34	0.06	0.04	-	-	0.06
distance from return air inlet	**2.0 m**	**5.0 m**	**8.0 m**	**11.0 m**	**2.0 m**	**5.0 m**	**8.0 m**	**11.0 m**	**2.4 m**	**4.8 m**	**7.2 m**	**11.0 m**	**2.4 m**	**4.8 m**	**7.2 m**	**11.0 m**
23 pallets	0.02	1.05	0.41	-	1.05	0.63	0.27	-	0.04	0.09	0.36	-	1.07	0.36	0.58	-

Table 30 Air velocities (m/s) measured in the air slit between pallet load and container wall at half the container height (blue squares in Fig. 24 till Fig. 27) with method of drive = diesel (Low Speed engine).

Container side:	**left**	**left**	**left**	**left**	**left**	**left**	**left**	**left**	**right**	**right**	**right**	**right**	**right**	**right**	**right**	**right**
flow direction (horizontal / vertical)	**vert.**	**vert.**	**vert.**	**vert.**	**hor.**	**hor.**	**hor.**	**hor.**	**vert.**	**vert.**	**vert.**	**vert.**	**hor.**	**hor.**	**hor.**	**hor.**
distance from return air inlet	**2.0 m**	**5.0 m**	**8.0 m**	**11.0 m**	**2.0 m**	**5.0 m**	**8.0 m**	**11.0 m**	**2.0 m**	**5.0 m**	**8.0 m**	**11.0 m**	**2.0 m**	**5.0 m**	**8.0 m**	**11.0 m**
reference	0.02	1.83	0.86	-	1.16	0.31	-	-	0.02	0.57	0.88	0.39	1.38	0.14	0.16	0.06
no air chute	0.29	1.04	0.36	-	0.07	0.30	-	-	0.74	0.44	0.36	0.09	0.10	-	-	0.06
distance from return air inlet	**2.0 m**	**5.0 m**	**8.0 m**	**11.0 m**	**2.0 m**	**5.0 m**	**8.0 m**	**11.0 m**	**2.4 m**	**4.8 m**	**7.2 m**	**11.0 m**	**2.4 m**	**4.8 m**	**7.2 m**	**11.0 m**
23 pallets	0.02	1.17	0.45	-	1.23	0.66	0.33	-	0.06	0.10	0.36	-	1.30	0.47	0.59	-

Table 31 Air velocities (m/s) measured in the air slit between pallet load and container wall at half the container height (blue squares in Fig. 24 till Fig. 27) with method of drive = diesel (High Speed engine).

Container side:	**left**	**left**	**left**	**left**	**left**	**left**	**left**	**left**	**right**	**right**	**right**	**right**	**right**	**right**	**right**	**right**
flow direction (horizontal / vertical)	**vert.**	**vert.**	**vert.**	**vert.**	**hor.**	**hor.**	**hor.**	**hor.**	**vert.**	**vert.**	**vert.**	**vert.**	**hor.**	**hor.**	**hor.**	**hor.**
distance from return air inlet	**2.0 m**	**5.0 m**	**8.0 m**	**11.0 m**	**2.0 m**	**5.0 m**	**8.0 m**	**11.0 m**	**2.0 m**	**5.0 m**	**8.0 m**	**11.0 m**	**2.0 m**	**5.0 m**	**8.0 m**	**11.0 m**
reference	0.02	2.17	0.99	-	1.49	0.35	-	-	0.02	0.54	1.16	0.44	1.73	0.31	0.38	0.13
no air chute	0.06	1.56	0.32	-	0.12	0.42	-	-	0.44	0.56	0.20	0.12	0.10	-	-	0.19
distance from return air inlet	**2.0 m**	**5.0 m**	**8.0 m**	**11.0 m**	**2.0 m**	**5.0 m**	**8.0 m**	**11.0 m**	**2.4 m**	**4.8 m**	**7.2 m**	**11.0 m**	**2.4 m**	**4.8 m**	**7.2 m**	**11.0 m**
23 pallets	0.03	1.30	0.70	-	1.55	0.84	0.30	-	0.13	0.13	0.63	-	1.68	0.66	0.82	-

Annex 5 Test log

Date	Activity
15-5-2020	Container arrives
16-5-2020 till 17-5-2020	K-value test
3-6-2020	Air velocities + Static pressure differences measured for configuration 2 (no air chute)
4-6-2020 till 8-6-2020	Temperature mappings for configuration 2
9-6-2020	Air velocities + Static pressure differences measured for configuration 1 (reference)
10-6-2020 till 18-6-2020	Temperature mappings for configuration 1
19-6-2020 till 23-6-2020	Repair of TK unit's evaporator fan
24-6-2020 till 4-7-2020	Continuation of temperature mappings for configuration 1
17-7-2020	Air velocities + Static pressure differences measured for configuration 3 (23 pallets)
18-7-2020 till 21-7-2020	Temperature mappings for configuration 3
27-7-2020	Measurement of supply air flow rate in empty container for multiple settings
27-7-2020	Container leaves

To explore the potential of nature to improve the quality of life

Wageningen Food & Biobased Research
Bornse Weilanden 9
6708 WG Wageningen
The Netherlands
www.wur.eu/wfbr
E info.wfbr@wur.nl

Report 2211

Confidential

The mission of Wageningen University & Research is "To explore the potential of nature to improve the quality of life". Under the banner Wageningen University & Research, Wageningen University and the specialised research institutes of the Wageningen Research Foundation have joined forces in contributing to finding solutions to important questions in the domain of healthy food and living environment. With its roughly 30 branches, 6,800 employees (6,000 fte) and 12,900 students, Wageningen University & Research is one of the leading organisations in its domain. The unique Wageningen approach lies in its integrated approach to issues and the collaboration between different disciplines.